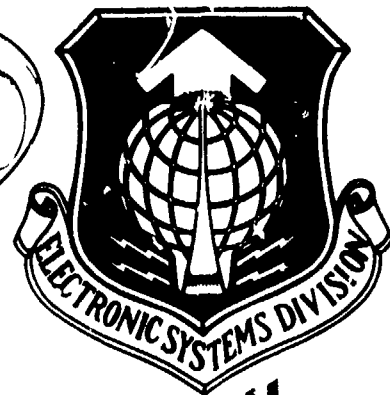


FG.

12



SPACEBORNE RADAR STUDY

Grumman Aerospace Corporation
Bethpage, New York 11714

28 June 1974

AD A 024679

Approved for Public Release;
Distribution Unlimited.

Prepared for

DEPUTY FOR DEVELOPMENT PLANS
ELECTRONIC SYSTEMS DIVISION
HANSCOM AIR FORCE BASE, MA 01731

RECEIVED
A -

UNCLASSIFIED

SECURITY CLASSIFICATION OF THIS PAGE (When Data Entered)

REPORT DOCUMENTATION PAGE		READ INSTRUCTIONS BEFORE COMPLETING FORM
1. REPORT NUMBER ESD-TR-76-144	2. GOVT ACCESSION NO.	3. RECIPIENT'S CATALOG NUMBER
4. TITLE (and Subtitle) Spaceborne Radar Study		5. TYPE OF REPORT & PERIOD COVERED Final Report 15 May 74 - 30 Jun 74
6. AUTHOR(s) Joseph/Greene, Richard/Kaplan, Gerald J./McNiff,		7. PERFORMING ORG. REPORT NUMBER
Paul/Nosal Jack L./Schultz John Wagner		8. CONTRACT OR GRANT NUMBER(s) F19628-74-R-0148/NEW
9. PERFORMING ORGANIZATION NAME AND ADDRESS Grumman Aerospace Corporation Bethpage, New York 11714		10. PROGRAM ELEMENT, PROJECT, TASK AREA & WORK UNIT NUMBERS PE: 63101F AFSC Project E150
11. CONTROLLING OFFICE NAME AND ADDRESS Deputy for Development Plans Electronic Systems Division, AFSC Hanscom Air Force Base, Bedford, MA 01731		12. REPORT DATE 28 Jun 74
14. MONITORING AGENCY NAME & ADDRESS (if different from Controlling Office)		13. NUMBER OF PAGES 169
(12) 173p.		15. SECURITY CLASS. (of this report) UNCLASSIFIED
16. DISTRIBUTION STATEMENT (of this Report) Approved for public release. Distribution unlimited.		
17. DISTRIBUTION STATEMENT (of the abstract entered in Block 20, if different from Report) Approved for public release. Distribution unlimited.		
18. SUPPLEMENTARY NOTES This study was in support of the Integrated Air Surveillance (IAS) Study, an in-house study conducted by the Electronic Systems Division (AFSC) and The MITRE Corporation, with participation by a number of U.S. and Canadian military and civil agencies.		
19. KEY WORDS (Continue on reverse side if necessary and identify by block number) Air Surveillance Bomber Warning Integrated Air Surveillance Satellite Radar Spaceborne Radar		
20. ABSTRACT (Continue on reverse side if necessary and identify by block number) Three air-defense radar surveillance systems are described, each consisting of active radar satellites capable of operating at earth-synchronous orbit altitude with associated ground control stations. System I (three satellites) provides a detection fence around the North American continent and does target tracking within the fence. System II (three satellites) provides detection fences around the USSR and China. System III (seven Satellites) provides worldwide coverage for aircraft detection and tracking. (continued)		

DD FORM 1 JAN 73 1473 EDITION OF 1 NOV 65 IS OBSOLETE

UNCLASSIFIED

SECURITY CLASSIFICATION OF THIS PAGE (When Data Entered)

388 847

mt

UNCLASSIFIED

SECURITY CLASSIFICATION OF THIS PAGE(When Data Entered)

Item 20 ABSTRACT (Cont)

The satellite carries a space-fed phased-array radar and the other necessary sub-systems for attitude control, station-keeping, and solar electrical power. Each ground station is capable of controlling three satellites. The ground station generates the transmitter pulse-burst chirp waveform, processes received signals, detects and tracks aircraft targets, and provides the communication interface with ADC and other users of the radar data.

The satellites can be launched on Titan 3-Centaur launch vehicles into earth-synchronous orbit. The phased-array antenna deploys in orbit to a 300-m diameter. It provides 15,700 mi of fence with .999 probability of detection of 1-m² targets, tracks 50 threat aircraft simultaneously, and requires an average radiated power of 2784 w.

Structural mechanics analysis, static and dynamic, of the vehicle configuration shows that the necessary tolerances can be held easily. Guidance and control analysis shows that the stationkeeping and attitude control thruster fuel requirements are modest.

Ten-year life-cycle cost forecasts are included.

UNCLASSIFIED

SECURITY CLASSIFICATION OF THIS PAGE(When Data Entered)

ABSTRACT

Three air-defense radar surveillance systems are described, each consisting of active radar satellites capable of operating at earth-synchronous orbit altitude with associated ground control stations. System I (three satellites) provides a detection fence around the North American continent and does target tracking within the fence. System II (three satellites) provides detection fences around the USSR and China. System III (seven Satellites) provides worldwide coverage for aircraft detection and tracking.

The satellite carries a space-fed phased-array radar and the other necessary subsystems for attitude control, stationkeeping, and solar electrical power. Each ground station is capable of controlling three satellites. The ground station generates the transmitter pulse-burst chirp waveform, processes received signals, detects and tracks aircraft targets, and provides the communication interface with ADC and other users of the radar data.

The satellites can be launched on Titan 3-Centaur launch vehicles into earth-synchronous orbit. The phased-array antenna deploys in orbit to a 300-m diameter. It provides 15,700 mi of fence with .999 probability of detection of 1-m^2 targets, tracks 50 threat aircraft simultaneously, and requires an average radiated power of 2784 w.

Structural mechanics analysis, static and dynamic, of the vehicle configuration shows that the necessary tolerances can be held easily. Guidance and control analysis shows that the stationkeeping and attitude control thruster fuel requirements are modest.

Ten-year life-cycle cost forecasts are included.

SIGNIFICANT CONTRIBUTORS TO THIS REPORT

<u>Name</u>	<u>Report Section</u>
Greene, Joseph	4
Kaplan, Richard	5
McNiff, Gerald J.	Appendix I
Nosal, Paul	2, 3, 4
Schultz, Jack L.	1
Wagner, John	6

NOTE: Ground Station Study by Sperry Gyroscope Division, see separate report. (*)

Previous and related contracts: None

* ESD-TR-76-145, Title: Ground Station Study for Spaceborne Radar Systems. (June 1974). Authors: P.M. Liebman, F.F. Kreussling, and R.S. Pierro

PREFACE

This report and the separately bound Sperry Gyroscope Division report were prepared in accordance with the contract description/specifications reproduced below.

F. DESCRIPTION/SPECIFICATIONS

Line Item 0001 - The contractor will perform a study to accomplish the following:

a. Develop spaceborne system designs for all weather air space surveillance for the U.S. and the North American continent for the purpose of air sovereignty and air traffic control. The contractor will also analyze these designs to identify relative advantages and disadvantages of each. Alternative designs shall include perimeter coverage and area coverage concepts.

b. The estimates of performance of the systems shall include the following parameters:

Aircraft Speeds: 100 knots to limit of military threat of 1985.

Aircraft altitudes: All feasible altitudes for civil and military aircraft.

Aircraft size: Down to 1 square meter of radar cross section.

Aircraft numbers: Detect and track all aircraft approaching the U.S. from the Atlantic Coast, Pacific, and Gulf Coasts, the Mexican Border, Alaska, and Northern Canada, until correlated with flight plan (or otherwise identified) with a probability of .999.

c. The designs should describe the system configuration of space and ground station elements, as well as a description of the launch platform.

d. The analysis will include calculations to confirm system performance of radar, communications, and data processing elements, interfaces with other agencies (civil and military) and provide estimates of item and life cycle costs of ten years of full system operation (including development).

TABLE OF CONTENTS

<u>Section</u>		<u>Page</u>
1	INTRODUCTION	11
	1.1 Geostationary Radar Satellite Coverage	13
	1.2 Satellite Configuration	13
	1.3 Satellite Radar Operation	15
	1.4 Ground Stations	18
2	MISSION ANALYSIS	19
	2.1 Scope	19
	2.2 Satellite Workload: System I	23
	2.2.1 Fence Generation	23
	2.2.2 Tracking	29
	2.2.3 Design Workload	30
3	SYSTEM SPECIFICATIONS	33
	3.1 Satellite Specifications	34
	3.2 Ground Station Specifications	35
	3.3 Radar Specifications	35
	3.4 Land and Sea Clutter	35
	3.5 Weather and Ionosphere	40
	3.6 Radar Parameters	40
	3.7 Resolution	41
	3.8 Accuracy	42
	3.9 Satellite Coverage	42
4	SYSTEM ELECTRICAL DESIGN	45
	4.1 Satellite	45
	4.1.1 Satellite Electronics (USP and LSP).	46
	4.1.2 System Operation	46
	4.2.3 Omni and Instrumentation	49
	4.1.4 Satellite Control	49

TABLE OF CONTENTS (Cont'd)

<u>Section</u>	<u>Page</u>
4.1.5 Beam Control Logic.....	50
4.1.6 Radar Antenna Array Electrical Design.....	53
4.1.7 Design of Subarrays of Main Radar Phased Array.....	63
4.1.8 Antenna Pattern Analysis.....	64
4.1.9 Feed Design.....	66
4.1.10 Radar System Noise Figure and Loss Budget.....	66
4.1.11 DC Power Distribution for RF Modules.....	68
4.2 Ground Station.....	70
4.3 Satellite Stationkeeping.....	75
4.3.1 Earth's Equatorial Ellipticity.....	75
4.3.2 Sun and Moon Gravitational Attraction.....	81
4.3.3 Solar Radiation Pressure.....	81
4.3.4 Summary.....	82
5 CONFIGURATION.....	95
6 LIFE-CYCLE COST ESTIMATE.....	101
7 STRUCTURAL MECHANICS AND RIGID BODY DYNAMICS.....	103
7.1 Static Structural Analysis.....	103
7.1.1 Structural Model.....	103
7.1.2 Static Analysis.....	110
7.2 Buckling Analysis.....	113
7.3 Vibration Analysis.....	113
7.4 Thermal Stress Analysis.....	116
7.5 Buckling Analysis.....	116
7.5.1 Buckling of Lower Systems Package Cylinder.....	116
7.5.2 Buckling of Battens.....	121
7.6 Dynamics of Controlled Orbiting Satellite.....	124
7.6.1 Rigid-Body Attitude Dynamics.....	124
7.6.2 Flexible Response to Control Jet Excitation.....	135
7.7 Dynamic Analysis of Gore Material During Launch.....	136

SUPPLEMENT TO THE
SPACEBORNE RADAR STUDY FINAL REPORT

20 September 1974

TABLE OF CONTENTS

<u>SECTION</u>	<u>TITLE</u>	<u>PAGE</u>
0	Introduction	145
1.0	Aircraft Track Initiation	145
2.0	Aircraft Traffic	145
2.1	Aircraft Fence Crossings	145
2.2	Traffic Density	149
3.0	Radar Average Power Calculation	151
3.1	Radar Range Equation Parameters	151
3.2	Fence Generation	152
3.3	Target Tracking	157
3.4	Power Summary	160
4.0	Integration Loss	161
5.0	Use of Shuttle	169

LIST OF ILLUSTRATIONS

<u>Figure</u>		<u>Page</u>
1-1	Geostationary Radar Satellite Coverage.....	14
1-2	Single-Satellite Coverage.....	16
2-1	Radar Fence Location.....	21
2-2	Fence Generation.....	25
2-3	Satellite Coverage.....	27
2-4	Worldwide Satellite Coverage.....	31
3-1	Sea Clutter at UHF, Vertical Polarization.....	38
3-2	Sea Clutter at UHF, Horizontal Polarization.....	38
3-3	Doppler Spectrum, UHF, State 3, Horizontal Polarization....	39
3-4	Geometry of Geostationary Radar Satellite Coverage.....	43
3-5	Principle of Double Coverage.....	43
3-6	Double Coverage Along the Equator.....	44
4-1	Satellite Onboard Radar System.....	47
4-2	Overall Time Signal Diagram.....	51
4-3	Pulse Format Received at Satellite from Ground Station.....	52
4-4	RF Module and Subarrays, Simplified Block Diagram.....	54
4-5	RF Module, Space Allocation.....	54
4-6	RF Module.....	57
4-7	Coordinate Reference System.....	59
4-8	Simplified Block Diagram, DC Power Distribution to RF Modules.....	59
4-9	Ground Station Locations.....	71
4-10	Effect of Earth's Ellipticity.....	78
4-11	Motion of Satellite Due to Earth's Ellipticity.....	79
4-12	ΔV Required to Correct for Earth's Triaxiality.....	80
4-13	Motion in Radial Direction Due to Earth's Equatorial Ellipticity.....	80
5-1	Deployed Configuration, 300-meter Diameter Phased-Array Radar Satellite.....	95-A
5-2	Axially Arrayed Components Deployed.....	95-B

LIST OF ILLUSTRATIONS (Cont'd)

<u>Figure</u>		<u>Page</u>
7-1	Structural Idealization	104
7-2	Back Stays and Br' dles	105
7-3	Gore Structure and Bridles	106
7-4	Front Stays and Bridles	107
7-5	Computer-Generated Structural Idealization	108
7-6	Axial Deflection of Rim Due to Broken Cable	111
7-7	Radial Deflection of Rim Due to Broken Cable	112
7-8	Mode Shape for Lowest Buckling Load	114
7-9	Second Vibration Mode, $f=10256$ cps	117
7-10	Temperature Variation of Stays	118
7-11	Structural Deformations From Thermal Stress Analysis . .	119
7-12	Axial Deflection of Rim Due to Temperature Distribution .	120
7-13	Radial Deflection of Rim Due to Temperature Distribution.	120
7-14	Arrangement of Battens in Deployed Configuration	122
7-15	Configuration and Mass Properties Used in Rigid Body Dynamics Study	125
7-16	Radiation Pressure for Specular and Diffuse Emission with Reflectivity = 1	126
7-17	Geometry of Orbit Assumed for Computing Solar Radiation Torques	128
7-18	Control Law Assumed for Attitude Position Control About Roll and Lens Axes	129
7-19	Torque Components about Axes Fixed in Satellite Due to Solar Radiation Pressure During One Orbit	131
7-20	Attitude Error Components About Axes Fixed in Satellite .	133
7-21	Transient Response of Deployed Satellite Due to Firing Pitch Control Jets	137
7-22	Transient Response of Deployed Satellite Due to Firing Yaw Attitude Control Jets	138

LIST OF ILLUSTRATIONS (Cont'd)

<u>Figure</u>		<u>Page</u>
7-23	Gore Material Packed for Launch.....	139
7-24	Unwrapped Gore Material.....	141
7-25	Force at Ends of Batten.....	141
7-26	Force and Stress Distribution Along the Length of the Outermost Batten Due to Sinusoidal Excitation.....	142

THIS PAGE HAS INTENTIONALLY BEEN LEFT BLANK

Section 1

INTRODUCTION

Three spaceborne radar systems are covered in this report. The systems differ only in the orbital locations of the satellites; the satellites are of one type. The proposed satellite can be launched on a Titan III/Centaur D-1T launch vehicle into earth-synchronous (geostationary) orbit, where it deploys on-station and operates as an active repeater of radar signals between a ground (control) station and the radar target. The satellite uses a phased-array radar antenna with electronic beam steering.

A number of techniques were combined to achieve the satellite concept described in this report:

- Deployable Wire-wheel Structure to Support the Antenna. The major question, answered affirmatively, is whether a practical antenna system can be designed that will be sufficiently large to enable a radar system at geosynchronous altitude to detect and track aircraft targets near the earth. Grumman has devised an antenna system, different from any used in space to date, that deploys into a wire-wheel configuration such that the physical structure matches the antenna's RF tolerance requirements
- Space-fed Phased-array Lens Antenna. The space-fed phased-array is at least ten times more tolerant to the structure's physical displacement than a reflector. In combination with the wire-wheel structure, the space-fed system results in a lightweight antenna that will provide the necessary gain and beamwidth and can be scanned electronically to cover the earth from geostationary orbit altitude
- Geostationary Orbit. It is not only possible, but necessary, that the satellite be geostationary. The stationary platform permits Doppler filtering to be used to detect moving aircraft in the presence of sea and land clutter. Any orbit other than geostationary would prohibit Doppler filtering and would prevent the radar from separating targets from clutter

- **Adaptive System.** The geostationary satellite system can be adaptive in a number of ways:
 - A radar fence can be established at any desired location. The fence can be moved at will or a new fence can be set up at any time
 - Continuous viewing provides random access to targets. The data rate can be changed to accommodate target speed, maneuvering, traffic density, and target priority
 - Continuous tracking, adapting the tracking data rate to traffic density and to the probability of crossing tracks, permits a target to be followed for as long as desired. Once a track is established and identified, the identity will be retained
 - Repeated looking is permitted. A target that is not detected on one attempt can be detected on a second or third try. The radar system adapts to the target detection probability
- **Track Detected Targets.** Large amounts of power are conserved by tracking only targets of interest. The geostationary system does not illuminate large areas, and waste energy, where no targets exist. The random-access nature of the coverage permits targets to be acquired, and thereafter tracked, in areas where traffic density is low and to be kept under surveillance anywhere. New targets can be acquired and old targets dropped at any time. Seven satellites, providing world-wide coverage (System III), permit all targets to be tracked continuously
- **Radar Repeater Satellite.** The radar system in the satellite is simplified, and hence made more reliable, by using the satellite as a repeater. The transmitter signal, generated by the ground station, is repeated by the satellite toward the target. Echoes from the area surrounding the target are repeated back to the ground station, where all signal processing and target tracking are accomplished.

The system will be an important asset to the Air Force surveillance mission. The system will provide 24-hour-per-day real-time position data on all targets that have been detected and are being tracked. These targets can be tracked until they have been identified by flight-plan matching, or until they have been visually identified by an interceptor.

Accurate target position and velocity data supplied by the spaceborne radar system will simplify the interceptor vectoring problem. The data obtained by combining the radar satellite system with other Air Force data sources will provide a high degree of confidence that no attack exists or that an attack is underway if such is the case, will permit reliable data to be transmitted to WWMCCS, and will allow the source of the attack to be determined.

1.1 GEOSTATIONARY RADAR SATELLITE COVERAGE

Figure 1-1 shows the basic coverage of a geostationary radar satellite orbiting the earth at the earth's rotation rate so that it remains stationary with respect to the earth's surface. The radar beam could be scanned to cover nearly a hemisphere, extending up to latitude 81.25° at 0° grazing angle. The open hole under the satellite occurs because radar operation is restricted to grazing angles of less than 70° by the need to use MTI to separate targets from clutter. The hole is covered by the adjacent satellites. Four satellites could provide full-earth radar coverage, except near the poles, on a single-satellite-per-area basis. Double coverage is desired, however, to avoid MTI blind-velocity problems. With double coverage, an aircraft moving tangentially to one radar beam will not be moving tangentially to the other, except at the equator. Seven satellites are required to obtain worldwide double coverage.

1.2 SATELLITE CONFIGURATION

The key element of the radar satellite is the 300-meter diameter antenna. Its design consists of a deployable, lightweight, wire-wheel structure. Electrically, the antenna is a space-fed active phased-array lens generating a pencil beam that can be directed to any point on the earth's surface within the satellite's view. A space-fed lens antenna is an order of magnitude less sensitive to dimensional errors than a reflector or a transmission-line-fed phased-array. The lens is zoned to permit the use of simple phase shifters. The satellite package at launch is a cylinder 15 meters long and 3.77 meters in diameter, weighing 7900 lb. In the deployed configuration the mast supports the upper system electronics package and the feed for the main antenna array. The main antenna structure has two dipole planes, one on each side of a ground plane. The dipoles are aluminum, supported on continuous tapes of fused-silica epoxy. Subarrays of 16 dipoles each are fed through binary manifolds driven by modules, one module per subarray. The manifolds are open-wire transmission lines-aluminum strips supported on continuous tapes of fused-silica

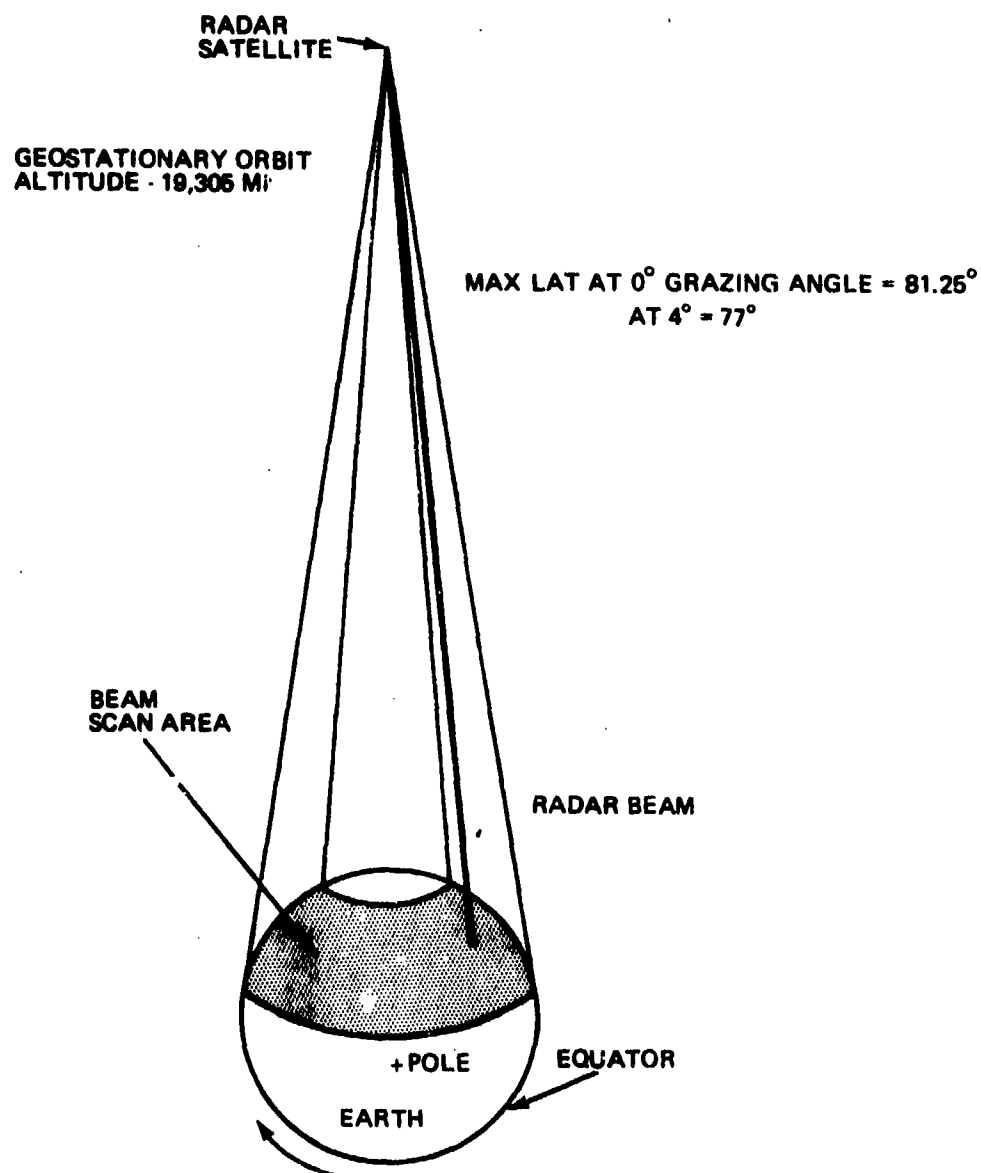


Fig. 1-1 Geostationary Radar Satellite Coverage

epoxy. The modules are mounted on the ground plane, which is an open mesh of aluminum conductors supported on graphite-epoxy tapes. The conductors are insulated from each other and distribute DC power to the modules.

The antenna mast and rim members are made of graphite epoxy. The temperature coefficient of this material, as well as that of the fused-silica epoxy, is very nearly zero; it is also very light for its strength.

1.3 SATELLITE RADAR OPERATION

The satellite operates as a radar-signal repeater. The radar pulse waveform (pulse burst) is transmitted to the satellite from the ground and then re-radiated toward the target. Target echoes are received by the satellite and re-radiated to the ground station. All signal processing (pulse compression, integration, Doppler filtering, and target detection) is accomplished by the ground system.

The control system responds to ground system commands for beam steering and for switching between transmitting and receiving modes. These commands are sent to the satellite through the communications antenna (comm beam) at all times except when comm beam contact is lost. A two-way omnidirectional (backup) command link is provided for initial stabilization and acquisition, or reacquisition, of the main beam.

The ground system commands are coded at the ground station and decoded by the satellite. The commands set the phase shifters in the main-array modules and synchronize the transmit-receive functions in the main-array modules and in the upper systems package (USP).

During transmission of a 64-pulse radar burst, the sequence is as follows (see Fig. 1-2). The communication beam points toward the ground station to receive a 225- μ sec chirp pulse. The pulse is delayed in a delay line in the USP and then transmitted toward the target by the main beam. The sequence repeats 64 times.

During reception of echoes, the receive gate is opened for a time corresponding to the length of the transmitter pulse burst. As the signal is being received, it is simultaneously repeated to the ground station through the communications array.

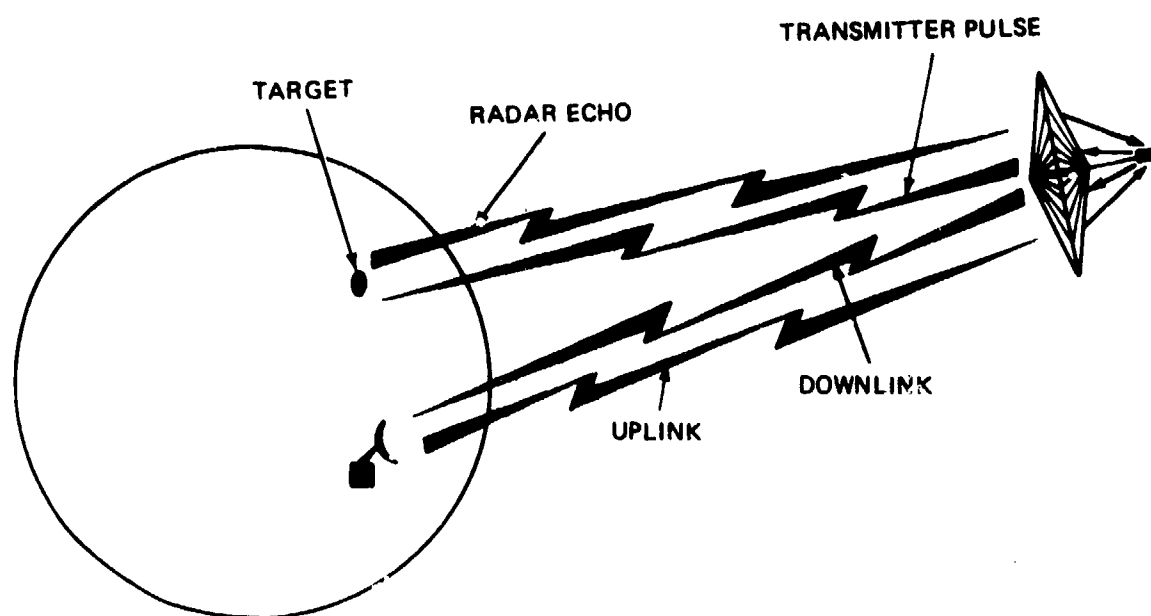


Fig. 1-2 Repeater Operation

Immediately preceding transmission of a pulse burst, a digital word is transmitted via the comm beam to insert the angular coordinates of the target in the digital memory of each module in the main array and in the communications array. Each module computes and stores the three bits it needs for each coordinate.

Immediately preceding reception of the 64 target echoes, the ground station transmits a synchronizing pulse (range gate trigger) for use in the main array and communication array modules and in the UPS to switch the amplifiers and gates to the receive mode. Commands for controlling other satellite functions, such as thruster firing and equipment switching, can be sent via either the comm beam or the omnichannel.

Satellite instrumentation data are sent to the ground station following every radar signal transmission. If comm beam contact is lost, the instrumentation data are sent via the omnichannel transmitter on command of the ground station.

There are six ways in which the geostationary radar satellite system can resolve the target it is tracking from other targets. A brief description of each follows:

- Radar Beam. The radar beam cross-sectional diameter on the earth is 60 miles. The projected beam on the earth is elongated along the range axis to 1000 miles at a 2° grazing angle. Range gating is employed to limit the active beam area to 60 miles when tracking aircraft. There will not be tracking interference when no other targets are in the active beam area simultaneously with the desired target.
- Range Bins. The active beam area is divided into 300-ft range bins along the range axis. The radar can separate the track from any other even in the same active beam area, providing they are in different range bins.
- Radial Speed. The MTI radar uses a Doppler filter that is capable of distinguishing differing radial speeds. Each range bin is treated independently and has a speed resolution of 7 kt. The narrow Doppler filters are used only to reduce clutter interference and to separate targets from other targets, not to measure target speed.
- Multiple Satellite Coverage. When two or more targets are in the range bin of a single radar beam, they will not be in the range bin of another radar beam covering the same area from a different angle.

- Variable Look Rate. The variable look rate capability of the proposed satellite radar allows an increase in the look rate when it appears that targets are approaching each other and could cross tracks. The increased look rate will greatly aid in keeping the tracks separated due to more accurate tracking of the individual targets.
- Smoothing. Smoothing is always used in radar target tracking. Position and velocity smoothing are employed using various amounts of radar data history. With smoothing, the track can, in most cases, be maintained through an area of crossing tracks where tracking would not otherwise be possible.

1.4 GROUND STATIONS

The ground station network for control of geostationary radar satellites will use existing or planned Air Force facilities wherever possible.

One satellite control ground station location can control three satellites. The location will be such that the elevation angle to any of the satellites exceeds 10° , thereby avoiding problems with troposphere bending or horizon reflection.

For redundancy, each satellite is in primary contact with one ground station and in backup contact with a second ground station. Three ground stations would provide control of seven satellites on a primary basis. Five ground stations will provide the primary and backup links for all satellites.

Three antenna systems are used at each ground station. These are assigned to the individual satellites such that, even if any one ground station became completely disabled, full control over all seven satellites could still be maintained.

It is desirable to have the stations sufficiently inland to prevent the enemy from jamming the uplink or downlink. The distance required depends on the grazing angle of the satellite beam at the ground station; it should be at least 600 n mi.

Section 2

MISSION ANALYSIS

2.1 SCOPE

The spaceborne radar system's primary mission is to provide surveillance against enemy air attack on the North American Continent. Other missions may be to provide interceptor control data, track designated aircraft, and provide surveillance of U.S. borders for unlawful aircraft crossing. Three systems are considered in this report.

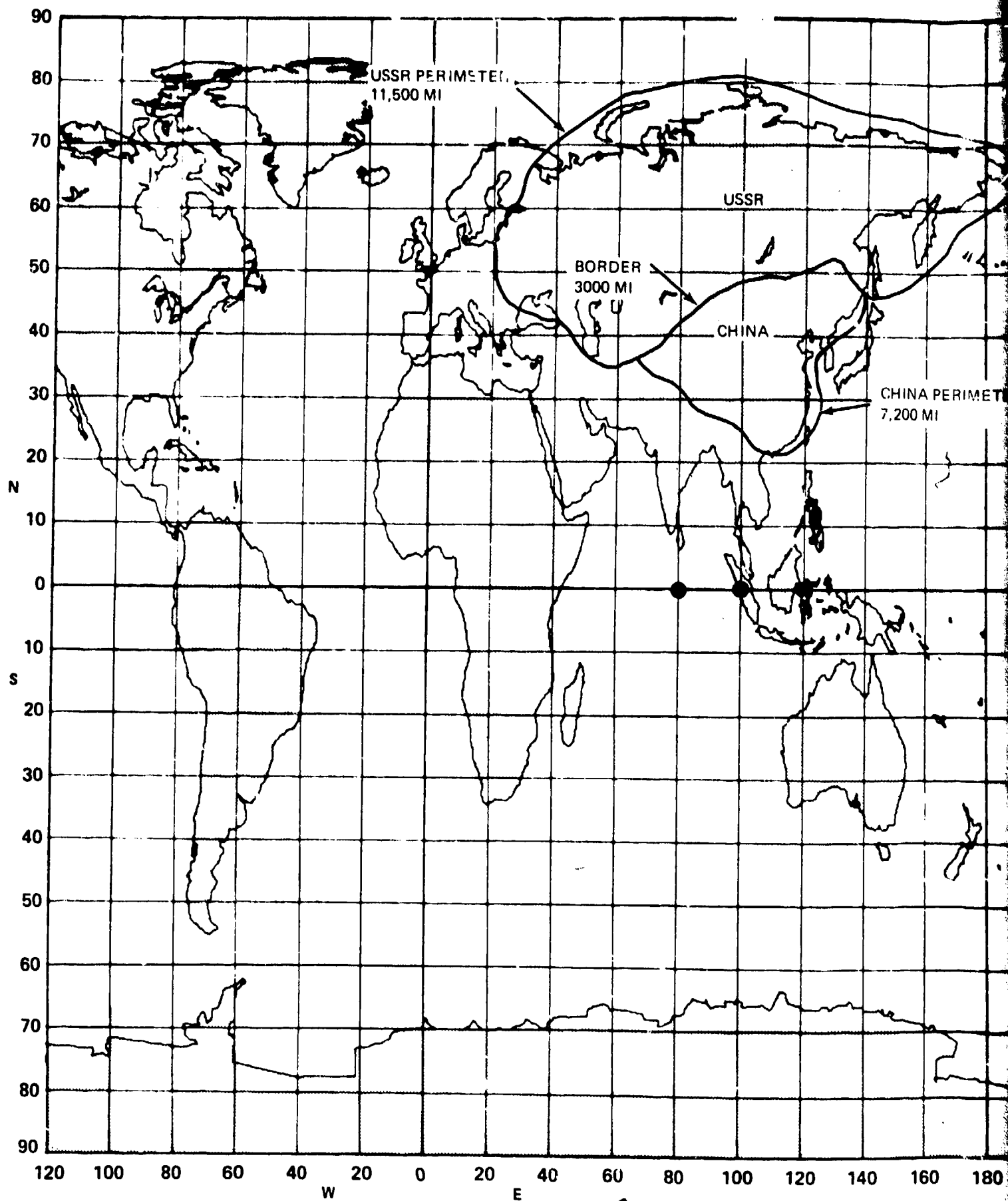
System I. Three Satellites. A radar fence is placed around the North American Continent at least 1,000 miles from coast, as shown in Fig. 2-1. The fence is just outside Alaska and Canada, at the limit of the satellite viewing area.

Aircraft crossing the fence are tracked by radar satellites until they are identified through flight plan correlation, IFF, or visual observation. The three satellites generate the fence and track penetrating aircraft.

System II. Three Satellites. A radar fence is placed around Russia and China and along their mutual border as shown in Fig. 2-1. Aircraft leaving these countries would be tracked while they are within the satellite radar coverage to determine their probable destination and to alert NORAD. Three satellites provide the fence and track penetrating aircraft.

System III. Seven Satellites. Spaced equally around the earth, seven satellites will provide world-wide coverage. Fences are placed in critical areas where the traffic density is low and aircraft are tracked worldwide, except at low altitude near the poles. Four satellites would cover the world on a single-coverage basis, but double coverage is required to fill the radar Doppler blind speeds that occur with single coverage.

THIS PAGE INTENTIONALLY LEFT BLANK



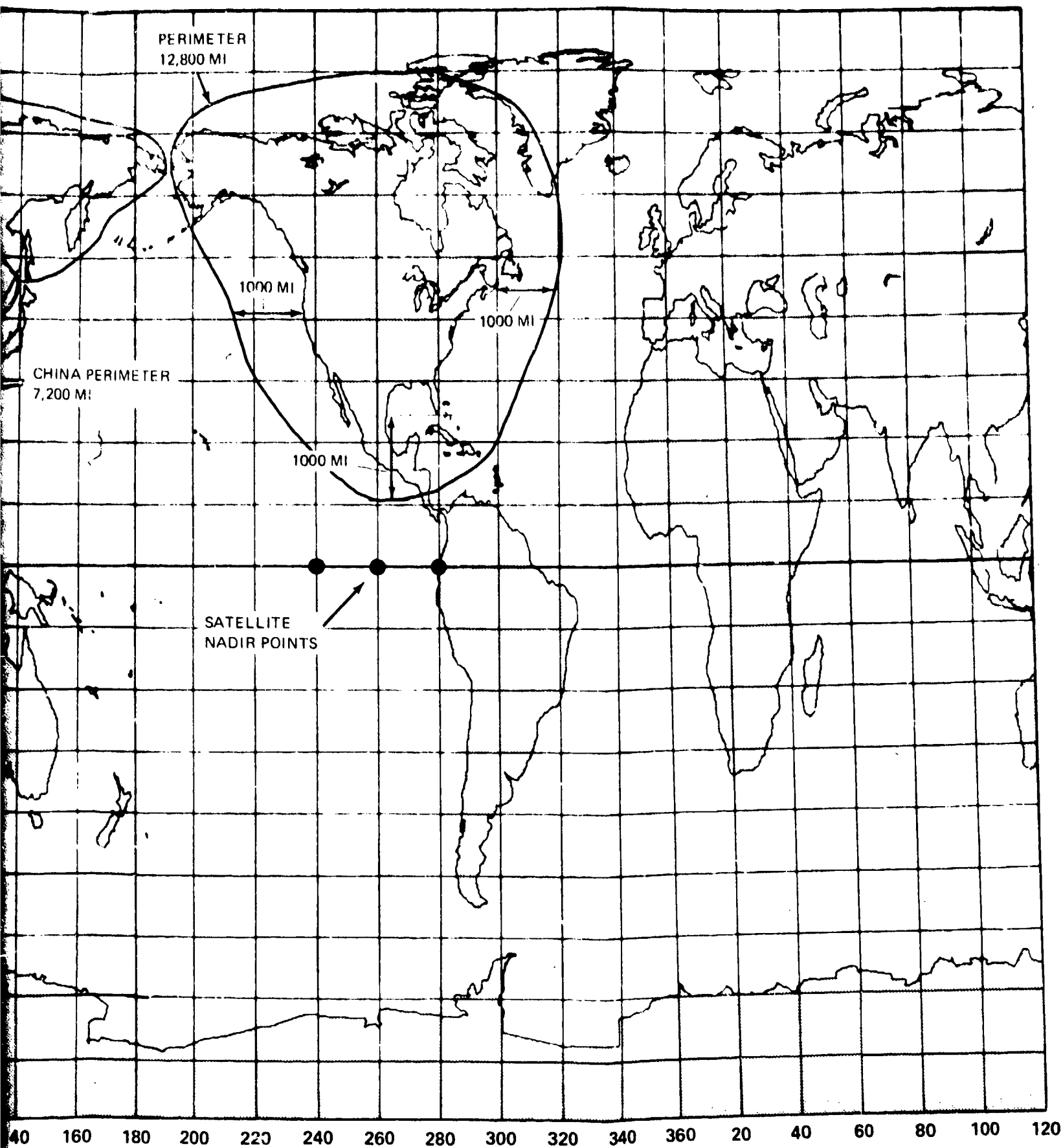


Fig. 2-1. Radar Fence Location

2.2 SATELLITE WORKLOAD: SYSTEM I

The length of the fence around the North American Continent, shown in Fig. 2-1, is 12,840 miles. Aircraft crossing the fence will have the following characteristics:

- Maximum Speed: Mach 3 (1800 kt)
- Minimum RCS: 1 m^2
- Altitude Range: 0 to 100,000 ft.

The probability of detection must exceed .999.

The fence may be located over land or sea. Its location will be flexible to avoid heavy clutter areas, such as cities, and may be changed at random to prevent enemy aircraft from making a high-speed dash (greater than Mach 3) across the fence, which they might attempt if they knew the exact fence location.

A maximum of 100 aircraft will be detected and tracked at any one time. The average speed for the 100 aircraft is estimated at Mach 1.75 based on the following distribution:

- 50 a/c at Mach 1
- 25 a/c at Mach 2
- 25 a/c at Mach 3.

2.2.1 Fence Generation

The fence is generated by successively pulsing adjacent beam positions at a scan rate fast enough to obtain the desired probability of detection.

The footprint made by a radar beam on the earth's surface is an ellipse, with the minor axis equal to the beam cross-sectional diameter and the major axis varying as a function of the grazing angle. For the System I radar parameters, the 3-dB radar beam diameter varies from 56.1 miles at a grazing angle of 70° to 64.4 miles at 2° due to the difference in range. The footprint's major axis varies from 59.7 miles to 1000 miles over the range of grazing angles.

Figure 2-2 shows the placement of footprints to generate the fence. Center-to-center overlap is used to provide approximately the same fence width from one beam position to the next. Examples of the fence are shown for low and high grazing angles over a short 90° turn (where the angle of ellipse remains nearly constant) to illustrate how fence width varies with the aspect angle between the fence and the satellite beam.

The number of footprints required per unit length of fence depends on the size of the ellipse and the aspect angle.

The time for a Mach 3 aircraft to cross the fence at the 3-dB cross-over point is a function of the ellipse size and the aspect angle. To obtain .999 probability of detection, two looks are made during this time. The number of looks required per hour per beam multiplied by the number of beams per fence gives the number of looks per hour required to generate the fence. A look consists of the transmission and reception of one pulse burst.

The number of looks per unit length of fence required at low grazing angles is several times less than that required at high grazing angles due to the different areas covered by one radar beam. Taking this into account and adding the number of extra looks required because of false alarms gives 16,302 looks per hour to generate the 12,840 miles of fence around the North American Continent.

A single geostationary radar satellite could produce the number of looks required, but one satellite is not sufficient to provide the .999 probability of detection because of the radar's blind speeds. A Doppler filter detector requires that the aircraft have a speed component toward the radar. An aircraft moving at right angles to the radar beam will not have any radial speed and will not be detected. For detection, the angle the aircraft heading must make with the tangential direction depends on the aircraft RCS, clutter level, aircraft speed, and grazing angle of the radar beam. An angle of approximately 10° will cover the worst-case situation. (In most cases, the angle is more nearly 1 to 2 degrees). Each spot in the fence must, therefore, be covered from two different angles separated by at least 10° . Three satellites are needed to provide double coverage; these share the workload. Figure 2-3 shows the placement of satellites and indicates their sub-orbital points and viewing areas. The maximum grazing angle is limited to 70° . At angles higher than 70° the clutter becomes severe, and the aircraft radial speed component is diminished.

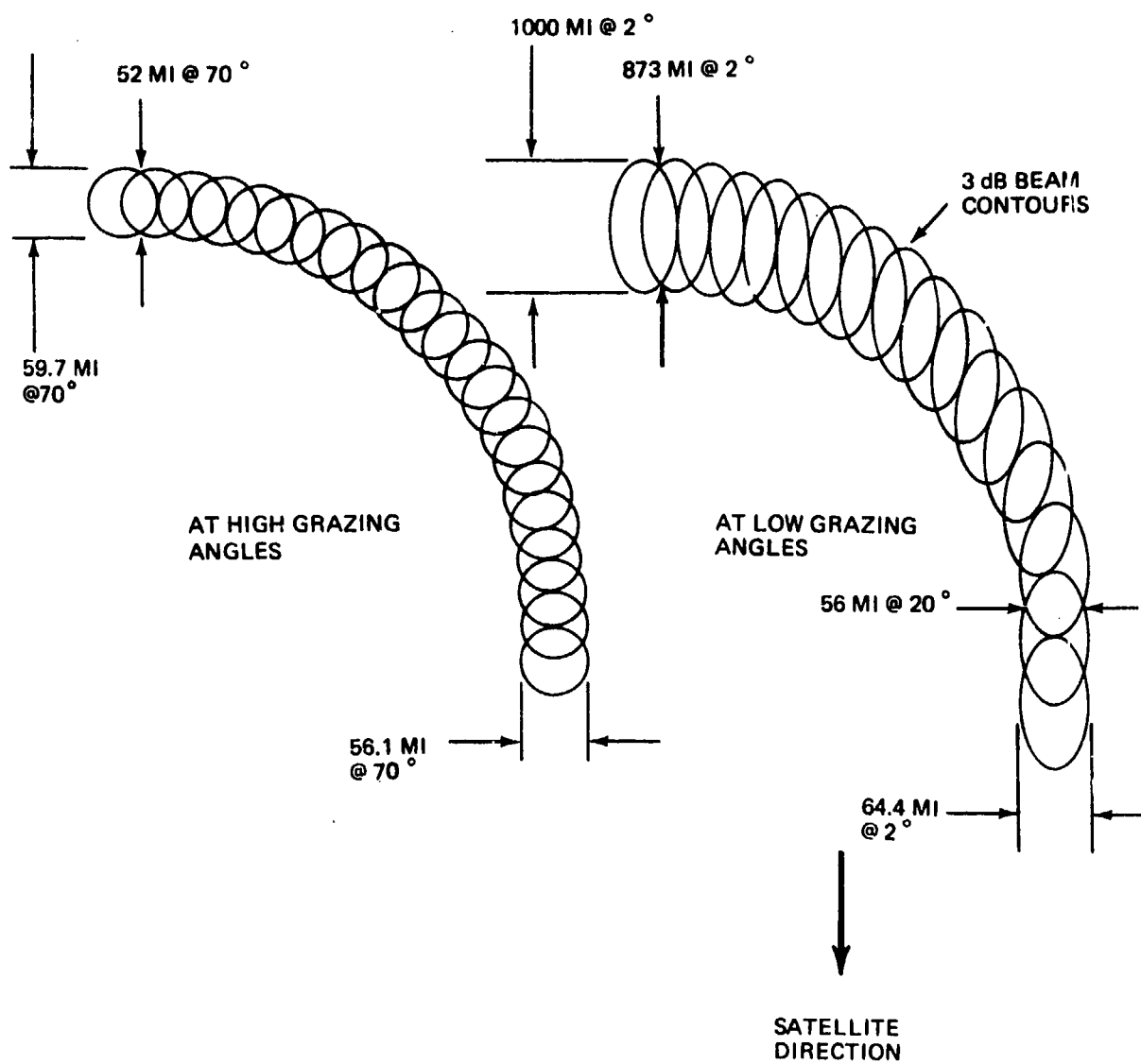
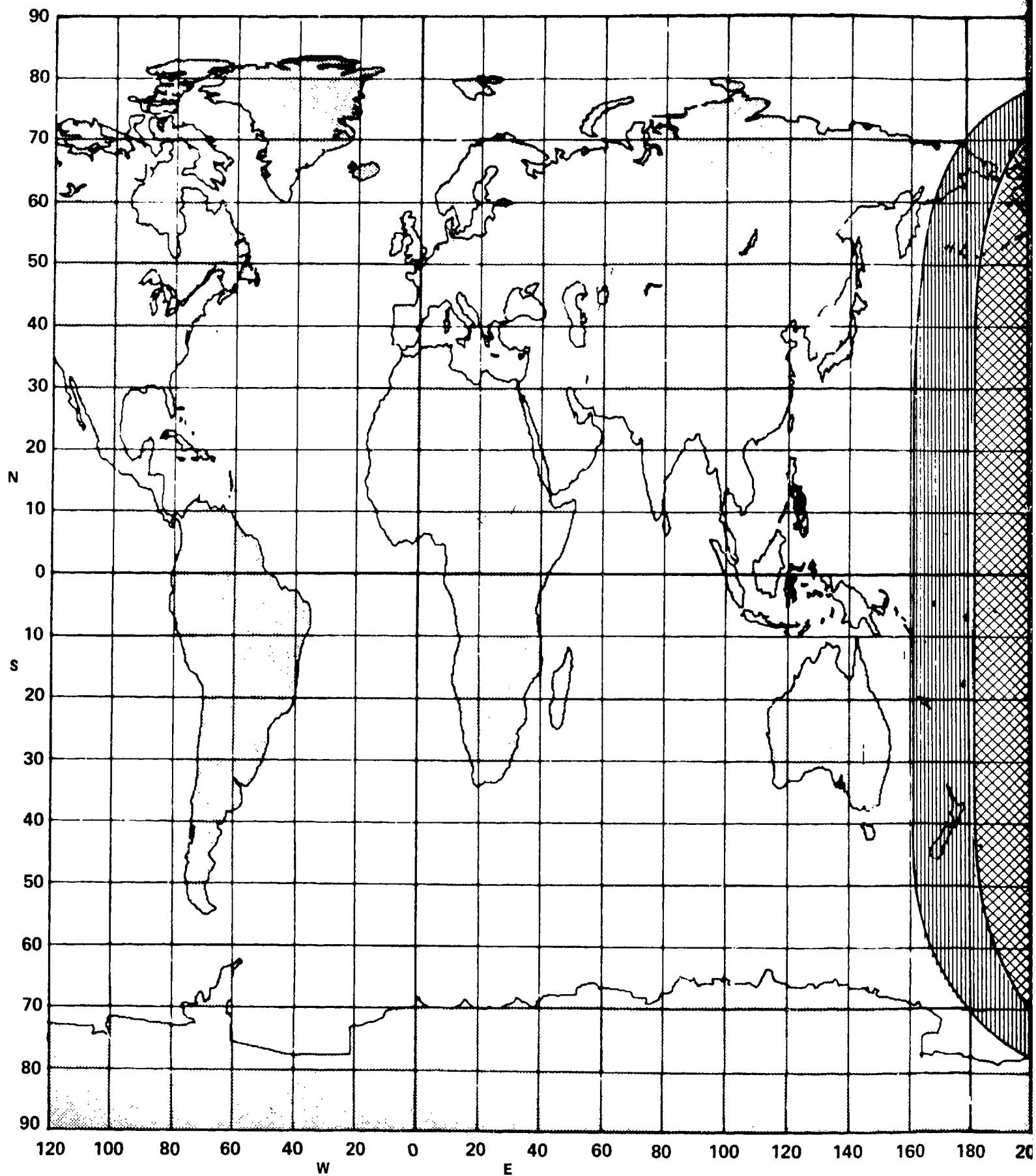


Fig. 2-2 Fence Generation

THIS PAGE HAS INTENTIONALLY BEEN LEFT BLANK



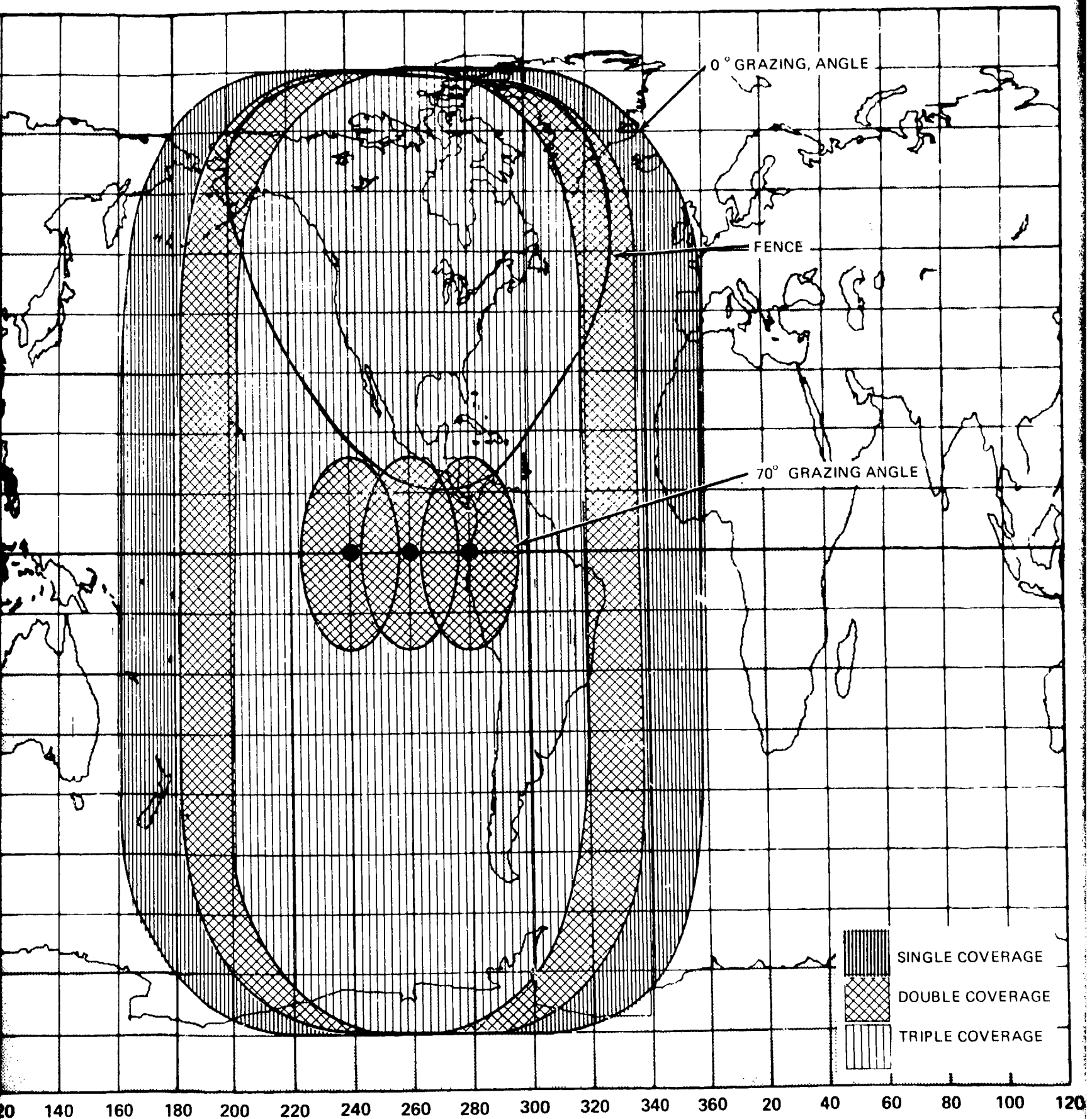


Fig. 2-3. Satellite Coverage

The look rate of 16,302 looks per hour required to generate the fence need not be doubled to provide two-angle detection. Instead, each fence element is looked at alternately by two of the satellites. Remembering that the rate provides two looks per aircraft crossing time, each of the two satellites gets at least one look at the aircraft. Combining the two satellites' looks produces a detection probability in excess of .999, providing the aircraft is not in the blind velocity zone of one of the radar satellites. For the case where the aircraft is in a blind zone (it cannot be in the blind zone of both satellites simultaneously except at the equator), the probability of detection drops to .995 when the crossing track and phase of the look and aircraft position are at the worst case. The probability of this situation occurring is very low since it requires the combination of the aircraft showing a 1 m^2 RCS and flying at the critical angle in the blind zone on the worst track through the fence with the worst look and position phase. An important point to note is that the alternate look technique from two satellites lowers the probability of detection only slightly when the aircraft is in the blind zone of one, as compared to no detection at all if only one satellite were used for all looks.

The number of looks needed for the fence is divided equally among the three satellites, resulting in 5,434 looks per hour per satellite.

2.2.2 Tracking

The track mode will be automatically initiated by the ground station upon detection of an aircraft penetrating the fence, and the aircraft will be tracked until it can be dropped.

Initially, the look rate is several times a minute until the aircraft direction and speed are established. Thereafter, the look rate is dependent on the aircraft's speed and maneuvers and on the active area of the radar beam spot as determined by the beam spot width and the range segment used out of the total range of the ellipse. Since the beam width averages 60 miles, a range segment of 60 miles is selected.

The look rate is set so that the aircraft cannot travel out of the active radar between looks. Using the average speed of Mach 1.75 for 100 aircraft, the average look period is 1/35th of an hour. Since each satellite does not cover the whole surveillance area, as indicated in Fig. 2-3, the tracking load is not divided by three but by two, resulting in 50 tracks per satellite. The look rate per satellite is then 50×35 or 1750 looks per hour for tracking the 50 aircraft.

Track mixup with other aircraft in the area is greatly minimized by the discrimination provided by the radar as follows:

- Aircraft in different beam spots are resolved
- Aircraft in the same beam spot but in different range bins are resolved
- Aircraft in the same beam spot and in the same range bin are resolved if they have different radial speeds
- Variable look rate permits more accurate smoothing for crossing tracks.

In the event a mixup does occur, each aircraft will be tracked until an identification is made.

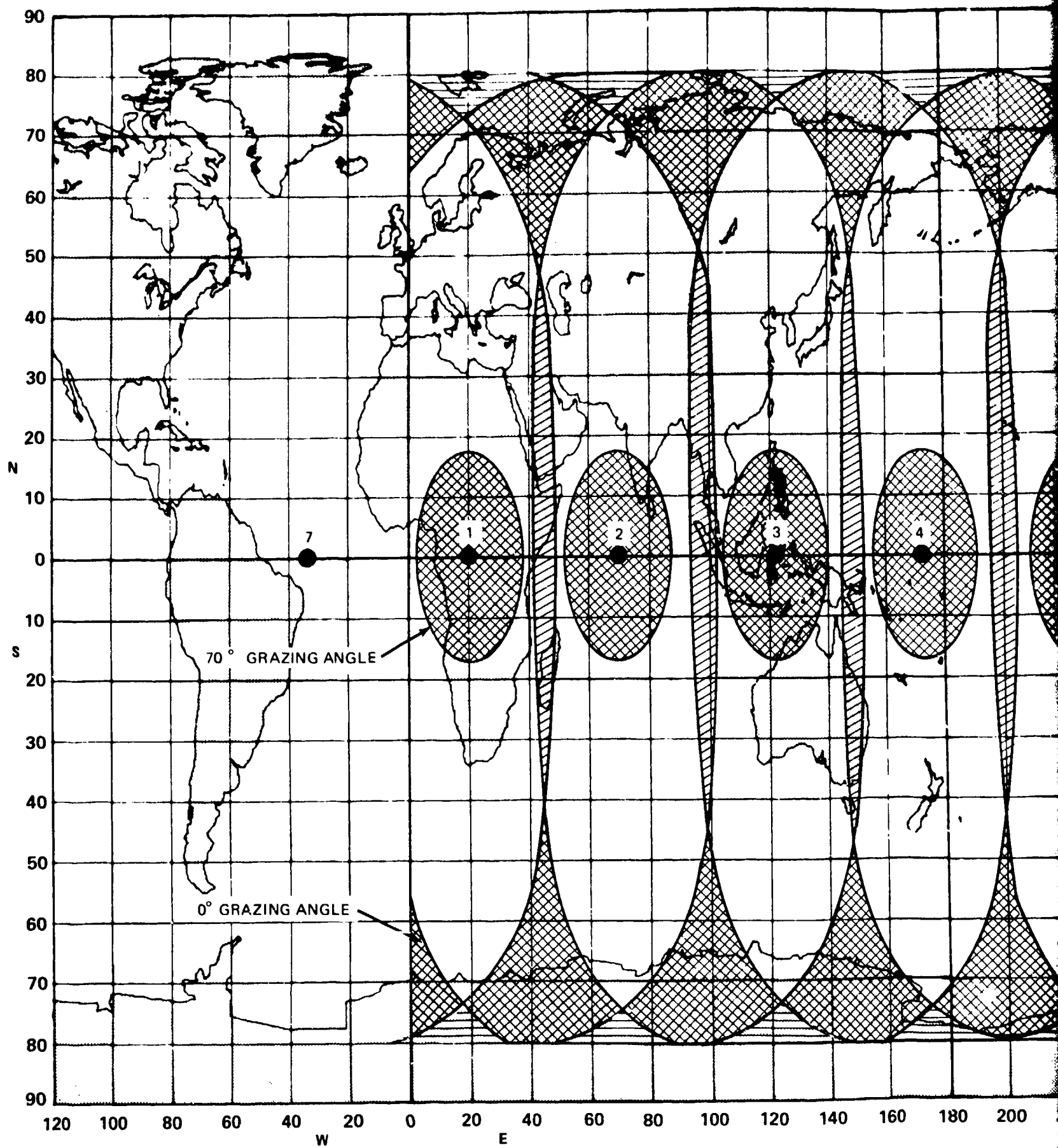
2.2.3 Design Workload

The System I total workload per satellite is the sum of 5,534 looks per hour to generate the fence and 1750 looks per hour to track 50 aircraft. The results is 7,184 looks per hour, about 2 looks per second.

System II consists of moving the three satellites to the locations shown in Fig. 2-1, generate the fence around the USSR and China.

The length of the fence around the USSR alone is 11,500 miles. Scaling the look rate with the length of the fence gives a fence workload per satellite of 4,867 looks per hour. A fence around the USSR and China is 12,700 miles long, requiring a look rate of 5,375 looks per hour per satellite. Keeping the USSR and China separate makes the fence length 15,700 miles, requiring a look rate of 6,644 looks per hour per satellite. Added to the fence workload is the tracking workload of 1750 looks per hour, totalling 8,394 looks per hour or 2.33 looks per second per satellite. The 2.33 looks per second are used as the design workload for the radar satellite.

System III consists of seven satellites equally spaced around the earth, each capable of 2.33 looks per second. Figure 2-4 shows the location and coverage provided.



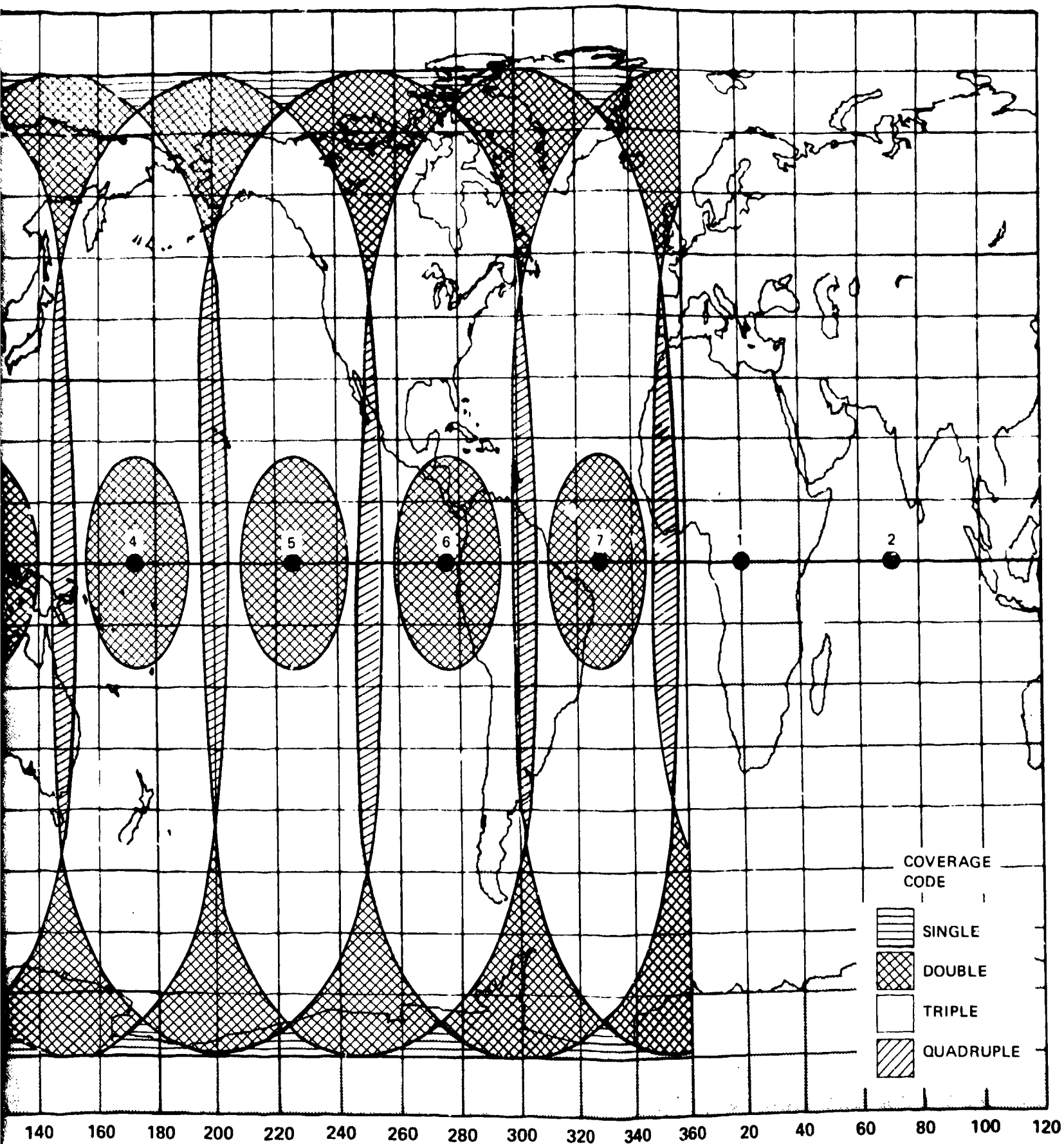


Fig. 2-4. Worldwide Satellite Coverage

Section 3

SYSTEM SPECIFICATIONS

The objectives of the aircraft detection and tracking satellite system design are to:

- Provide a radar satellite that will
 - Handle the workload: generate 5,233 miles of fence and track 50 aircraft per satellite with the necessary accuracies and data rates
 - Operate in earth synchronous equatorial orbit (19,300-mile altitude) to provide full-time viewing and high data rates when necessary
 - Use available technology
 - Be lightweight and low cost
 - Provide coverage of the North American continent (3 satellites), or of the USSR and China (3 satellites), or worldwide (7 satellites)
 - Be inherently reliable for 5 years operating life
- Provide a ground station that will
 - Control the satellite
 - Process the satellite radar data for detection of aircraft, and maintain tracks as required
 - Accept direction from NORAD for fence placement and for tracking aircraft
 - Transmit data to NORAD on aircraft penetrations and tracks.

3.1 SATELLITE SPECIFICATIONS

Radar Antenna Diameter	-----	300 m
Mast Length (F number = 2.5)	-----	750 m
Launch Weight	-----	6000 lb
Electrical Power System (Solar Array and Battery)	---	20 kw

Lower Solar Arrays (2) Dia, ea. -----	36 ft
Attitude Control System -----	50- μ lb teflon-electrical thrusters, radar-derived attitude, horizon sensor and sun sensor for backup
Stationkeeping System -----	Same thrusters, radar position deter- mination
Initial Orbit -----	2.1° inclination, equatorial orbit
Telemetry System:	
• Primary -----	Via main beam of satellite
• Backup -----	S-band, 50 kilobits/sec
Onboard Electronics -----	Radar repeater system; instrumentation system; command data system; intra- satellite communication.

3.2 GROUND STATION SPECIFICATIONS

Location -----	Inland, preferably at existing communi- cation sites
Antenna Size -----	60-ft dish
Transmitted Power -----	10 kw peak
Transponder -----	Radar beacon
Satellite Control System -----	Data display, manual command via telemetry
Radar Electronics -----	Radar signal processing; radar data processing; earth-to-satellite-to-earth coordinate conversion
Communication System to NORAD -----	Radio, wire and/or communications satellite.

3.3 RADAR SPECIFICATIONS

The radar specifications of the geostationary satellite, given in Table 3-1, will produce the performance required for all three aircraft surveillance systems described in Section 2.

In selecting radar parameters, the compromise between size, power and performance was biased in favor of a minimum-launch-weight system. Two items having a very large input on selection are the power required for generating the fence and the radar resolution needed to separate moving aircraft from land and sea clutter.

The average transmitter power required to generate a fence is given by $P_{AVG} \sim LV/D^2 \sigma$, where L is the fence length, V the maximum aircraft velocity expected, D the antenna diameter, and σ the minimum RCS of the aircraft. The radar resolution required for target detection in clutter is determined by target backscatter cross section and speed, and by the amplitude and spectrum of the clutter.

The average power required to track an aircraft is $P_{AVG} \sim \lambda V/D^3 \sigma$. The radar resolution is a function of beam spot size, size of the range bins, and bandwidth of the Doppler filters. The resolution required to separate one target from all others in operational use is adequately met by the required resolution for target detection.

3.4 LAND AND SEA CLUTTER

From the data obtained by the four-frequency radar system tests* made by NRL in sea states ranging from 0 to 7, it is concluded that an upper bound for the sea clutter radar cross section (RCS) exists and is closely approached when wind speed exceeds 10 kt (5 m/sec). Saturation was indicated by an approximately 3-dB increase in RCS for an increase in wind velocity from the 7- to 12-kt range to the 48-kt range.

* "Experimental Study of a Sea Clutter Model", N. V. Guinard and J. C. Daley of NRL, in Proceeding of IEEE Vol 58, No. 4, April 1970.

TABLE 3-1 RADAR SPECIFICATION FOR GEOSTATIONARY SATELLITE

Parameter	Specification	Parameter	Specification	Parameter	Specification
Antenna Type	Space-Fed Phased Array	Signal-to-Noise Ratio, dB	14.6	Radar Transmitter Primary Power Input	53
Antenna Dia, Meters	300	Transmitter Signal Format		• During Pulse Burst (Max), Kw	6.96
Frequency, MHz	408 - 450	• Pulses per Burst	64	• Long-Term Average, Kw	
Wavelength, CM (Center)	72	• Stretched Pulse Length, μ sec	225	LSP Satellite Primary Power, Kw	20.3
Polarization	Circular	• Pulse Compression Ratio, Max	375		
F Number	2.5	• Interpulse Period, μ sec	1562.5		
Feed (Monopulse)	Phased-Array Fixed	• PRF	640	Solar Array Sca, 2 m	36
Number of Dipoles (Unthinned)	192,000	• Bursts Per Second (Max) (Variable Power)	2.33	Dia, ft	7,900
Dipole Spacing, Wavelengths	.75	Target Backscatter Cross-Section, M ²	1	Satellite Weight, lb	
No. of Active Modules	12,000	Length of Fence, n mi	5,233	Launch Vehicle	Trident III C/Centaur
Antenna Beamwidth		No. of Aircraft Tracks	50	Orbit	Equatorial, 24 hr
• Milliradians	2.88	Aircraft Speed, (Max), Mach	3	No. of Satellites per Launch	3
• Degrees	165	System RF Peak Power Output, Kw	144		
Beam Spot Dia at Earth, N mi	60	System RF Average Power Output, (Max), Kw	2,784	No. of Satellites	3
Range Resolution, ft	300	Module RF Peak Power Output, W	12	• Type I System	3
Receiver Bandwidth, MHz	167	Module RF Average Power Output		• Type II System	3
		• During Burst (Max), W	1.73	• Type III System	7
System Losses (Two-Way, Max), dB	5.33	• Long-Term Average, W	0.232		
Effective System Temperature, deg (Referred to Antenna Input, including only resistive losses)	470	DC to RF Efficiency for Transmitter, %	40		

Figures 3-1 and 3-2 are plots of the UHF clutter data for vertical and horizontal polarization, respectively.

In addition to clutter backscatter measurements, measurements of sea clutter spectra were also made during the four frequency radar system tests by NRL. A summary of some of the results is as follows:

- The spectrum width of radar sea-echo is frequency dependent, and decreases with increasing radar frequency
- The bandwidth is widest for horizontal polarization, narrowest for vertical polarization, and intermediate for the depolarized spectrum
- The bandwidths of the spectra for all polarizations increase with wave height
- The spectrum bandwidth for vertical polarization is almost independent of depression angles between 5° and 30°; that for horizontal polarization decreases toward the width of the vertical spectra with increasing grazing angle.

Figure 3-3 is a plot of the spectrum at the UHF frequency for sea state 3 and horizontal polarization taken from the NRL report. Minor variations have been smoothed. The half-power bandwidth of the spectrum is approximately doubled for sea state 7.

Extrapolation of the curve indicates that components of sea clutter exist that have frequencies as high as 20 knots that must be considered in the Doppler filter design for detection of aircraft with a RCS of 1 m^2 .

Land clutter reflectivity varies with terrain type and grazing angle. For example, for UHF at a grazing angle of 10°, the σ_0 is approximately -10 dB for cities, -22 dB for wooded hills, and -38 dB for a desert. The σ_0 for wooded hills varies from about -24 dB at 1° grazing angles to about -15 dB at 70°.

There are discrete scatterers, such as large buildings, that can be many times larger than the average numbers indicated above. Fortunately, the spectrum of these objects is usually very narrow and can be fairly easily filtered. The spectrum from vegetated terrain arises from the relative motion of the scatterers as they move about in the wind. The standard deviation of this spectrum seldom exceeds a few knots.

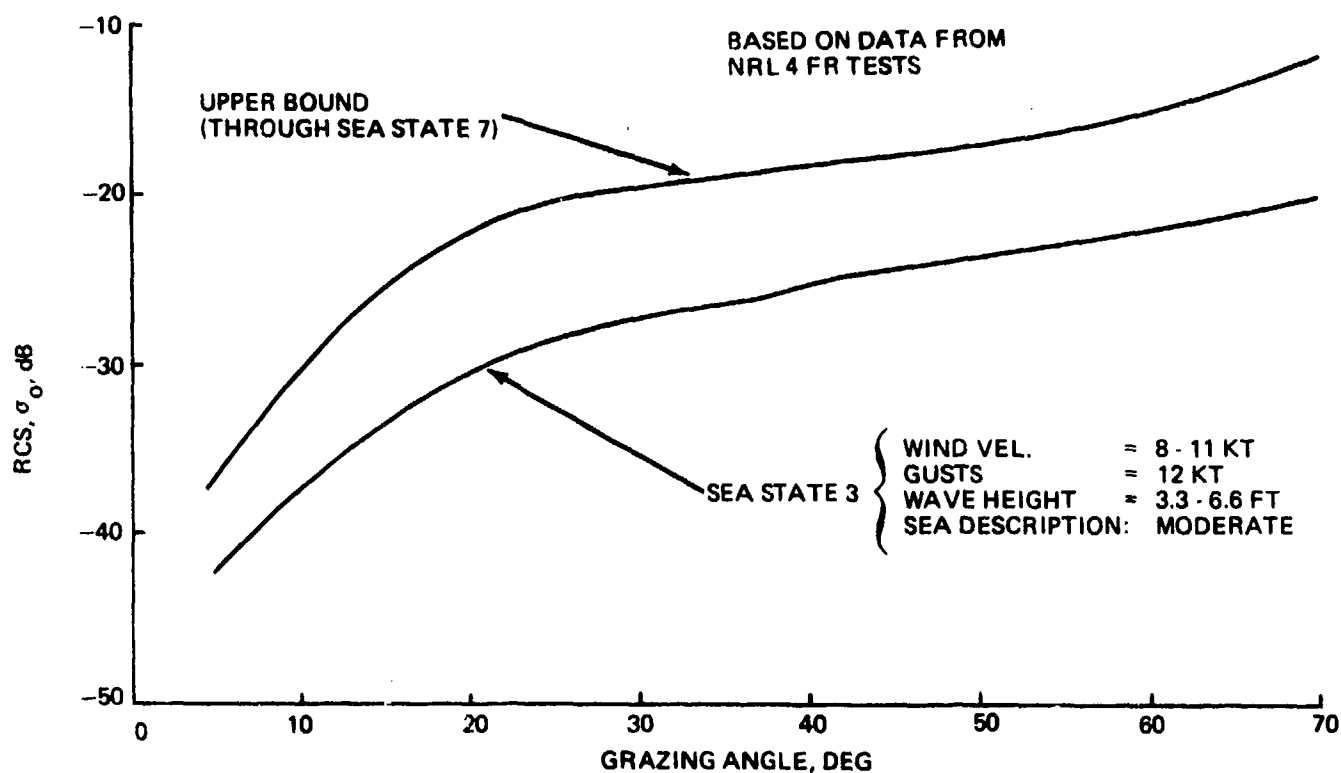


Fig. 3-1. Sea Clutter at UHF, Vertical Polarization

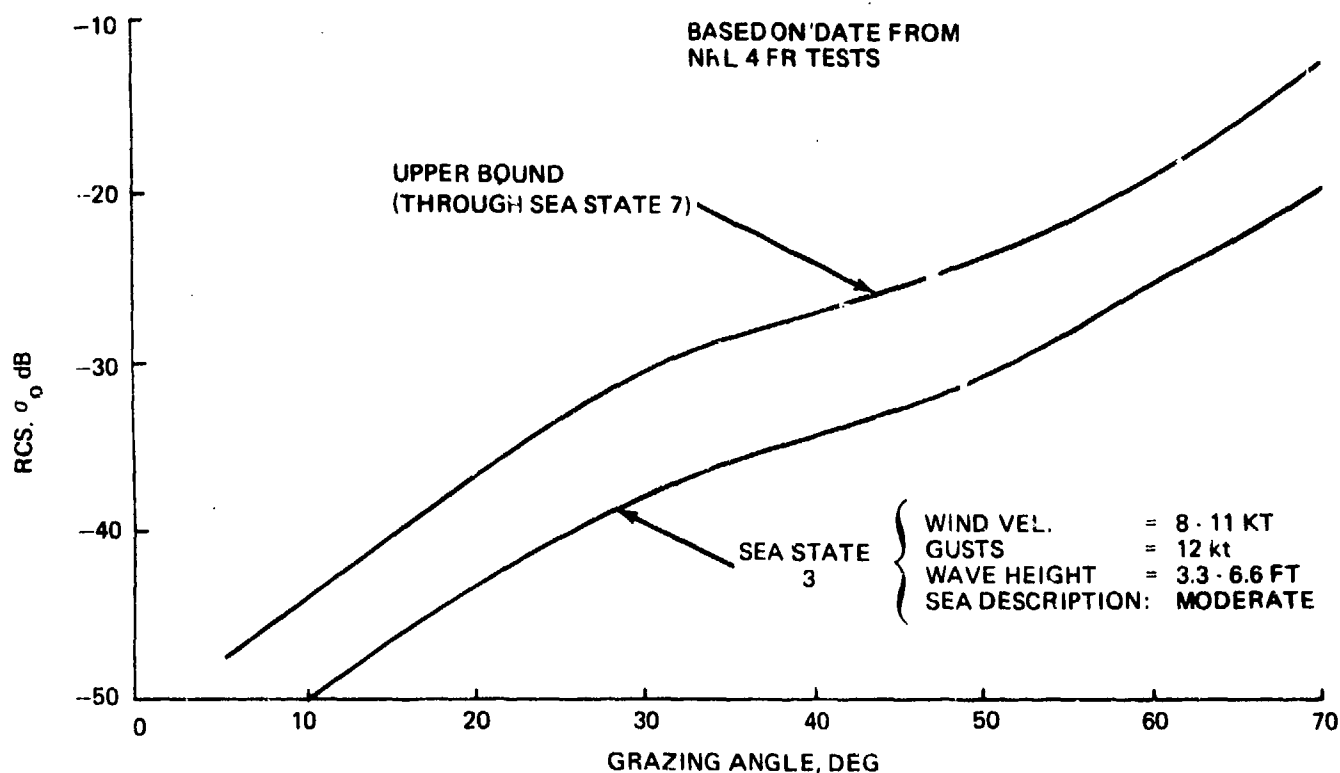


Fig. 3-2 Sea Clutter at UHF, Horizontal Polarization

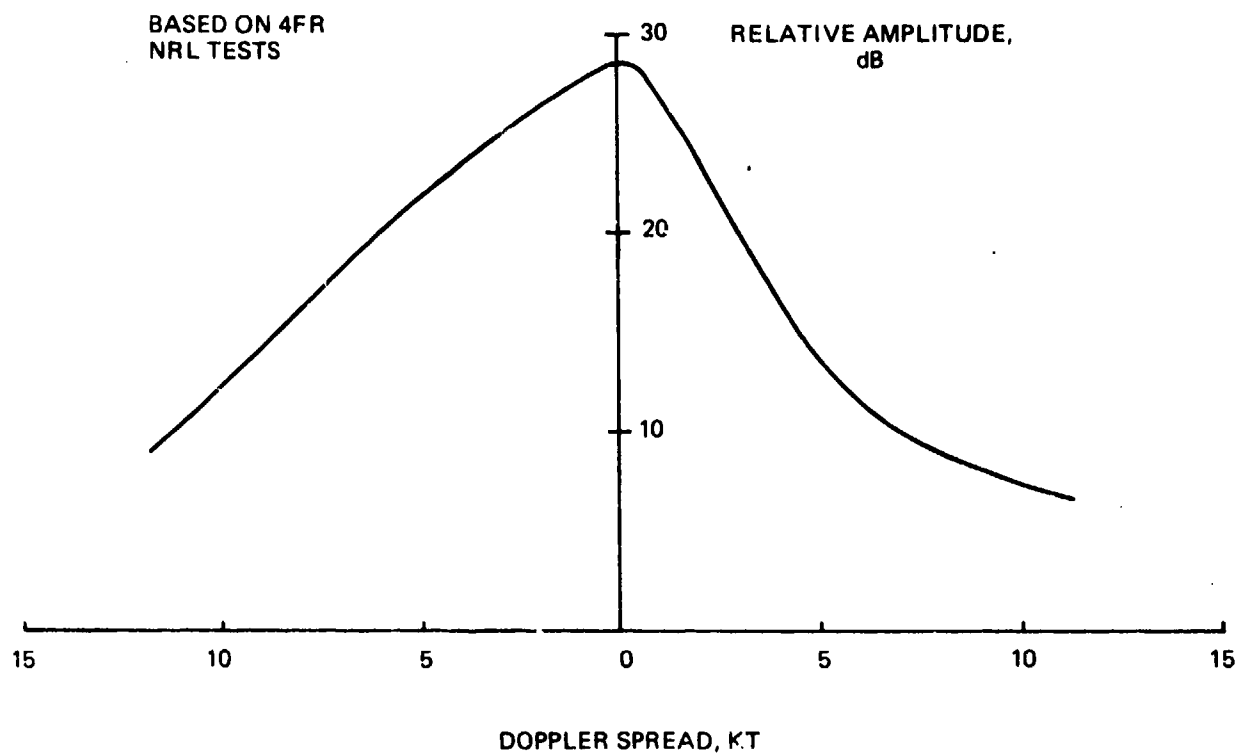


Fig. 3-3 Doppler Spectrum, UHF, Sea State 3, Horizontal Polarization

3.5 WEATHER AND IONOSPHERE

Attenuation due to weather of any kind at the UHF frequency is negligible. Rotation of the signal by the ionosphere at UHF is quite large. Circular polarization is used in the antenna with the direction of polarization changed from transmit to receive. The ionosphere decorrelation time is variable, but never less than 0.25 sec. Since the correlation time needed for the radar signal selected is only 0.1 sec, no problems are expected.

3.6 RADAR PARAMETERS

Consideration of the above factors led to the selection of a pulse-burst Doppler radar, with a 300-m diameter antenna, operating at a frequency of 417 MHz \pm 5%.

A range resolution of 300 ft is used, long enough to permit full integration of all the pulses for an aircraft travelling at Mach 3, requiring a system bandwidth of 1.67 MHz which is within the bandwidth of the large antenna.

The resolution element is therefore 300 by 360,000 ft (the beam-width of 60 miles on the ground), or 10^7 m^2 . Using a σ_0 of -20 dB for the clutter gives a clutter RCS of 10^5 m^2 , 50 dB above 1 m^2 . Detection of an aircraft with a RCS of 1 m^2 in this clutter with a signal-to-clutter ratio of 15 dB requires a clutter reduction of 65 dB. Clutter reduction is done with a bank of Doppler filters produced at the ground station from the pulse-burst signal.

The transmitter pulse-burst is 64 pulses, at a PRF of 640 Hz, a duration of 0.1 sec. The PRF determines the first blind speed, 452 kt. The burst duration determines the width of the Doppler filters, 7.07 kt.

In Section 2, Mission Analysis, we determined that the maximum look rate each satellite must provide for the fence and tracking is 2.33 looks per second. This consists of 1.844 looks per second for the fence and 0.486 looks per second for tracking.

To minimize the average transmitter power required for the mission, the power per look is adjusted for each target to compensate for the range to the target and antenna scan loss at the scan angle of the target. For system I, the satellite radar antenna is bore-sighted off vertical to 3.5° north, or roughly at Mexico City, to reduce scan angle losses. There is approximately a 3:1 variation in the power required over the extent of the fence.

The power is adjusted by varying the amount of transmitter pulse compression. For the maximum power look, the pulse compression ratio is 375, which expands the $0.6\text{-}\mu\text{sec}$ pulse (300 ft range resolution) to $225\text{-}\mu\text{sec}$. The shortest pulse length is $83.5\text{-}\mu\text{sec}$, with a compression ratio of 139. The average power required for the fence around the North American continent is 1710 w per satellite. The average power for tracking 50 aircraft is 693 w. The total maximum power output required from the satellite radar transmitter is 2403 w.

The satellite radar is designed for the largest workload, which is for System II (China and the USSR). The total maximum power output for this system is 2784 w.

The satellite operates as a radar repeater, with the transmitter pulse burst, pulse compression, and all signal processing done at the ground station. Section 4 describes the electrical design and operation of the radar satellite system.

3.7 RESOLUTION

The radar is capable of resolving one aircraft from all others by antenna directivity (beamwidth), range resolution, and velocity resolution:

- The radar beam cross-sectional diameter at the earth is 60 miles. The projected beam on the earth is elongated along the range axis to 1,000 miles at the 2° grazing angle. Targets are resolved if they do not appear simultaneously in the area covered by the beam
- The radar beam is divided into range increments, each 300-ft long in the range direction. Aircraft are resolved if they appear in different range increments
- After Doppler filtering, each range bin contains 64 velocity increments, each with 7.07-kt width. Aircraft are resolved if their radial speed components differ sufficiently to appear in separate velocity increments
- If, by chance, the aircraft are in the same range bins and have the same radial speed components, they may still be resolved by another radar covering the same area from a different angle.

3.8 ACCURACY

The radar's location accuracy is determined by two factors:

- The location accuracy within the beam is determined by the size of the range bins and by the beam-splitting capability of the azimuth monopulse system. The range accuracy is 300 ft. The azimuth accuracy depends on the signal-to-noise ratio and, for most cases, will be on the order of 1 n mi.
- The location accuracy with respect to earth coordinates depends on the accuracy to which the radar satellite location is known and that with which the radar beam can be pointed. Beacon calibration stations at known earth locations will be used to correct the data. The overall absolute (earth coordinates) location accuracy is expected to be within 5 n mi, and the relative accuracy (within 300 miles of a reference) will be about 2 n mi.

3.9 SATELLITE COVERAGE

In Section 2, Mission Analysis, the satellite coverage is shown on a Mercator map. It was pointed out that the radar beam is not scanned to grazing angles higher than 70° because of the large clutter σ_0 and the greatly diminished radial speeds at higher angles. This leaves a hole directly under the satellite which must be covered by adjacent satellites. It was also shown that each area must have at least double coverage to circumvent the blind spots of any single radar.

To illustrate how the hole is covered and the double coverage obtained, three sketches of the coverage geometry are shown. Figure 3-4 shows the geometry of the coverage of a single satellite arranged to produce coverage bands of width equal to the diameter of the hole. Figure 3-5 shows the coverage of three satellites, giving double coverage of the hole. Figure 3-6 shows double coverage of the equator as provided by the seven satellites.

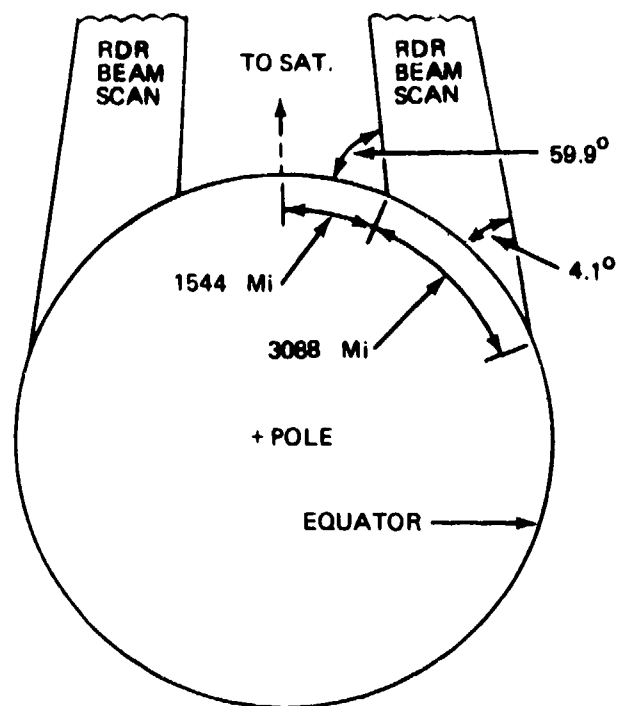


Fig. 3-4 Geometry of Geostationary Radar Satellite Coverage

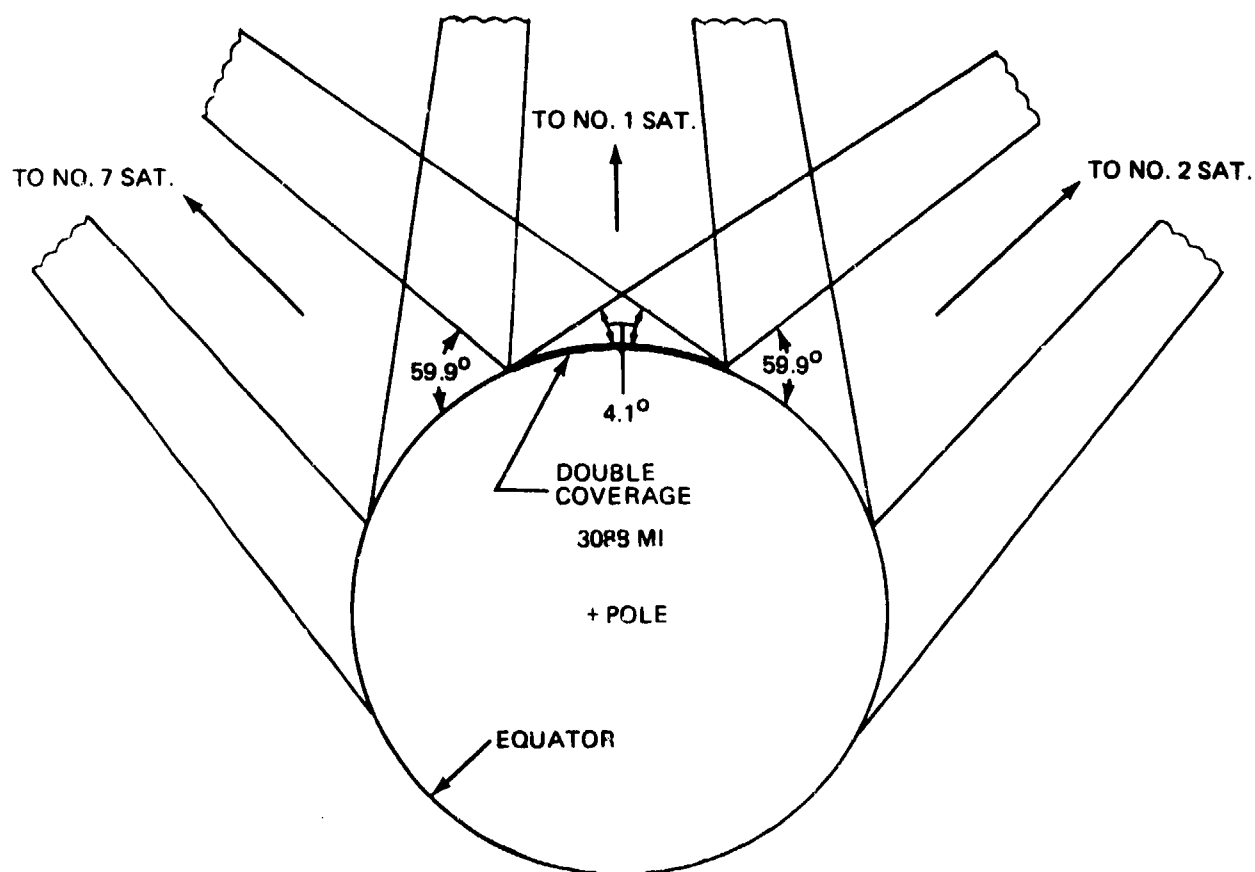


Fig. 3-5 Principle of Double Coverage

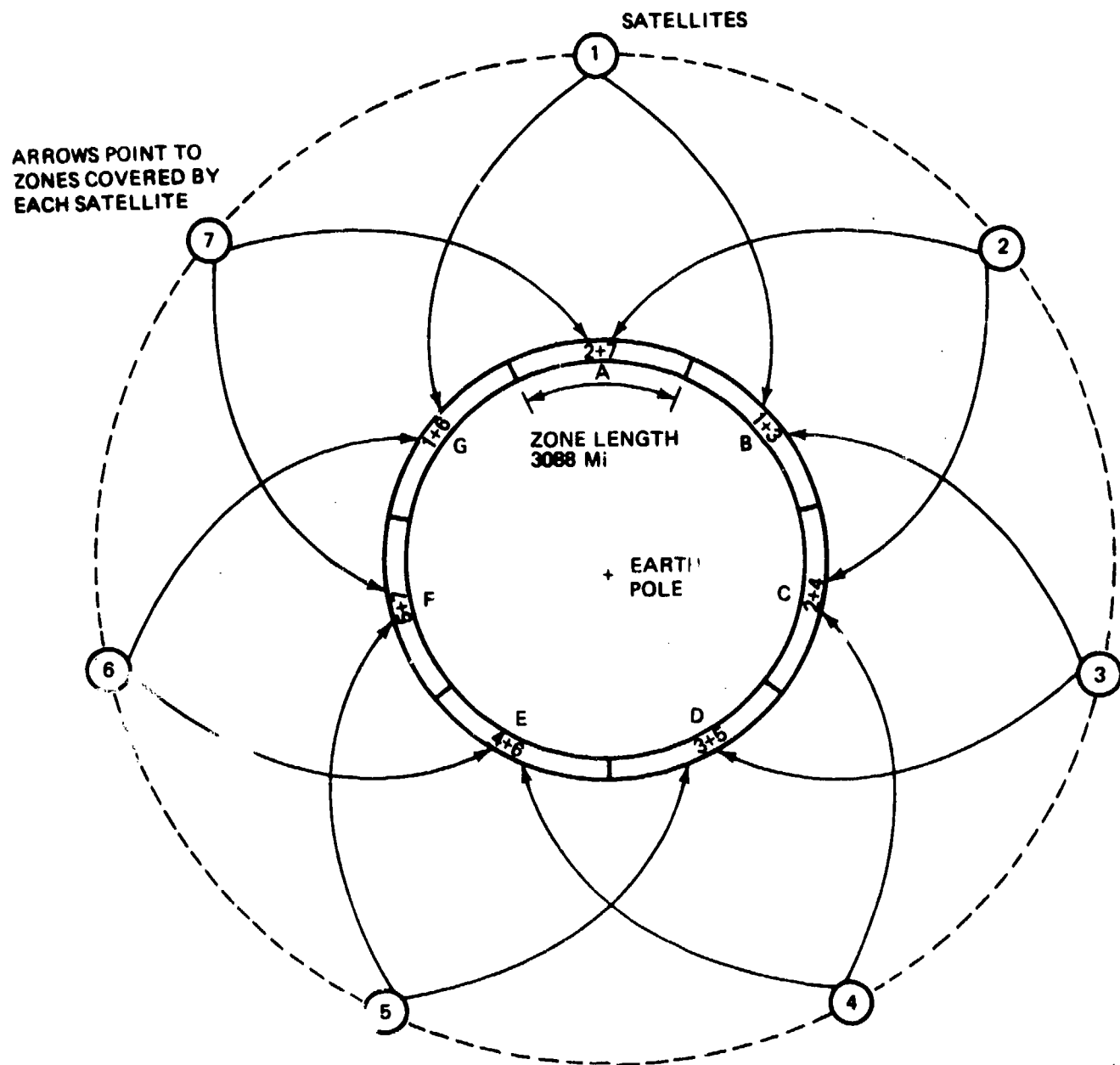


Fig. 3-6 Double Coverage Along the Equator

Section 4

SYSTEM ELECTRICAL DESIGN

4.1 SATELLITE

The design of a repeater satellite for radar use requires transmission and reception of signals from a ground station, as well as transmission and reception of radar signals to and from the target. For the proposed system, the signals to and from the target are generated at $417 \text{ MHz} \pm 5\%$ and directed by the radar antenna (300-m dia). The signals to the ground station are also at UHF but at a frequency sufficiently different that the radar echoes received by the radar antenna can be simultaneously repeated to the ground station by the communication antenna without interfering with the radar receiver. The communication antenna, 28 m in diameter, is located in the center of the radar antenna.

In normal operation, the signal from the ground station to the satellite consists of beam pointing commands and the transmitter pulse-burst. A delay equal to the maximum pulse length ($225 \mu\text{sec}$) is inserted in the repeater loop to prevent interference between the high-power pulse-burst transmission by the radar antenna and pulse reception by the communications beam receiver. This delay permits reception of the complete pulse before transmission begins. The delay is not in the loop for repeating the radar echo signal to the ground station.

The electrical design involves three positions on the satellite. The subarrays and RF modules for both the radar array and communications array are located in the main antenna structure and supported within the compression rim. The DC battery and power distribution system for the RF modules are in the LSP; the solar arrays which are the primary source are located nearby. The antenna feed array, monopulse circuitry, feed amplifiers, and radar receivers are located in the upper systems package (USP), with the smaller solar array and battery source. The main antenna is space-fed; the communication antenna uses a corporate feed network between the antenna modules and the amplifiers in the LSP.

4.1.1 Satellite Electronics (USP and LSP)

Figure 4-1 is a block diagram of the satellite on-board electronic system showing the major system elements, the signal flows via hard lines and space, and the different antenna types. Note that there are no hard lines for signal flow between the USP and LSP. The phase shifters and switches in the main array module are controlled by coded RF signals received from the main array feed located at the USP.

Control of the communication array modules and transfer of radar signals, instrumentation data, and commands between the USP and LSP is accomplished by the intra satellite communication system. This system consists of a receiver, transmitter, and dipole antenna located at each end; it operates at the communication beam frequency.

During normal operation, communications with the satellite are via the communication beam which is pointed at all times at the ground station. An omni-antenna system is provided for satellite control and instrumentation data readout during deployment and in case contact is temporarily lost through the communication beam after deployment. An omni-system is required on both the USP and the LSP to ensure communications contact regardless of the satellite's attitude. In normal operation, the upper omni-antenna is blocked by the radar antenna.

4.1.2 System Operation

Basic system operation of the satellite electronics will be explained below by describing the signal flow and equipment functions for the three principal operations: control of the beam direction, transmission of the radar pulse-burst, and the reception of the radar echo signal.

4.1.2.1 Control of Beam Direction

Crypto-encoded beam direction pulses and the synchronizing code are received by the communication beam receiver in the LSP. The signals are amplified and transmitted via the intra satellite communications system to the USP. After crypto decoding, the pulses are sent to the frequency translator where two RF signals are generated: one at the radar frequency and the other at the communication frequency. The radar beam signal is delayed by 225 μ sec, amplified by the radar array transmitter and sent to the sum channel of the

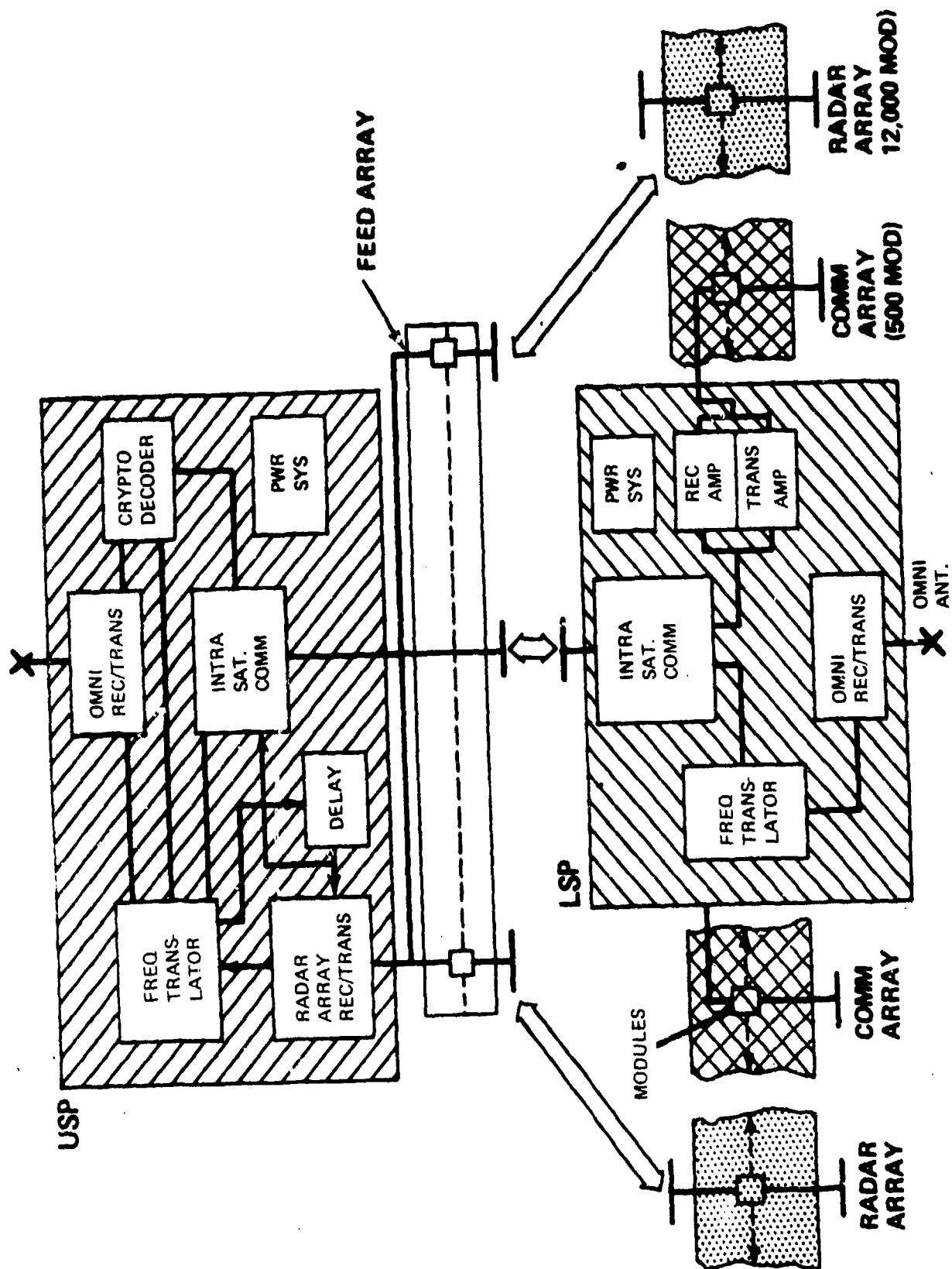


Fig. 4-1 Satellite Onboard Radar System

radar array feed. The signal is picked up by the feed side dipoles of the radar array and fed to the modules. Simultaneously, the communication beam signal is delayed and sent, via the intra satellite communication system, through the transmitter amplifier and the corporate feed to the communications array modules. The modules in both arrays detect the signals and use the code for setting the phase shifters that control the beam direction.

4.1.2.2 Transmission of Radar Pulse Burst

Immediately following the beam direction pulses are the 64 chirp pulses for transmission by the radar array. These follow the same path as the beam direction pulses up to the frequency translator. The frequency is translated to the radar frequency, delayed by 225 μ sec, amplified by the transmitter amplifier, and space-fed via the feed array to the radar array. The pulses are amplified by the power amplifiers in the modules and transmitted towards the target. The radar beam remains pointed at the target during transmission of all 64 pulses. Two pulse bursts may be transmitted at two different targets before the radar echo returns from the first burst.

4.1.2.3 Reception of Radar Echo Signal

The radar echo signal is received by the radar array, amplified by the receiver pre-amplifiers in the modules, and space-fed to the radar array feed in the USP.

The corporate feed output consists of a sum channel and two difference channels that provide monopulse information for splitting the beam to obtain precise location of the target in azimuth. The three outputs, each with a bandwidth of 1.67 MHz, are separated into three RF channels by a frequency shift of two of them, resulting in a frequency multiplexed signal with a 6-MHz bandwidth. After amplification, the multiplexed signal frequency is translated to the communication beam frequency and sent via the intra satellite communication system to the communication array by which it is transmitted to the ground station. The radar echo signal is retransmitted by the communication array at the same time it is received by the radar array. The 225- μ sec delay is bypassed. The communications array power output is approximately 22 watts peak, and care must be used in selecting the frequency and designing the filters to prevent interference.

4.1.3 Omni and Instrumentation

The omni units in the USP and LSP are identical and consist of a transmitter, receiver, and associated omni antenna. The standard satellite control frequency of 2.2 GHz is used for the uplink, and 1.8 GHz for the downlink. The data rate capacity is 51.2 kilobits/sec.

To route the control signals coming in on one of the omni receivers in either the USP or LSP to the opposite systems package, the omni frequency is translated to the communications frequency and transmitted via the intra satellite communications system.

Instrumentation data are continually being acquired and stored. All data are in digital form, obtained either directly from the instruments or by using signal conditioners. Before transmission to the ground station, the data are crypto-encoded.

Instrumentation data are transmitted to the ground station following each radar transmission. Data can also be sent via the omni transmitter on command from the ground station.

4.1.4 Satellite Control

The satellite attitude sensors consist of a sun sensor and a horizon sensor. On initial deployment, sun sensor and horizon sensor data are sent to the ground station via the omni communication system. The ground station, using these data, will direct the satellite to fire the appropriate thrusters until the satellite attitude comes within the sensors' accuracy limits, about one degree.

The ground station will then direct the satellite to point the communications beam at the ground station. A step-by-step search may be necessary to obtain a beam lock-on. For precise satellite attitude control, the main radar beam will be directed to point at calibration stations on the ground and, if the error exceeds prescribed limits, the satellite will be directed to fire the appropriate thrusters to correct the attitude. For attitude errors within the limits, the radar data will be corrected before transmission to the users.

4.1.5 Beam Control Logic

The overall sequence of transmission and reception of signals between ground station and radar satellite is shown in Figure 4-2. Operation begins with the transmission of a pair of pulses (sync 1) that synchronize the RF module timing circuit. (See Fig. 4-3.) A 4-MHz parallel comparator senses the presence, spacing, and pulsewidth of this signal before using it to start the pulse burst cycle in the satellite. Synchronization starts a 1-MHz timing clock in each module. A 12-bit frame code is used to identify the proper ground station and a bonafide transmission, thus reducing the possibility of accidental or intentional enemy destruction of previously stored information. Control data are next transmitted as a 12-bit pulse-code-modulated signal for each of the following:

- Target 1 radar beam position in azimuth
- Target 1 radar beam position in elevation
- Target 2 radar beam position in azimuth
- Target 2 radar beam position in elevation
- Frequency ratio
- Interpulse period
- Ground station communication beam position in azimuth
- Ground station communication beam position in elevation.

These data (called "command control" data) are transmitted within one PRF interval and are used to compute the individual RF module phase-shifter commands for radar and communication beam steering.

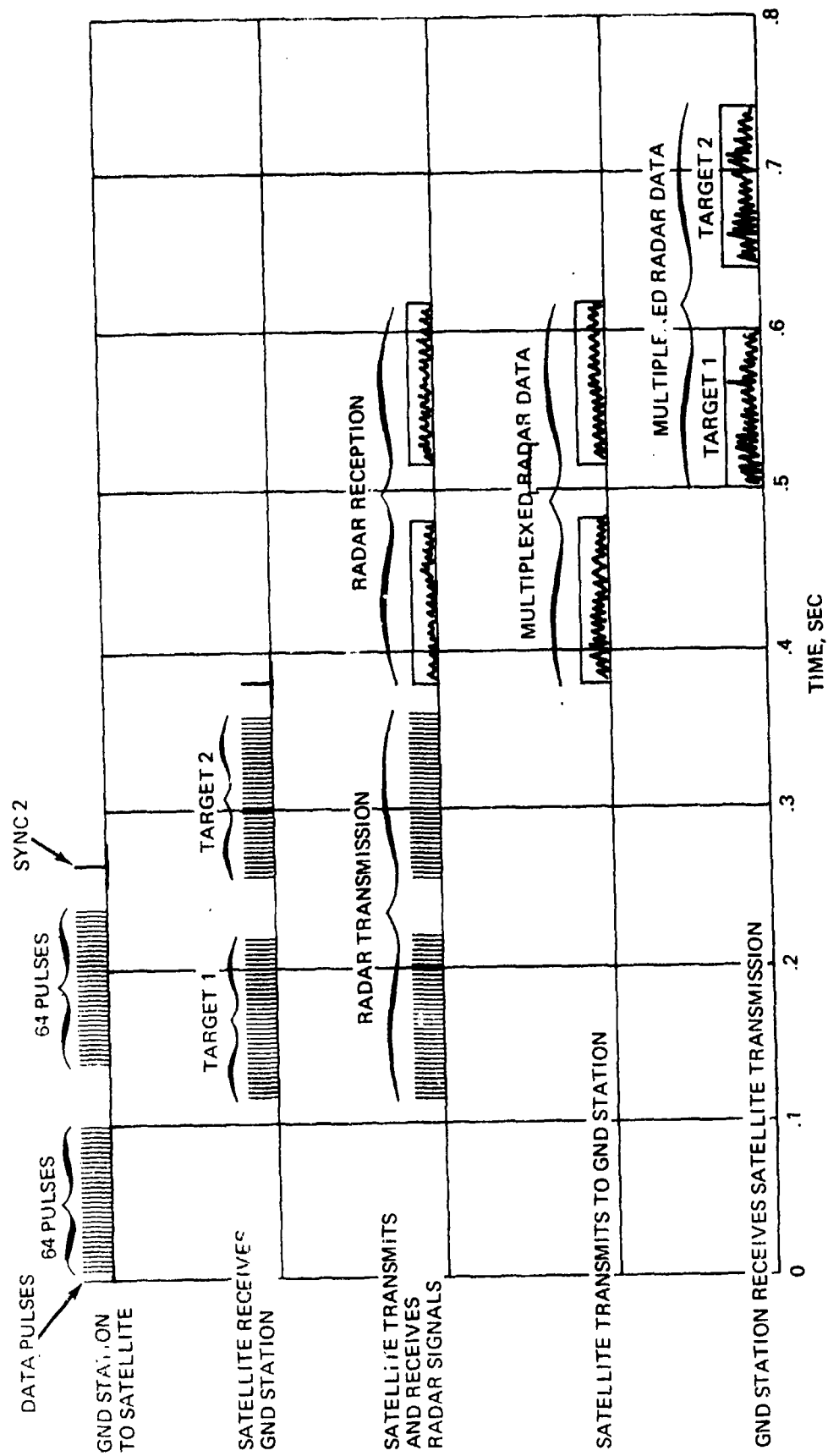
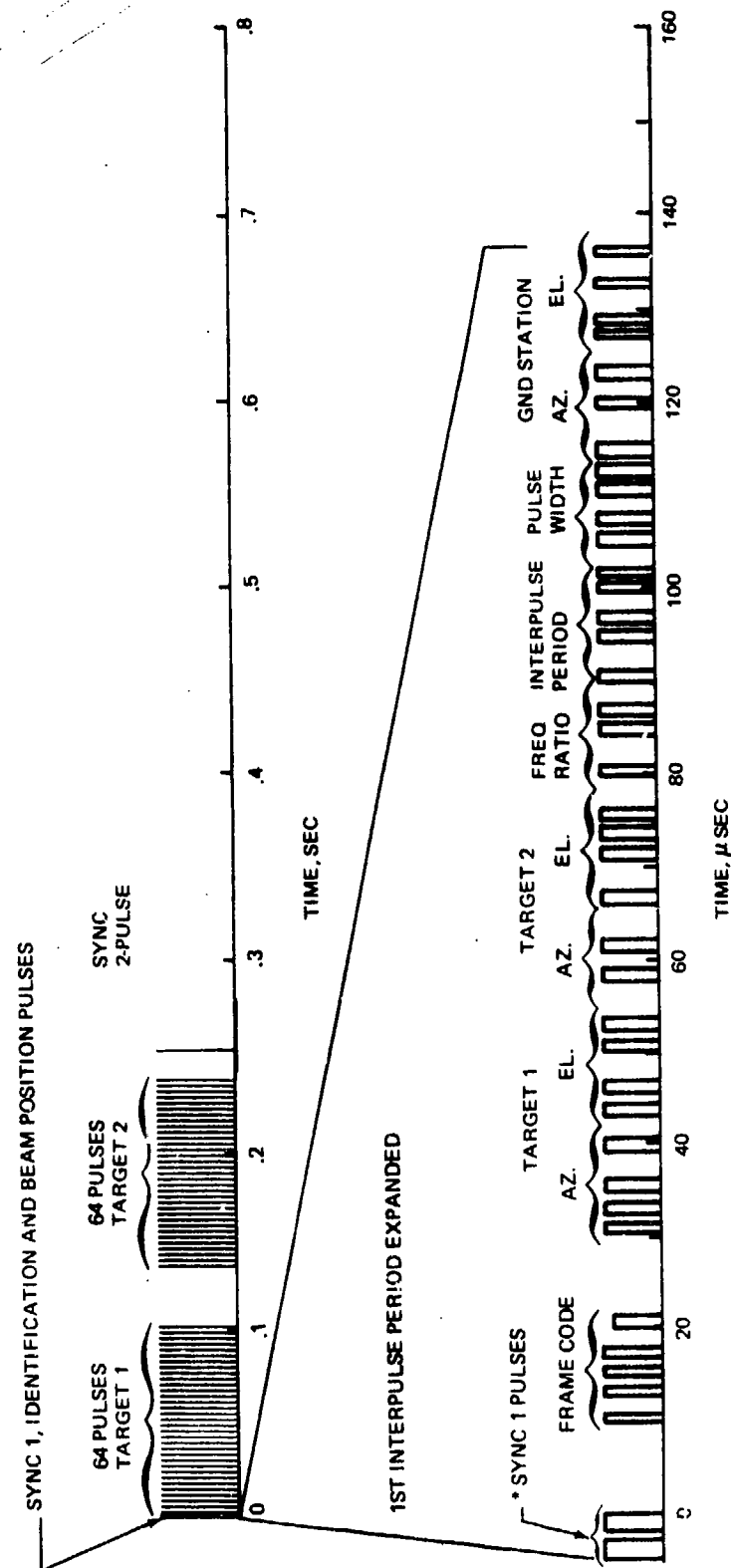


Fig 4-2 Overall Time-Signal Diagram



* PULSE TRAINS SHOWN
ARE SYMBOLIC

Fig 4-3 Pulse Format Received at Satellite from Ground Station

The information needed to steer the radar and communication beams is transmitted to the satellite via the communications link during the first interpulse period following the synchronizing pulses. The signal is routed to the USP where it is crypto-decoded, frequency offset to the radar frequency, and retransmitted toward the radar antenna array. The digital logic in each T/R module selects the appropriate data train to determine the phase shifter settings for both the radar-link and ground-link modules. The radar array modules will store phase-shift data for two targets in two separate memories; the communication array modules will store the phase-shift data for the ground station in its memory.

One interpulse period after the sync 1 pulse, the first 225- μ sec radar pulse is received at the satellite and stored in a 225- μ sec delay line in the USP.

4.1.6 Radar Antenna Array Electrical Design

The electrical design of the radar antenna array can be subdivided into the following tasks:

- Design of an RF transmit/receive module
- Design of subarrays for both sides of the array antenna, including transmission lines and corporate feed networks to interconnect the radiating elements with each module.

4.1.6.1 RF Transmit/Receive Module Design

Figure 4-4 shows the RF module, connected to radiating subarrays, in simplified form. The major circuit subdivisions are:

- RF circuits
- Digital circuits
- Power supply components.

Figure 4-5 shows the space allocation for the major subunits of the RF module.

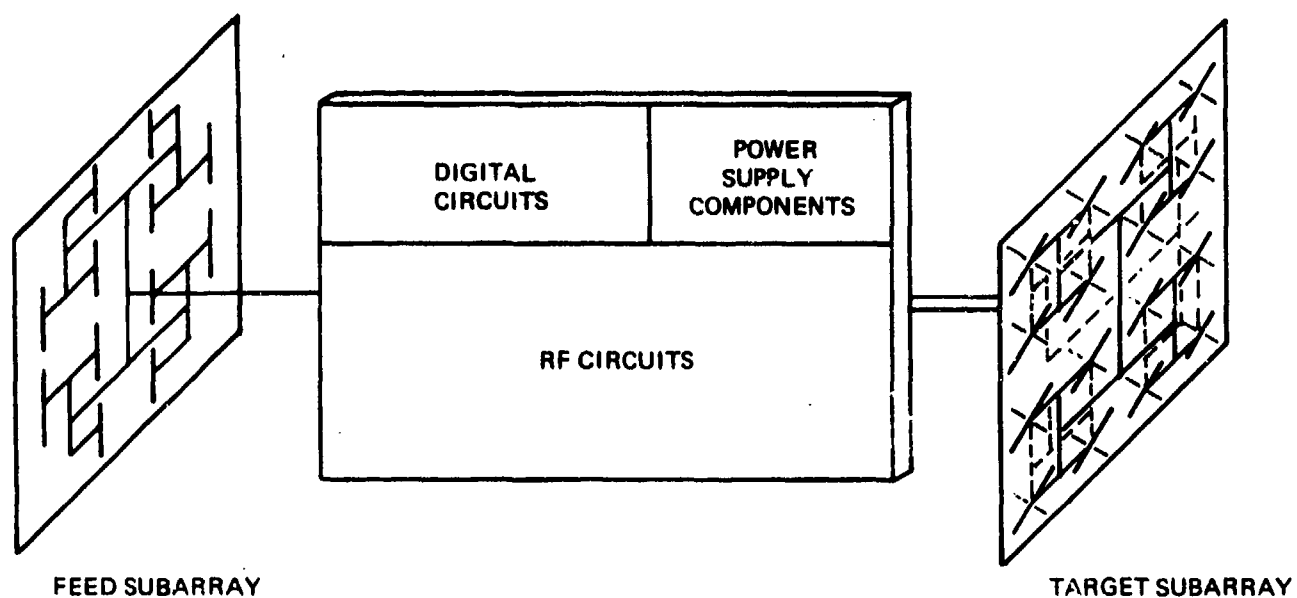


Fig. 4-4 RF Module and Subarrays, Simplified Block Diagram

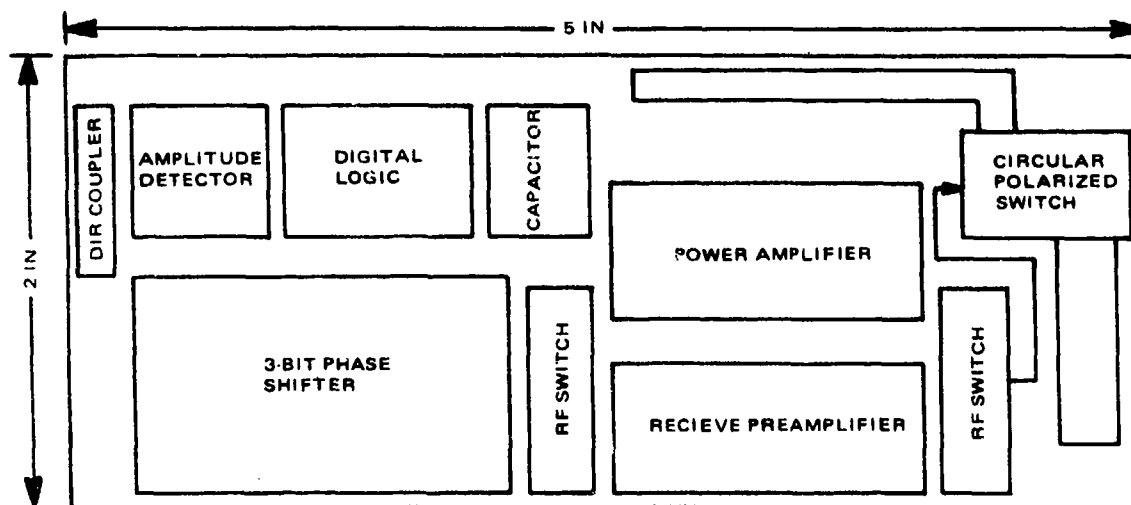


Fig. 4-5 RF Module, Space Allocation

RCA was invited to submit an informal proposal for realizing the goals for the T/R module. Their letter response is enclosed as Appendix B.

Digital logic may be provided by the Hughes Aircraft in accordance with their letter, Appendix C.

The 22- μ fd power supply capacitor will be provided by Union Carbide as a tantalum chip. This is the T-370 "Micron" tantalum chip capacitor designed for 35 vdcw.

4.1.6.2 RF Power Amplifier

The RF power amplifier is a 3-stage, 4-transistor, class C amplifier built on a 10-mil Al_2O_3 substrate. It is designed for +28-volt operation and has the following parameters:

- Gain: 23 dB, +6 to -1 dB
- Nominal Output Power: 12w peak
- Frequency: $417 \pm 5\%$ MHz
- Pulsewidths: 83.5 to 225 μ sec
- Input and Output Impedance: 75 ohms nominal
- Current Drain: < 0.25 ma with +30 vdc on amplifier and no input signal
- Duty Factor: 14.4% during pulse burst, 3.36% overall
- Weight: 3 grams max
- Heat Sink Temperature: 0 to 50°C
- Efficiency: 50% min.

4.1.6.3 Digital Logic

Figure 4-6 shows the connection between the digital logic circuits and the other parts of the module.

The primary purpose of the digital logic is:

- Synchronization and timing of all module functions
- Computation of module target 1 and target 2 phase-shifter commands
- Control of all module switching.

The following information defines the computation of phase-shifter commands. Figure 4-7 shows the reference coordinate system defined for the main array antenna.

To provide unipolar signals for beam steering, the reference position at -8.6° is defined as $n = 0$. All beam steering commands and computed phase shifts are therefore with respect to -8.6° and the phase shifts associated with -8.6° beam steering. The phase differential across the diameter of the antenna required to steer the beam 17.2° from reference zero (to $+8.6^\circ$) is nominally 44,800 degrees at $f_o = 417$ MHz. As shown in Fig. 4-7, the phase of any module phase shifter in azimuth or elevation can be written as:

$$\phi_n = \frac{n_x}{8.65} \cdot 9362 \left(\frac{f_i}{f_o} \right) \sin \frac{m_x}{162.8} - 8.6^\circ + 1400 = \frac{n_x N_{px}}{8.65} \text{ (degrees)}$$

where

$$N_{px} = 9362 \left(\frac{f_i}{f_o} \right) \sin \frac{m_x}{162.8} - 8.6^\circ + 1400$$

and

N_{px} = pulse code number sent from ground station to satellite for "x" coordinate beam steering (integer value only)

n_x = module index number in "x" coordinate direction

f_o = nominal center frequency, 417 MHz

f_i = operating frequency for next pulse burst transmission

m_x = beam position index number in "x" direction

ϕ_x = total phase shift for "x" direction for all modules with index number " n_x " (prior to modulo 2π extraction).

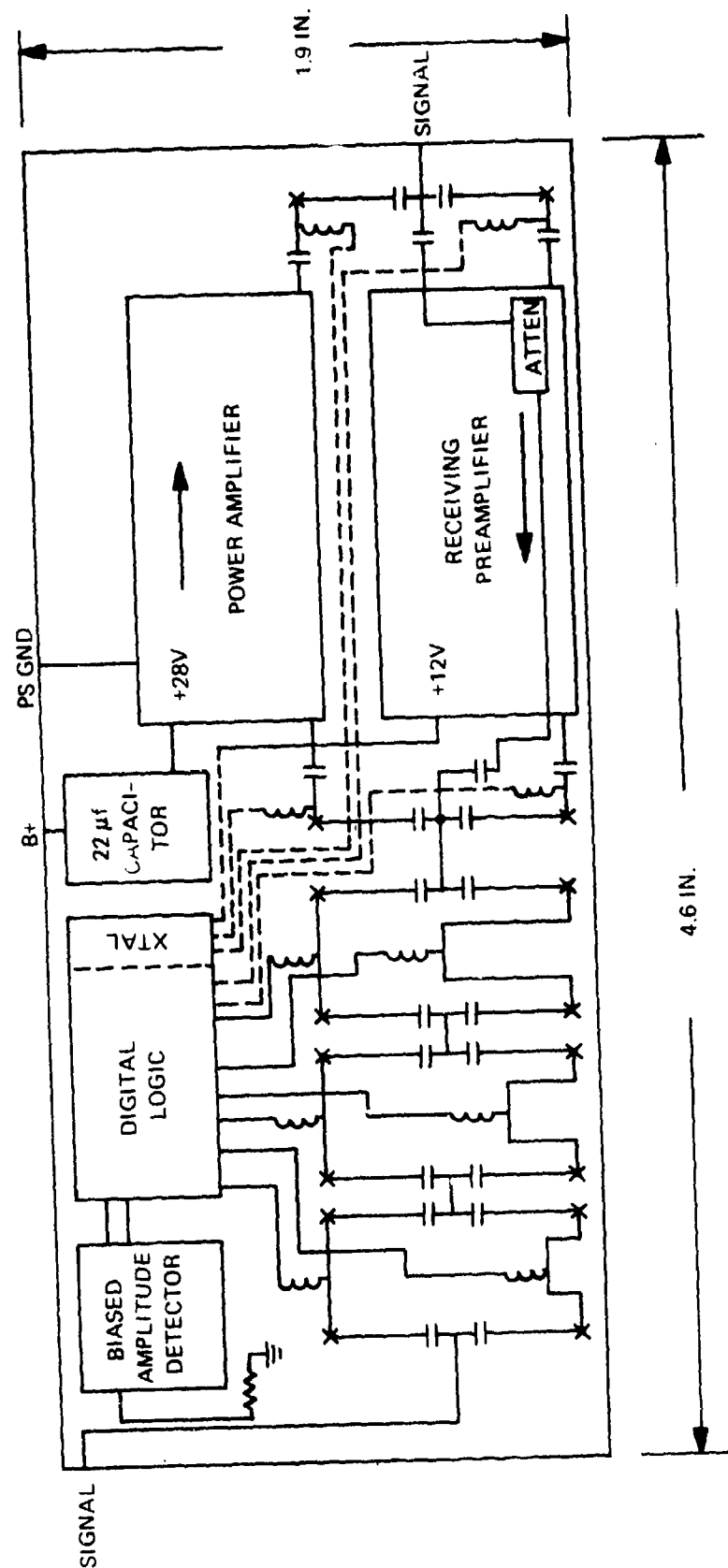
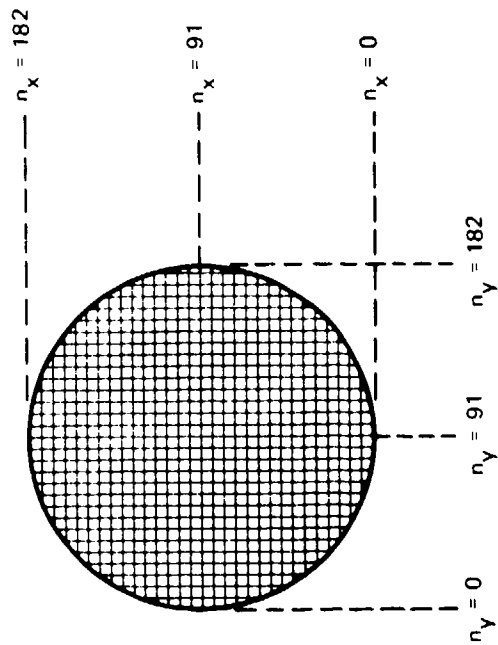


Fig. 4-6 RF Module

THIS PAGE HAS INTENTIONALLY BEEN LEFT BLANK



$$d/\lambda = 0.75$$

$$\lambda = 2.36 \text{ ft}$$

$$S = X \sin (\theta - 8.6^\circ)$$

$$\text{Total phase differential across diameter } \phi_x = 2 \left[\frac{2\pi S}{\lambda} \right]$$

$$\text{Sub-Array spacing} = 4d \text{ where } d = \text{dipole spacing}$$

$$(4d) (n_{x_{\max}} + 1) = D$$

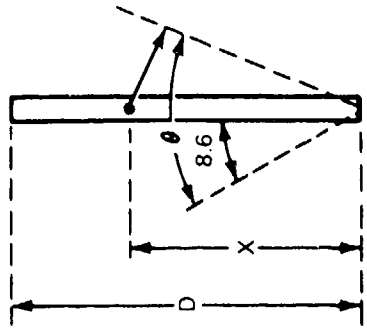
$$n_{x_{\max}} = \frac{D}{4d} - 1 = \frac{D/\lambda}{4d/\lambda} - 1 = \frac{585}{4(.8)} - 1 = 138$$

$$\text{also } n_{y_{\max}} = 138$$

$$\text{at any frequency "f"}$$

$$\phi_{x1} = \frac{4\pi S}{\lambda_1} = \frac{4\pi S}{\lambda_0} \left(\frac{\lambda_0}{\lambda_1} \right) = \frac{4\pi S}{\lambda_0} \left(\frac{f_1}{f_0} \right)$$

$$\text{but } X = 4d n_x = 4 \left(\frac{d}{\lambda} \right) \lambda \quad n_x = 7.08 n_x \text{ ft}$$



$$\phi_{x1} = \frac{4\pi S}{\lambda_1} = \frac{4\pi S}{\lambda_0} \left(\frac{\lambda_0}{\lambda_1} \right) = \frac{4\pi S}{\lambda_0} \left(\frac{1}{f_o} \right)$$

but $X = 4d n_x = 4 \left(\frac{d}{\lambda} \right) \lambda \quad n_x = 7.08 n_x \text{ ft}$

$$\phi_x = \frac{4\pi (7.08 n_x)}{\lambda} \left(\frac{f_1}{f_o} \right) \sin \left(\theta_x - 8.6^\circ \right) \text{ rads}$$

$$\phi_x = 2160 n_x \left(\frac{f_1}{f_o} \right) \sin \left(\theta - 8.6^\circ \right) \text{ degrees}$$

If ϕ is the angle to the target in the "X" coordinate direction and the range of ϕ_x is from 0° to 17.2° which is divided into 2800 intervals with index numbers "m" then

$$m_x = (\phi / 17.2^\circ) 2800 = 163 \phi_x$$

$$\phi_x = \frac{m_x}{163}$$

If ϕ_x is biased to always be a positive quantity then

$$\phi_{x1} = \frac{n_x}{8.669} \left[\underbrace{9362 \left(\frac{f_1}{f_o} \right) \sin \left(\frac{m_x}{163} - 8.6^\circ \right) + 1400}_{N_{px1}} \right]$$

The term in the brackets is defined at N_{px1} which is the number of pulses transmitted to the satellite for setting the beam in the "X" direction to a beam position whose "X" index is "m". The term outside the bracket is the module index number and a constant. The module performs the arithmetic of $\phi_{x1} = (n_x / 8.669) N_{px1}$

At 417 MHz

- $\leq m_x \leq 2800$
- $\leq n_x \leq 138$
- $\leq N_{px} \leq 2800 \text{ pulses}$
- $\leq \phi_{x1} \leq 44, 860 \text{ degree}$

Fig. 4-7 Beam Steering Calculation

At 438 MHz, the bounds for the various parameters are:

$$0 \leq n_x \leq 138$$

$$0 \leq m_x \leq 2800$$

$$0 \leq N_{p_x} \leq 2941 \text{ pulses}$$

$$0 \leq \theta_x \leq 47,103 \text{ deg}$$

The accuracy required for the phase information at each module prior to extracting modulo 2π is 22.5° out of 44,860 degrees or one part in 2000. All computations, including the correction of quadratic phase errors, must be made to at least this accuracy. Although the frequency compensation for beam steering does not require sending the operating frequency data to the satellite explicitly, the quadratic phase error correction will require explicit transmission of the operating frequency to the satellite. The quadratic phase error correction is:

$$\Delta \phi = 1.783 \times 10^5 \left[\sqrt{1 + 8.932 \times 10^{-6} \left(n_x'^2 + n_y'^2 \right)} - 1 \right] \frac{f_i}{f_o} \text{ (deg)}$$

where

$$n_x' = n_x - 69$$

$$n_y' = n_y - 69$$

$$n_x = \text{module index in "x" direction}$$

$$n_y = \text{module index number in "y" direction}$$

For subarrays assembled on a $\rho - \Theta$ coordinate system

$$n_x' = \rho_k \cos \Theta_{k'}, \quad n_y' = \rho_k \sin \Theta_{k'}$$

$$\rho_k = \text{radius to kth ring}$$

$$\Theta_{k'} = \text{angle from reference of the k'th module in kth ring}$$

The frequency ratio f_1/f_o is sent as a binary-coded digital signal as part of the command data signal. The compensation is performed at each module with an accuracy exceeding 22.5° . The quadratic phase correction must be combined with the beam steering phase

angle data prior to performing the extraction of modulo 2π . The total phase angle for a single module can be expressed as:

$$\phi_{n_x n_y} = \frac{n_x N_{px}}{8.65} + \frac{n_y N_{py}}{8.65} + \Delta\phi$$

where the terms have their previous definitions. The digital logic performs the function of calculating $\phi_{n_x m_y}$ for its particular module. For example, if the module is in the 5th row in the array then $n_x = 5$. If it is in the 14th column, then $n_y = 14$.

$$\phi = 1.344 \times 10^5 \left(\sqrt{1 + 8.932 \times 10^{-6} \left[(n_x - 69)^2 + (n_y - 69)^2 \right]} - 1 \right) \frac{f_1}{f_0}$$

For $n_x = 5$ and $n_y = 14$, the function within the brackets is a constant and

$$\phi = \text{constant} \times \frac{f_1}{f_0}$$

N_{px} and N_{py} are the pulse-coded beam position information transmitted to the satellite from the ground station.

The target side subarrays are circular polarized and, from gore-to-gore, the dipoles rotate by the gore angle. A phase correction for this rotation (constant for a whole gore) will be provided by changing the electrical length of the drop-line from the subarrays to the RF modules.

Digital logic of comparable complexity was estimated to require two 140 x 140 mil chips using CMOS logic.

4.1.6.4 Receiver Preamplifier

- Frequency: 417 ±5% MHz
- Noise Figure: 2 dB
- Gain: 23 dB nominal
- Dynamic Range: 36 dB
- Plan Area: 1 inch²

We plan to utilize lumped-element phase shifters, duplexes switches, and amplifier input-output matching networks similar to those described in an article entitled "Status of

Lumped Elements in Microwave Integrated Circuits - Present and Future" by Caulton, Hershenov, Knight, and DeBrecht of RCA Laboratories, IEEE Transactions on Microwave Theory and Techniques - Vol. MTT-19, No. 7, July 1971.

4.1.7 Design of Subarrays of Main Radar Phased Array

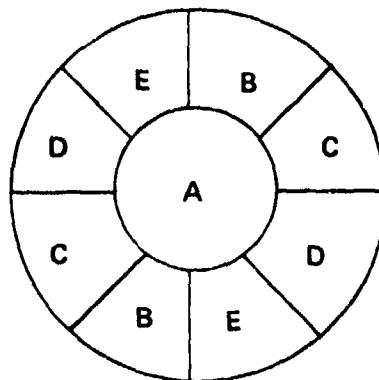
The transmitted signal will be right-hand circularly polarized and echoes will be received through a left-hand circularly polarized antenna. Circular polarization is used to minimize loss due to ionospheric polarization rotation.

With an element spacing of 0.75λ and uniform amplitude distribution across the 16 element (4 x 4) subarray, the subarray loss is approximately 1.44 dB at a scan angle of 6.1° . The circularly polarized elements on the target side of the main array can be structurally oriented on each gore. Subarray rotation resulting from this construction causes a phase shift between gores which is compensated for by adjusting the electrical line length between the subarrays and the modules.

The design of the circularly polarized subarray is based on a successful C-P array design which Grumman used on another program. Sixteen folded dipoles and a corporate feed network are printed on each side of a 1/2-mil flexible dielectric substrate. The dipoles on the two sides are orthogonal to each other, as are the corporate feed networks. There are four lines which fall on top of each other on the two sides of the corporate feed network. Each network along these lines will be displaced laterally in opposite directions to eliminate coupling between them. The corporate feed networks are three-wire printed circuit lines representing a degenerate coaxial line configuration. Folded dipole impedances of 600 ohms are utilized with matched transmission lines. Two quarter-wave transformers provide a net resultant drop-line impedance of 75 ohms to the RF module. Two three-wire printed circuit drop lines connect the subarray to the RF module. The RF module includes a lumped element quadrature hybrid which is connected to the high power duplexing switches to provide an equal power split and 90° phase shift between the two subarray feeder transmission lines. The polarization is changed from RCP to LCP by the duplexer diode switches controlled by the digital logic chips.

The subarray for the feed side of the main array is linearly polarized. The array consists of 12 dipoles (4 x 4 array with the corner elements eliminated). The element spacing is 0.75λ . The arrays are mounted in a circular frame which can be rotated to the

proper angle in each gore. The basic subarray must be squinted to point at the feed. This is accomplished by providing five different phase tapers for subarrays in different locations. The squint angle required at the edge of the antenna is 11.3° . The loss due to the subarray pattern at 11.3° is 2.68 dB. The antenna is subdivided as shown below:



Central sector "A" has subarrays without squint. The other sectors have squinted subarrays in the repeating pattern shown. The subarray loss will be between 0.3 dB and 1 dB, depending on the squint angle of the phase-shift sections.

The feed is a corporate-fed array designed to provide main array amplitude illumination with less than 1 dB ripple across the aperture and 1 dB spillover loss. It is described below.

4.1.8 Antenna Pattern Analysis

A computer program that uses ray tracing from the feed to the far field was used to compute the pattern of a space-fed phased-array antenna similar to the one described in this report. Although the results are not directly applicable, they will be described in the next paragraph as an example of the results that can be expected from a similar analysis of the UHF antenna system described herein.

The antenna analyzed operates at a wavelength of 10 cm and consists of a standard four-phase-center monopulse feed which space-feeds the active primary lens array. The lens array is composed of 22,460 subarrays on the feed side. There are five kinds, each having a different set of squint angles. Behind the subarrays are RF modules, each containing a 3-bit digital phase shifter, duplexer switches, a power amplifier used in the transmit mode, and a receiver preamplifier used in the receive mode. The phase shifter

provides beam steering and quadratic phase-error correction. There are 22,460 subarrays on the radiator side of the primary lens. The subarrays are amplitude-tapered to reduce scan loss. The analysis included the effects of the above items in addition to a vibrational displacement of the antenna surface. The computer antenna simulation produced the desired mainlobe and sidelobes which rapidly decreased to -40 dB at an angle 1.2° away from the peak of the beam. The average far-out sidelobe level was about -40 dB one way. The clutter is therefore primarily determined by the main beamwidth and not the sidelobe level. The 3-bit phase shifter does not produce quantization lobes because of the randomization caused by the quadratic phase-error correction. The basic design of the primary lens is corroborated by the computer study results.

Table 4-1 is a summary of the computed 417-MHz antenna performance

TABLE 4-1 ONE-WAY ANTENNA PARAMETERS

Parameter	UHF
Frequency	417 MHz \pm 5%
Diameter	300 meters
No. of dipoles	172,000
No. of Modules	12,000
Directive Gain	62.3 dB
Beamwidth	0.17°
1st Sidelobe	-15 dB
Far out (8°) sidelobes	below -40 dB
Scan Loss 6.1	1.44 dB

4.1.9 Feed Design

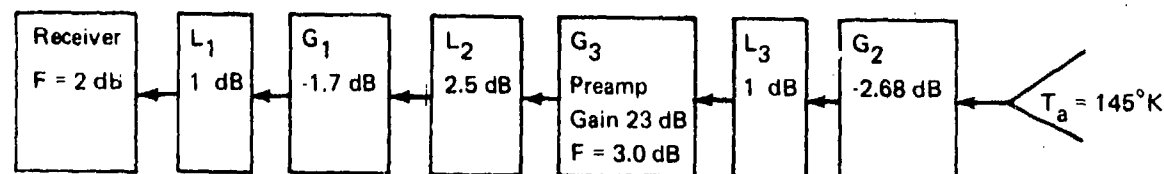
The basic antenna design consists of a space-fed phased-array. The radar array is active with receive/transmit modules connected to radiating subarrays. To minimize feed spillover losses and keep the main array nearly uniformly illuminated, a special feed design was made. With a low-amplitude ripple across the main array, all the class C RF module power amplifiers will be operating in a highly efficient region. Main array aperture efficiency is also aided by uniform illumination. To obtain the feed design, the synthesis program described in Appendix A was used. The feed is composed of radiating dipoles arrayed on rings. The feed diameter is 36 ft and contains 716 dipoles on 15 rings. The amplitude ripple across the main array is expected to be less than 1 dB, with the spillover loss also less than 1 dB.

4.1.10 Radar System Noise Figure and Loss Budget

A loss budget is shown below.

	One-way Loss, dB	
	Γ_R^2	Gain
Beam Steering Loss, Subarray, Target Side		-1.45
Polarization Loss		-1.0
Time Delay Loss, Beam-steered, Target Side		- .23
		} G2
Corporate Feed, High Power	0.5	}
Duplexer Switch, High Power & Polarizer	0.5	
		} L3
Duplexer, Low Power	0.5	}
Phase Shifter, 3-bit	1.5	
Corporate Feed, Low Power	0.5	
		} L2
Subarray Loss, Feed Side		-0.5
Time Delay Loss, Feed Side		-0.2
Spillover Loss, Feed Side		-1.0
		} G1
Monopulse Feed Loss	0.5	}
Sum Channel Duplexer Loss	0.5	
		} L1

A model for noise figure computation is shown in the diagram below. To be conservative, the preamp gain was reduced to 20 dB.

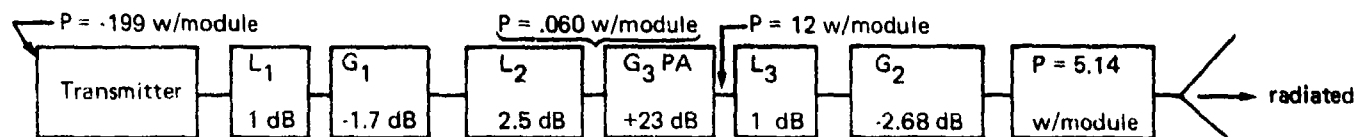


Loss Model, Receiver With Preamplifier

$$T_e = T_a + \frac{T_o (L_3 - 1)}{G_2} + \frac{T_o (F - 1) L_2}{G_2} + \frac{T_o (L_2 - 1) L_3}{G_2 G_3} + \frac{T_o (L_1 - 1) L_2 L_3}{G_1 G_2 G_3} + \frac{(F - 1) L_1 L_2 L_3 T_o}{G_1 G_2 G_3}$$

$$T_e = 688.5^\circ\text{K at antenna input.}$$

$$F_{\text{effective}} = 10 \log \frac{T_e}{T_o} = 3.75 \text{ dB}$$



Gain/Loss Model for Radar Signal Transmit Mode

The input to the power amplifier is 60 mw peak per module. Assuming a minimum specification gain of 23 dB in the amplifier, the output is 12 w peak per module. When the antenna is scanned 6.1° from broadside, the radiated power in the main beam is 5.14 w peak per module. The above model neglects amplitude taper across the feed side of the array aperture and assumes power amplifier hard limits at 12 w peak output.

4.1.11 DC Power Distribution for RF Modules

Figure 4-8 shows the DC power distribution system for the RF modules in simplified form.

The solar cell paddes are located near the LSP and rotate to face the sun. Rotary joints will bring DC power into the LSP where secondary batteries store this energy. The DC power is distributed to the modules in each gore via ribbon conductors running on or parallel to the gore edge tapes. The energy is carried from the edge tape conductors via conductors carried on the battens to conductive tapes composing the ground plane. The ground plane carries the ground conductors as well as the B+ conductors. Each module will have seven ground tapes and seven tapes carrying B+, to provide redundant power feeders to the module. The average path resistance from the battery to a module will be about 0.76 ohm. The DC power from the secondary battery is used to charge an energy storage capacitor on each RF module through the 0.76-ohm feeder line resistance. During the pulse burst, it takes 39 volts at the battery to produce steady state 28 vdc in a 22- μ f capacitor on each module at the maximum pulse compression ratio. To reduce the ripple across the capacitor to a minimum, the voltage is switched from 28 to 39 vdc during pulse burst transmission from the RF module. The peak-to-peak ripple is 3.8 volts; the efficiency is 67%. At the lowest pulse compression ratio, the required voltage is 32 v and the efficiency is 77%.

The direct current to each gore is 129 amp. and is switched using high-power switching transistors. The voltage is switched to the appropriate voltage 800 μ sec after receipt of the sync 1 pulses and switched back to 28 vdc 800 μ sec after transmission of the 64th radar pulse. This is repeated for each pulse burst cycle. To control the battery switches, a subarray antenna and an RF module are mounted on the LSP so that it receives the same signal as the modules in the main array. The logic will be modified to provide 80 switch drivers gated in accordance with the required switch on-off times. The system, as described, has been designed for a PRF = 640 pulses/sec during the pulse burst.

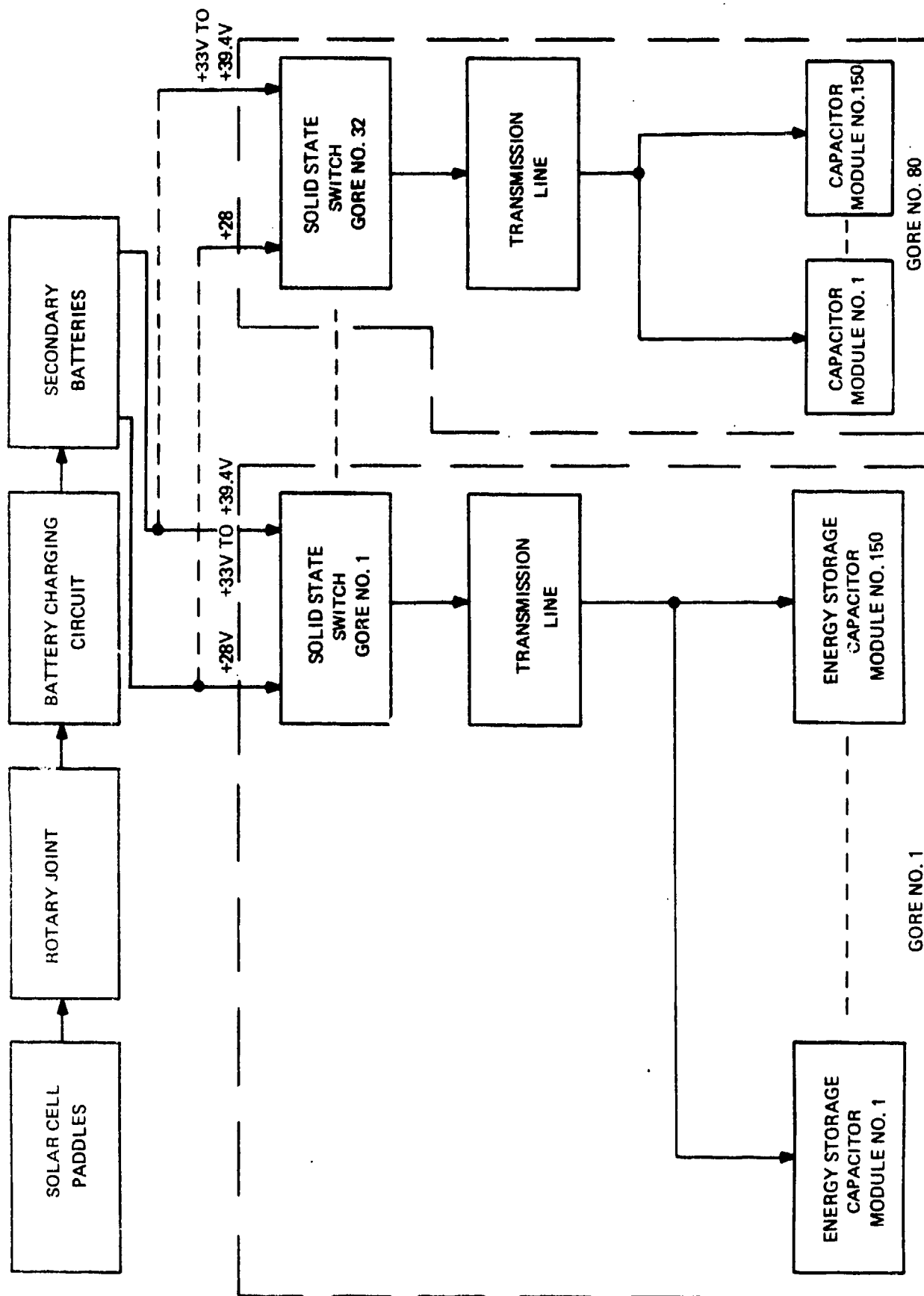


Fig. 4-8 Simplified Block Diagram, DC Power Distribution to RF Modules

4.2 GROUND STATION

Ground Station design analysis was performed by Sperry Gyroscope Division under subcontract to Grumman. The Sperry report is a separate document delivered with this Grumman report. This subsection of the Grumman report presents the ground station requirements and gives a general description of the principal functions.

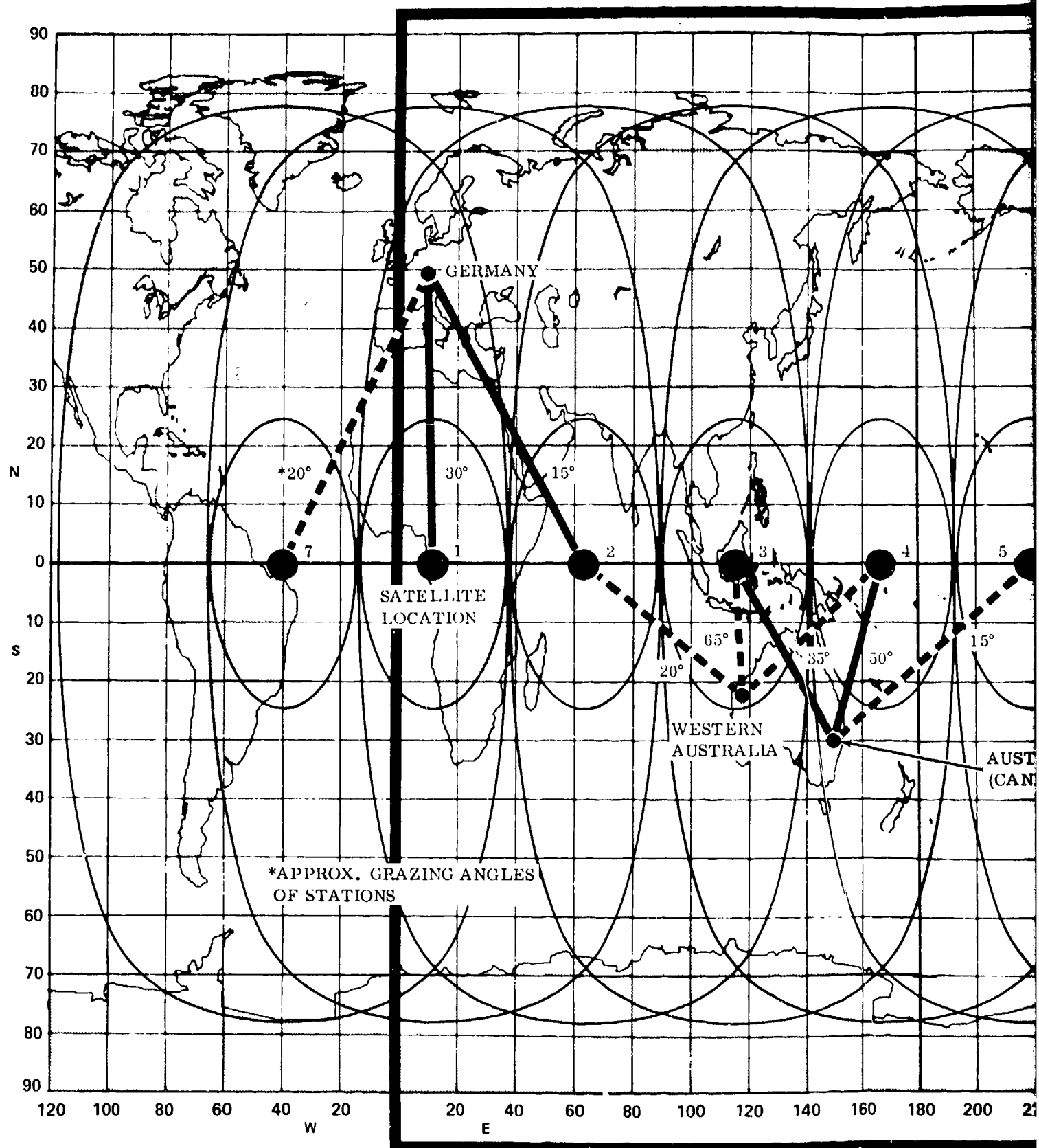
Because the satellites are radar repeaters, dedicated ground stations are required. It is possible to control three satellites from one ground station. Two ground stations are proposed for Systems I and II - one for normal operation and the other as backup.

For the North American Continent both ground stations could be located in the United States or Canada, but should be one to two thousand miles apart to reduce the chances of simultaneous destruction by enemy action. For the Russia and China fence, the stations will be located in Australia. Wherever possible, the stations will be located at existing satellite control sites.

For System III, worldwide coverage, three ground stations could provide control over all seven satellites. Five ground stations are proposed for backup capability. Three antenna systems at each ground station are assigned to individual satellites in a way such that, should any one ground station be completely disabled, full control of all seven satellites will still be available. Figure 4-9 shows the ground station locations selected, with their primary and backup links indicated to illustrate system redundancy.

The principal functions of a ground station are to:

- Accept instructions from NORAD or other Commands for placement of the fence and for tracking designated aircraft
- Perform the necessary radar function using the satellites as radar repeaters
- Send the acquired surveillance data to NORAD or other Commands as required
- Monitor and control the satellite position and attitude.



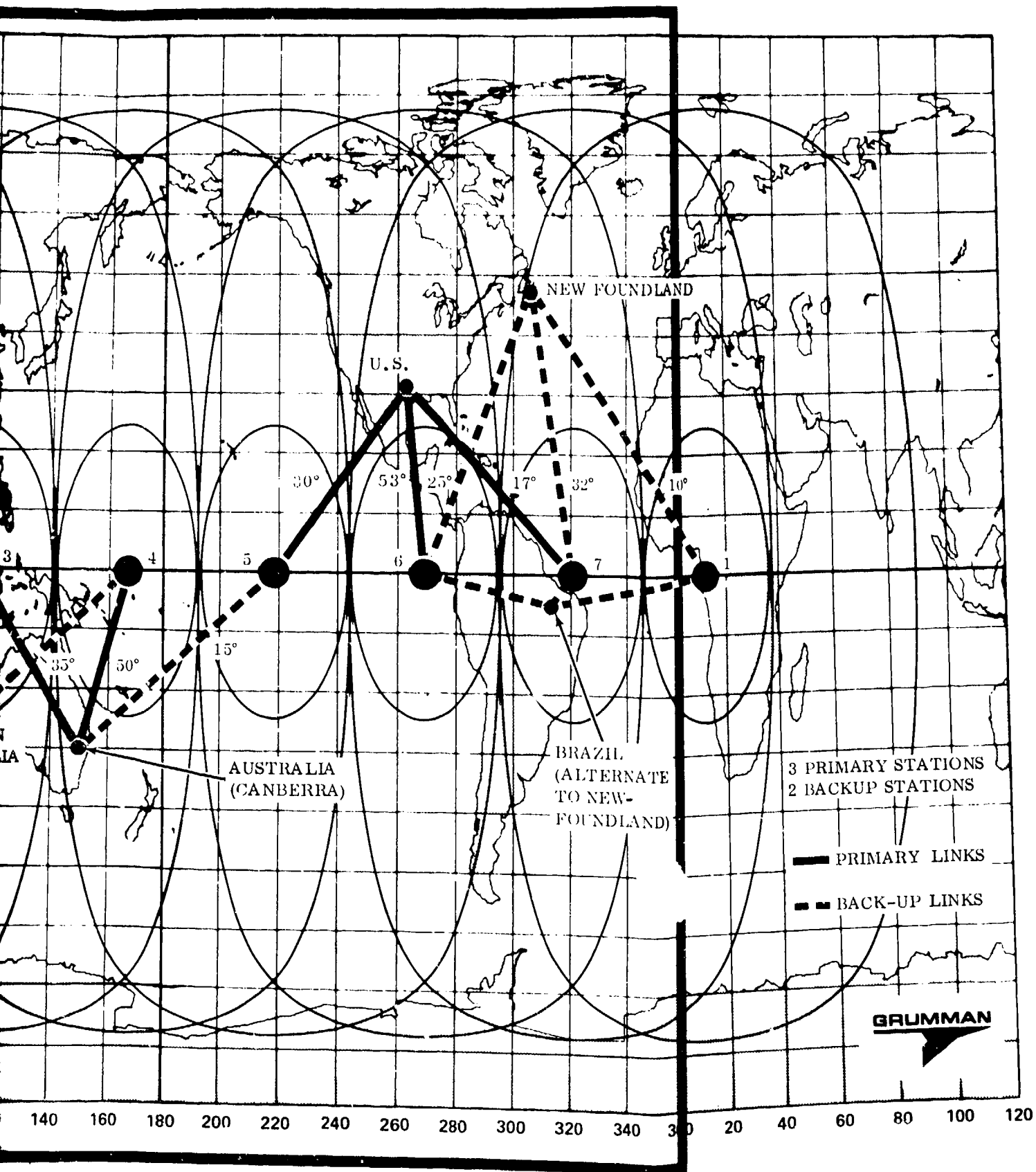


Fig. 4-9 Ground Station Locations

Each station will have three separate antenna systems and associated RF hardware for operation with the three satellites within its view. Each antenna will be 60 ft in diameter, providing a gain of 38.3 dB at the UHF frequency of the communications link. The combined gain of the ground antenna with the 42-dB gain of the satellite communications antenna permits operation with a peak power of approximately 22 w for a signal-to-noise (S/N) ratio of 47 dB. The high S/N ratio is needed to prevent distortion of the radar echo signal. Using 10 Kw at the ground station instead of 22 w will provide greatly increased immunity to jamming of the communication link.

In addition to the three UHF antennas, there will be an antenna for the satellite omni communication link. Wherever possible, this link will be the standard satellite control system using a frequency of 2.2 GHz for the uplink and 1.8 GHz for the downlink. One system can be shared by the three satellites, since this link is used only during deployment or if contact is lost through the main link.

The principal radar functions performed by the ground station are:

- Generation and transmission of signals for pointing the satellite radar beam at the target and the communication beam at the ground station
- Generation and transmission of the radar pulse burst signal to the satellite
- Processing of received radar signals.

The signal processing consists of pulse compression, integration, Doppler filtering, and target detection. A coordinate converter translates earth latitude and longitude coordinates into radar range and azimuth and elevation. Radar processing and display are accomplished in radar coordinates for accuracy and simpler displays. Position data are sent to the user systems in latitude-longitude earth coordinates.

The ground station also provides the necessary computations and storage for generating the fence and for tracking aircraft. A computation is required for each fence segment because the number of beams, the look rate, and the transmitter power vary with the fence location. Tracking requires an additional computation based on target speed, traffic density, and target priority.

Satellite position and attitude control and radar beam direction calibration are done from the ground station using calibration stations. The error is determined by periodically pointing the main radar beam at calibration stations with known positions. Two of these can be the ground stations assigned to control the satellite; additional calibration stations can be placed elsewhere if needed. A calibration station is a radar signal transponder for obtaining a high signal-to-noise ratio at the radar receiver, permitting an accurate azimuth determination from the monopulse signal.

Communications data links are required between the ground stations and the directing Commands. The data rates required are very modest, not more than a few hundred bits per second; but the time delay is a function of the tactical situation and may have to be quite short - on the order of a few minutes.

4.3 SATELLITE STATIONKEEPING

An equatorial, circular, geosynchronous satellite experiences perturbing forces from a number of sources and, if uncorrected by delta-V applications, may depart significantly from the desired geosynchronous position. The satellite's motion as perceived by an earth-fixed observer is the result of a combination of various superimposed deviations from the expected stationary condition usually associated with equatorial, circular, synchronous orbits.

This subsection will discuss the motions of a satellite which result from (1) higher-order earth potential terms, J_2 and J_{22} , due to equator ellipticity, (2) gravitational attraction of the sun and moon, and (3) forces resulting from solar radiation impinging upon the satellite's surface areas.

4.3.1 Earth's Equatorial Ellipticity

The earth's gravitational potential energy function, U , contains terms which depend upon latitude and longitude. The dominant term is the "central force" potential, $-\mu/r$; the remaining (infinite) series terms are of descending relative importance in their energy contribution. For present purposes, the series is truncated to

$$U = -\frac{\mu}{r} \left[1 - \frac{1}{2} J_2 \frac{R^2}{r^2} (3 \sin^2 \lambda - 1) - 3 J_{22} \frac{R^2}{r^2} \cos^2 \phi \cos 2\Gamma \right]$$

where λ = latitude of satellite position

Γ = longitude of satellite position, measured from minor axis of elliptic equator

r = radius from earth's center to satellite position

R = semi-major axis of elliptic equator = 3443.934 n mi

$$\mu = .225902135 \times 10^9 \frac{\text{n mi}^3}{\text{min}^2}$$

$$J_2 = .1082637 \times 10^{-2}$$

$$J_{22} = .1789187 \times 10^{-5}$$

This non-spherical dependency of U is often referred to as triaxiality.

The forces derived from this energy potential function create tangential east-west satellite accelerations. The resulting motion appears to an earth-fixed observer as a long-period, east-west oscillation about the elliptic equator's minor axis. Two positions

exist on the minor axis (on diametrically opposite sides of the earth) such that, if the satellite is initially placed at one of these, at rest in the earth's rotating frame, no departure from this earth-fixed position would ensue. Two similar positions also exist on the major axis except that, whereas perturbed satellites will remain "near" the two (stable) points on the minor axis, the two major axis equilibrium positions are unstable.

The location of the equator's minor axis does not, as yet, appear to be well defined. Various investigators have listed a stable point (relative to the Greenwich meridian) to be located at:

- 104.74° W (from a list of constants by Goddard)
- 116.4° W (C.A. Wagner, Goddard, Feb. 1964)
- 123. ° W (Frick and Garber, RAND 1962)
- 123. ° W (Izsak, 1961)
- 127.5° W (Kozai, 1961)
- 129. ° W (Kaula, 1962)

This range of longitudes may be characterized as "western Pacific Ocean region". The diametrically opposite stable point would have a longitude in the range 51 to 75° E, which is in the Indian Ocean region.

The near-equatorial, geosynchronous orbit subjected to the influence of the J_{22} term will undergo long-period east-west, radial, and north-south oscillations. The last may be ignored since the inclination varies from its mean by only one part in 10^6 . The illustration below shows the motion in the orbit plane as seen in an earth-fixed coordinate frame. Each closed curve is characterized by a maximum east-west deviation, Γ_{max} , from the equator's minor axis.

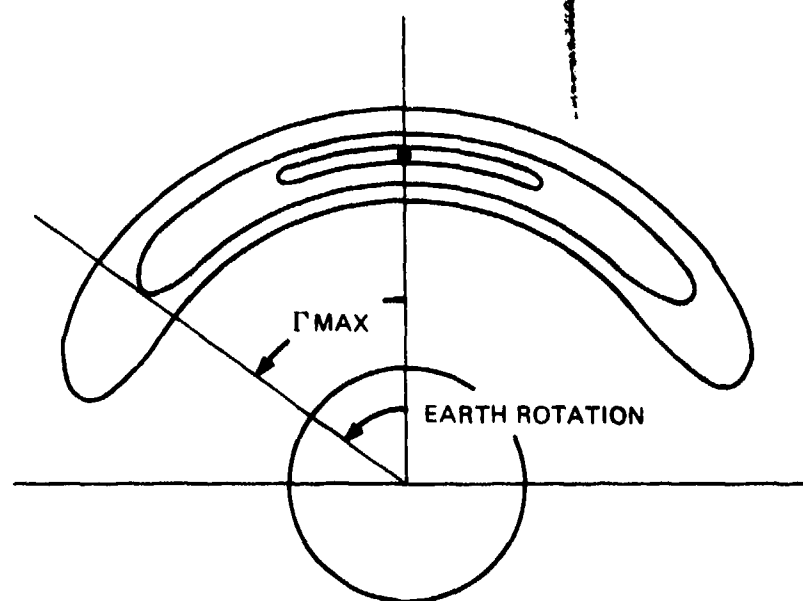


Figure 4-10 gives the time it takes to transmit one-quarter of the closed figure (either in the upper or lower section) as a function of r_{\max} . Note that the motion is of long period compared to a synchronous orbit. Even for a small oscillation about the stable point, the full period is 820 days. Since the satellites will be required to hold positions approximately every 52° (seven satellite system) or 45° (eight satellites), it is evident that stationkeeping action will be needed to counter the triaxiality influence.

A possible stationkeeping procedure would be to select, for each desired satellite longitude, that contour for which r_{\max} yields the required mean longitude plus the acceptable longitudinal deviation limit. For example, if the desired mean longitude is 105°E , the allowed deviation 1° , and the nearest stable point (assumed) 75°E , then the selected contour would have $r_{\max} = 105^\circ + 1^\circ - 75^\circ = 31^\circ$. Then, whenever the satellite deviates from r_{\max} by 2° (a position 1° closer to the minor axis than is the desired mean position), a Hohmann transfer is made to return the satellite to that portion of the contour wherein the motion is again directed toward r_{\max} , thereby reducing the deviation. Figure 4-11 indicates the positions of the first and second burns of the Hohmann transfer orbit. The time spent in transfer from position 1 to position 2 is about 12 hr. Figure 4-11 also shows the time spent in circuit from position 2 to position 1 as a function of both r_{\max} and the allowed longitudinal deviation. Note that positions near $r_{\max} = \pm 45^\circ$ require the most frequent corrective action for stationkeeping.

Figure 4-12 provides the delta-V required over a 5-yr period to perform the Hohmann transfer outlined above when the allowed deviation from the mean position is 1° . The maximum delta-V of about 30 ft/sec occurs for $r_{\max} = 45^\circ$.

Motion in the radial direction has the same period as the east-west motion. The amplitude of the radial motion is the monotonically increasing function of r_{\max} shown Figure 4-13.

Both the radial and the east-west satellite speeds relative to the earth-fixed frame are small. The radial speed component does not exceed $\pm 10^{-2}$ ft/sec. The longitudinal component of earth-relative satellite speed always remains less than ± 5 ft/sec when crossing the minor axis. At the extreme point of the contour, this latter component approaches zero.

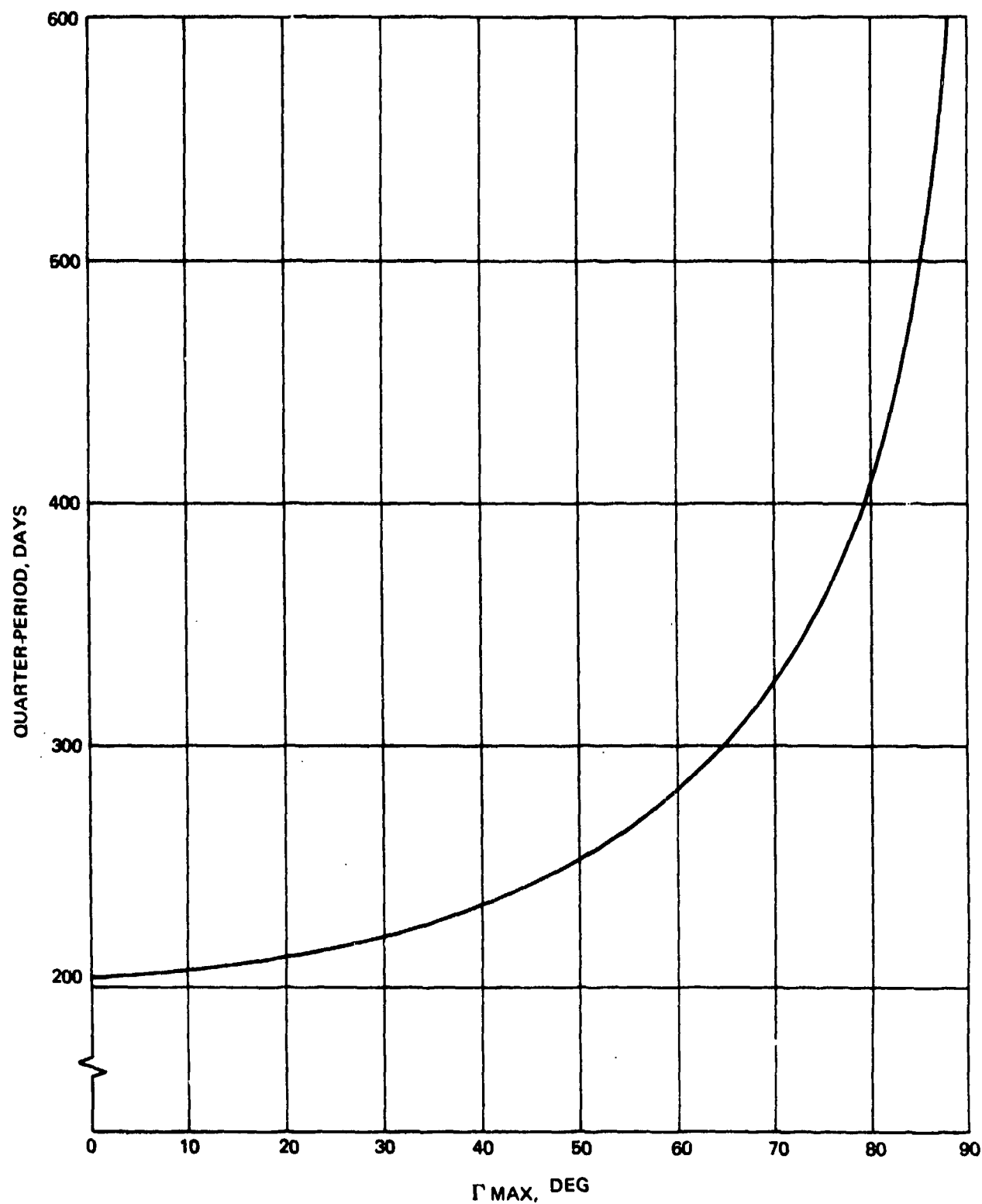


Fig. 4-10 Effect of Earth's Ellipticity

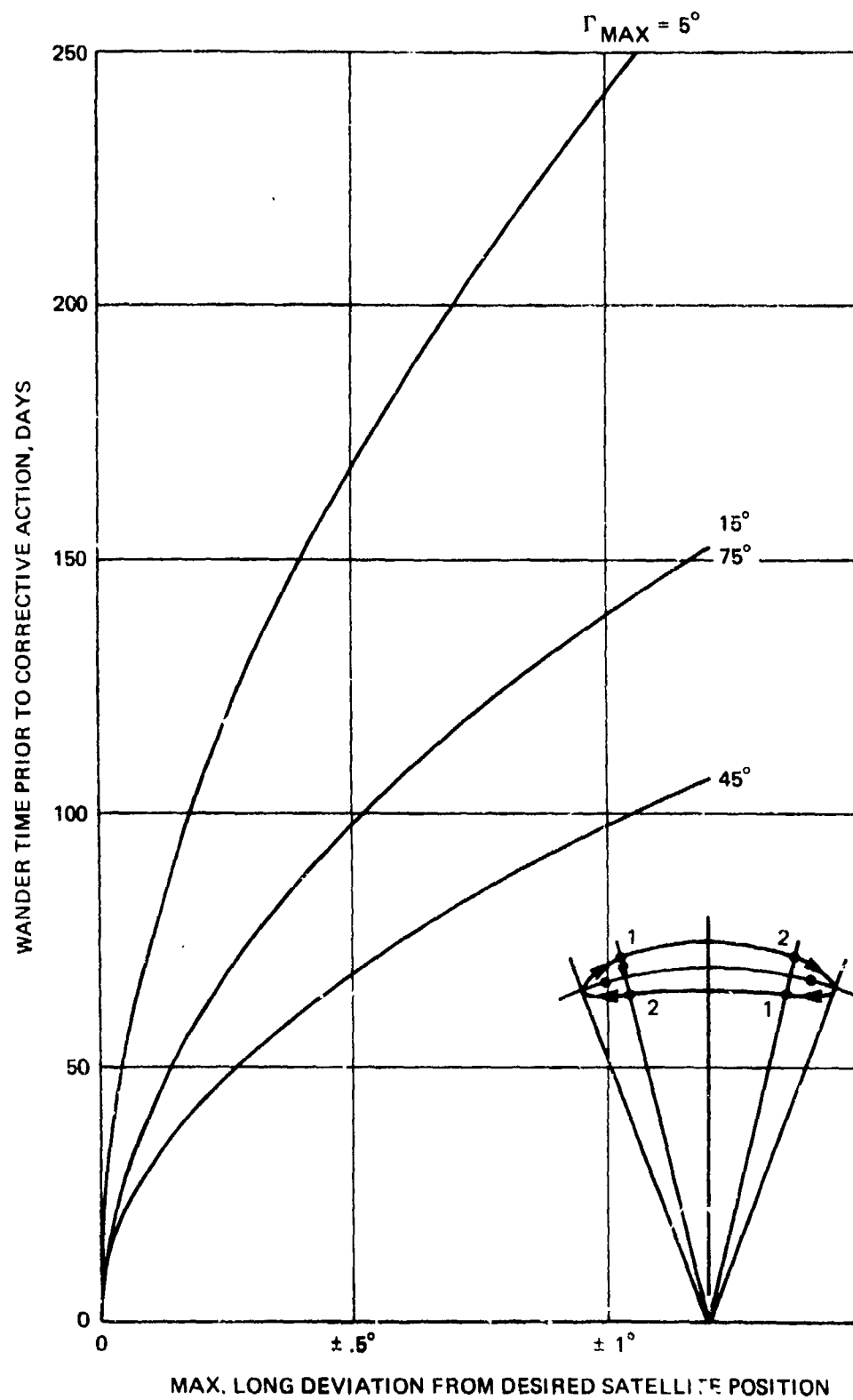


Fig. 4-11 Motion of Satellite Due to Earth's Ellipticity

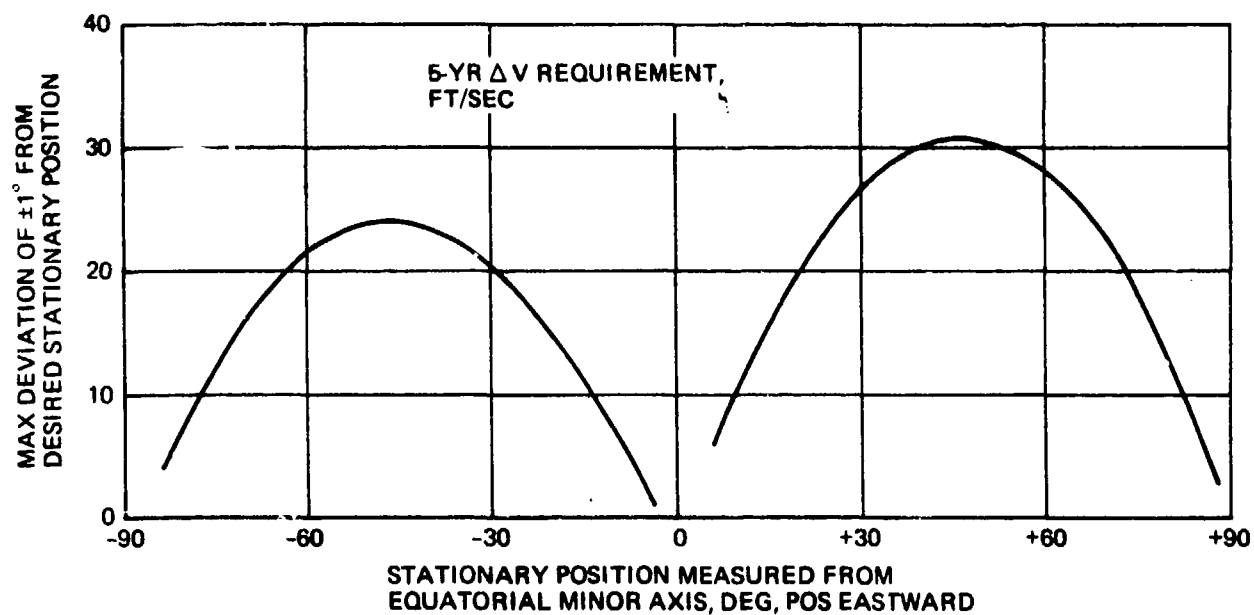


Fig. 4-12 ΔV Required to Correct for Earth's Triaxiality

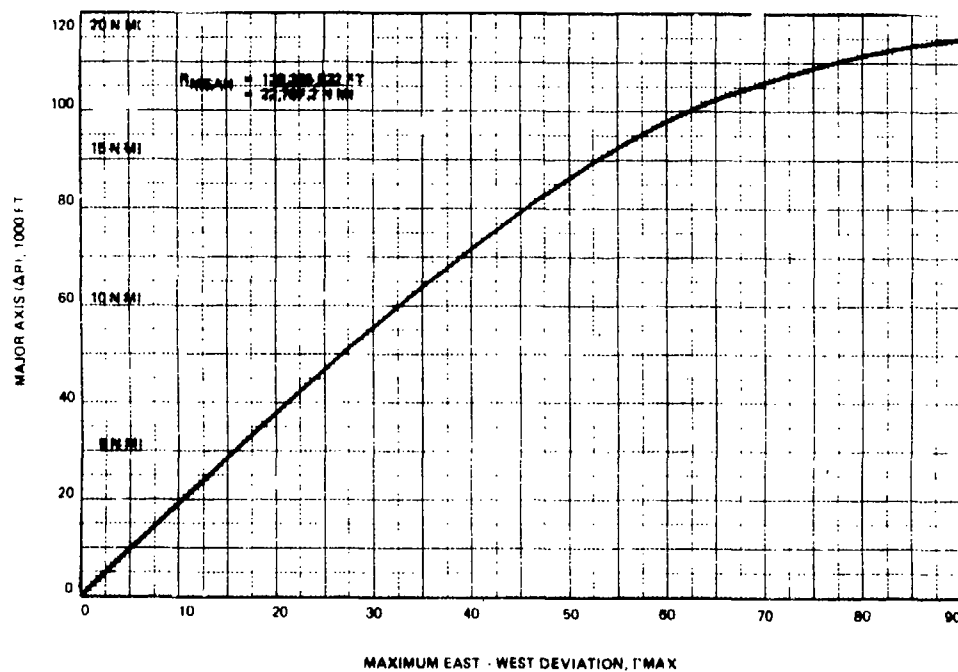


Fig. 4-13 Motion in Radial Direction Due to Earth's Equatorial Ellipticity

4.3.2 Sun and Moon Gravitational Attraction

The principle effect of sun and moon attraction on a near-equatorial geosynchronous satellite is to alter the orbit's inclination to the equator. Only when the orbit's ascending node is at the vernal equinox ($\Omega = 0$) and the orbit's inclination $i = 7.5^\circ$ does the orbit plane inertial orientation remain invariant. Any other orbit orientation will lead to a long-period (~ 53 yr) oscillation of the orbit inclination about $i = 7.5^\circ$. When the orbit inclination is near zero, the inclination rate is about .853 deg/yr. Then, if the orbit is initially oriented to $i = 0$ it will tend to rotate about the vernal equinox direction, reducing the angle it makes with the ecliptic plane and, in 5 yr, accumulating an inclination to the equator of about 4° .

To return the orbit to $i = 0$ after it has wandered by Δi requires a delta-V of about 175 ft/sec for each degree of correction. If the correction is made each year (after an accumulation of $i = .853^\circ$), then, over the 5-yr period, four corrections are required for a total delta-V of 600 ft/sec. For a satellite weighing 2200 lb utilizing a fuel with $I_{sp} = 200$ sec, this delta-V would require an additional fuel weight of about 140 lb.

If, however, a $\pm 2.1^\circ$ north-south deviation from the equator can be tolerated, then it is possible, by selecting an initial orbit orientation $i = 2.1^\circ$ and $\Omega = 100^\circ$, to ensure that, during a 5-yr mission period, the inclination will not exceed the initial value and, therefore, no north-south delta-V would be required. What occurs is a reduction of inclination to zero during the first half of the mission period, followed by an increase in the latter half. The orbit plane rotates in the same sense during the 5-yr period with a discontinuity in the ascending node of 180° as the inclination passes through $i = 0^\circ$. With the orbit inclination at its maximum value of 2.1° , the sub-orbital point has a maximum north-south speed of 33.0 kt.

The required initial orbit, described above, to avoid the otherwise large delta-V applies to each satellite in the seven or eight satellite system. This implies that each satellite starts off in the same orbit, uniformly separated by selecting the appropriate initial true anomaly. At any given instant, then, each satellite would be at a different position in its respective "figure 8" trace, each trace being the same in size and shape.

4.3.3 Solar Radiation Pressure

The effect of solar radiation pressure on the initially equatorial, geosynchronous (circular) orbit is to induce orbit eccentricity with only minor changes in orbit period. The orbit period increases gradually so that, 5 yr later, the satellite has experienced an accumulated westward drift of only 1° .

Superimposed upon this slow drift of the satellite's mean position, however, is an oscillatory east-west motion resulting from the orbit's eccentricity. The following computations lead to an estimate of the eccentricity and the oscillator motion.

At the earth's distance from the sun, fully absorbed solar radiation produces a pressure of 1×10^{-7} lb/ft². The 200-ft diameter lens is assumed to be 80% transparent to solar radiation and 20% absorptive. With a mass of 2200 lb (= 68.323 slugs), the satellite then experiences an acceleration of

$$a = (.2 \times 10^{-7}) (\pi \times 10^4) / 68.323 = 9.196 \times 10^{-6} \text{ ft/sec}^2$$

Since the satellite is earth-oriented, the effective acceleration of the satellite over the course of each orbit is $(2/\pi) a$ or $\bar{a} = 5.855 \times 10^{-6} \text{ ft/sec}^2$. The eccentricity, starting at zero, grows to a maximum in 6 months and then returns to zero after one year. The maximum eccentricity may be found from

$$e_{\max} = 3 \frac{r_c^2}{k \mu} \bar{a} \cos \epsilon$$

where

$$r_c = \text{radius to stable point} = 138,335,932 \text{ ft}$$

$$\mu = \text{gravitational constant} = 1.407654 \times 10^{16}$$

$$k = .273 \times 10^{-2}$$

$$\epsilon = \text{angle between equatorial and ecliptic planes} = 23^\circ 27'$$

This yields

$$e_{\max} = .8024 \times 10^{-2}$$

The resulting difference between apogee and perigee at maximum eccentricity is

$$(r_a - r_p)_{\max} = 2 r_c e_{\max} = 365 \text{ n mi}$$

Assuming the motion between apogee and perigee to be sinusoidal, the maximum radial velocity would be

$$\dot{r} = \frac{365}{2} \frac{\pi}{12} \frac{\text{n mi}}{\text{hr}} = 23.9 \text{ kt}$$

The apparent east-west oscillatory motion for $e = e_{\max}$ is $\pm .92^\circ$ about the mean position. This yields a maximum longitudinal rate for the sub-orbital point of $\dot{L} = .92^\circ \times 60 \frac{\text{n mi}}{\text{deg}} \times \frac{\pi}{12 \text{ hr}} = 15 \text{ kt}$. No corrective action is required for these effects.

4.3.4 Summary

This subsection discussed the stationkeeping requirements on a large geosynchronous satellite due to (1) earth's equatorial ellipticity, (2) sun and moon

gravitational attraction, and (3) solar radiation pressure. Over the 5-yr operational period required of the seven-satellite system, a judicious choice in the initial configuration of the various satellite orbits will result in acceptable uncorrected motion from all perturbative sources except equatorial ellipticity. This perturbation can be controlled over the five years by an expenditure of up to 30 ft/sec. Table 4-2 summarizes the perturbed motions and the required corrections. Solar pressure torque effects on attitude are discussed in Section 7.

TABLE 4-2 PRIMARY PERTURBING SOURCES AND THE MOTIONS THEY GENERATE

Effect	Source	Uncorrected Drift	5 - Yr Delta-V Req
Longitudinal Mean Drift	Sun & Moon Attraction Solar Press	1° westward in 5 yr	None
Longitudinal Oscillation	Triaxiality Sun & Moon Attr., Solar Pressure	0 - ±90° (very long term) 0 - ± .92°/day	Up to ~30 ft/sec None
Latitudinal Oscillation	Sun & Moon Attraction	.853°/yr	None

Appendix A

A CONCENTRIC RING ARRAY TECHNIQUE FOR APPROXIMATING ARBITRARY AXIALLY SYMMETRIC ANTENNA PATTERNS

A. 1 INTRODUCTION

A short study was undertaken to devise a technique for determining the aperture distribution of a circular array whose far-field pattern closely approximates a predetermined functional shape. The ideal function of interest takes on a constant value over a conical angle, and is zero elsewhere. The technique described herein is, however, quite general in nature, and may be used to synthesize any desired axially symmetric antenna pattern, within the limitations of the available aperture size.

A. 2 IDEALIZED RING ELEMENT

Consider a circular ring current source with radius r , current density I_0 amp/meter, and infinitesimal thickness. Mathematically, this source may be written in cylindrical coordinates (ρ, ϕ, Z) as:

$$I(\rho, \phi, Z) = I_0 \delta(\rho - r) \delta(Z) \quad (1)$$

The far-zone electric field due to this source is obtained as a Fraunhofer integral:

$$\begin{aligned} E(\theta) &= c \iiint I_0 \delta(\rho - r) \delta(Z) e^{j \frac{2\pi}{\lambda} [\rho \sin \theta \cos(\phi - \psi) + Z \cos \theta]} \rho d\phi d\rho dZ \quad (2) \\ &= c I_0 r \int_{-\pi}^{\pi} e^{j \frac{2\pi}{\lambda} r \sin \theta \cos(\phi - \psi)} d\phi \\ &= c I_0 r J_0 \left(\frac{2\pi}{\lambda} r \sin \theta \right) \end{aligned}$$

where θ and ϕ are the axial and radial angles, respectively, of a conical coordinate system relative to the ring axis, and C is a constant independent of r which will be neglected from here on.

Appendix A

A.3 RING ARRAY

Assume that N current sources of various radii are arrayed concentrically in a plane. If r_k and I_k are the radius and current density, respectively, of the k th source, then the far field of the array may be written:

$$E(u) = \sum_{k=1}^N I_k r_k J_0\left(\frac{2\pi}{\lambda} r_k u\right) \quad (3)$$

where $u = \sin \theta$.

In examining the form of Eq (3), note that the set of Bessel functions $\{J_0(Z_k u): k=1, 2, \dots\}$, where Z_k is the k th zero of $J_0(Z)$, form a complete orthonormal basis with respect to the set of all piecewise continuous functions on the interval $0 \leq u \leq 1$. Consequently, choosing the ring diameters r_k according to the equation

$$r_k = \frac{\lambda Z_k}{2\pi} \left(\approx (k - \frac{1}{4}) \frac{\lambda}{2} \text{ for large } k \right) \quad (4)$$

will guarantee that any desired pattern may be approximated (except at points of discontinuity) by choosing a sufficiently large number N of rings in the array. The Gibbs Phenomenon, which occurs at the discontinuities, may be avoided by approximating the desired pattern with a continuous function. For example, the "conical step function" described earlier may be approximated by a high-order Butterworth characteristic of the form:

$$E_M(u) = \frac{1}{1 + (u/u_0)^M} \quad (5)$$

A.4 SOLUTION FOR OPTIMUM EXPANSION COEFFICIENTS

The final step in applying this technique is to find a "best" set of currents ($I_k; 1 \leq k \leq N$) in Eq (3) to approximate the desired pattern $E_d(u)$ using N ring sources. The "goodness" criterion used here will be a weighted least-mean-squares criterion which seeks to minimize the integral expression $F(I_1, \dots, I_N)$, given by:

$$F(I_1, \dots, I_N) = \int_0^1 W(u) \left| E_d(u) - \sum_{k=1}^N I_k r_k J_0(Z_k u) \right|^2 du \quad (6)$$

Where $W(u)$ is a non-negative weighting function.

Appendix A

Equation (6) may be expanded as follows:

$$F(I_1, \dots, I_N) = \int_0^1 W(u) \left| E_d(u) \right|^2 du - 2 \sum_{k=1}^N I_k r_k \int_0^1 W(u) E_d(u) J_0(Z_k u) du \quad (7)$$

$$+ \sum_{k=1}^N \sum_{n=1}^N I_k r_k I_n r_n \int_0^1 W(u) J_0(Z_k u) J_0(Z_n u) du$$

Define:

$$e_k = I_k r_k \quad (8a)$$

$$v_k = \int_0^1 W(u) E_d(u) J_0(Z_k u) du \quad (8b)$$

$$h_{kn} = \int_0^1 W(u) J_0(Z_k u) J_0(Z_n u) du \quad (8c)$$

$$c_1 = \int_0^1 W(u) \left| E_d(u) \right|^2 du \quad (8d)$$

Using these definitions, Eq (7) may be written:

$$F(e_1, \dots, e_N) = c_1 - 2 \sum_{k=1}^N v_k e_k + \sum_{k=1}^N \sum_{n=1}^N h_{kn} e_k e_n \quad (9)$$

$$= c_1 - 2 \bar{V}_T \bar{e} + \bar{e}_T \bar{H} \bar{e}$$

where matrix notation has been used, the T-subscript denoting matrix transpose.

Appendix A

It is shown later than the coefficient vector \bar{e} which minimizes the expression in Eq (8) is given by:

$$\bar{e}_{\min} = \tilde{H}^{-1} \tilde{V} \quad (10)$$

This equation, together with the definitions in Eq (8a) through (8c), yield the desired ring currents.

A.5 COMPUTER PROGRAM

A FORTRAN IV computer program was written to compute the optimum ring currents according to the above theory.

The pattern resulting from a typical program run is shown in Fig. A-1. The ideal pattern was approximated by a Butterworth characteristic with $M = 20$ and $u_0 = 0.22$, or $\Theta_0 = \sin^{-1}(0.22) = 12.7^\circ$. The weighting function $W(u)$ was a constant value of unity for this run, and the number of concentric rings in the array is 20.

The problem of finding the coefficient vector \bar{e}_{\min} , which minimizes the symmetric quadratic form given in Eq (9), is treated as follows.

Let \tilde{y} be an arbitrary bounded vector, and ϵ a small scalar. Then if $\epsilon\tilde{y}$ is a small perturbation of \bar{e} , the functional value F becomes

$$\begin{aligned} F(\bar{e} + \epsilon\tilde{y}) &= c_1 - 2\tilde{V}_T (\bar{e} + \epsilon\tilde{y}) + (\bar{e}_T + \epsilon\tilde{y}_T) \tilde{H} (\bar{e} + \epsilon\tilde{y}) \\ &= F(\bar{e}) + \epsilon (\tilde{y}_T \tilde{H} \bar{e} + \bar{e}_T \tilde{H} \tilde{y} - 2\tilde{V}_T \tilde{y}) + o(\epsilon) \end{aligned} \quad (11)$$

A necessary condition for \bar{e} to be a stationary point of the functional F is that the first variational derivative, given by the coefficient of ϵ in Eq (11), must be identically zero for all allowable perturbation vectors \tilde{y} . This term may be written

$$0 = y_T H e + y_T H_T e - 2y_T V \quad (12)$$

Appendix A

Since H is a symmetric matrix, Eq (12) may be written

$$\vec{2y}_T (\vec{H}\vec{e} - \vec{V}) = 0 \quad (13)$$

Since this expression must hold for all bounded vectors \vec{V} , the bracketed term must be identically zero:

$$\vec{H}\vec{e} - \vec{V} = 0 \quad (14)$$

or

$$\vec{H}\vec{e} = \vec{V}$$

Assuming \vec{H} to be nonsingular, Eq (14) may be inverted to give the desired solution:

$$\vec{e}_{\min} = \vec{H}^{-1} \vec{V} \quad (15)$$

A.6 SUMMARY

The technique described here seems to be a reasonable means of approximating arbitrary axially symmetric antenna patterns using circular phased arrays. In practice, the idealized ring element would be approximated by a ring of equally spaced, identically fed elements such as dipoles. Although mutual coupling effects would be variable around such a ring, the element patterns should all be sufficiently broad to allow the ring array theory to be applied within a reasonably broad angle near boresight.

Appendix B

RCA | Government and Commercial Systems | Missile and Surface Radar Division
Moorestown, New Jersey 08057 | Telephone (609) 963-8000

Mr. J. Schultz
Grumman Aircraft Corporation
Building 25
Bethpage, New York 11714

RCA

Subject: Spaceborne Radar Transceiver

Dear Mr. Schultz:

7 June 1974

In response to your request during our meeting at your facility on 31 May 1974, I am pleased to confirm that RCA has the facilities and qualified personnel to fabricate the transceiver modules for your spaceborne phased array radar. We have evaluated your requirements and believe that our approach briefly described in Attachment A will provide a satisfactory design completely compatible with your system.

The Missile and Surface Radar Division here in Moorestown, New Jersey has the facilities, personnel and specific experience to supply the complete transceiver as a space-qualified completely-tested assembly ready for installation by the Grumman Aircraft Corporation into your array. Our Solid-State Division in Somerville, New Jersey will participate as a supplier of power amplifier subassemblies. It is our intention to arrange for at least two qualified suppliers of each functional circuit subassembly, as well as develop in-house (MSRD) capability for certain of these subassemblies, to ensure timely availability of these parts at a highly competitive cost.

RCA's extensive experience in providing space-qualified equipment directly to the Government, and to prime contractors such as Grumman, provides the necessary background to ensure success of this program. The facilities and expertise of our Astro Electronics Division in Hightstown, New Jersey, augmented by the scientific resources of the David Sarnoff Research Center in Princeton, New Jersey, will be utilized to provide and confirm the design for the space environment.

Appendix B

Mr. J. Schultz

-2-

7 June 1974

I hope that the enclosed attachments provide adequate information for your current study, and will serve as a sound basis for further joint participation in subsequent phases of the project. In the event that we can be of assistance to you in subsequent phases of this program, please contact Mr. J. Cavacini, Manager Contract Operations on extension PM 3744. If additional specific data is required, please do not hesitate to call me.

Very truly yours,

Frank Klawnsnik
Frank Klawnsnik

FK:jas

cc: Mr. J. Greene Grumman
 Mr. F. Rohr RCA-Solid-State Division

Attachment A

Technical Description
of a
Spaceborne Radar Transceiver

A complete microwave transceiver for a space-fed spaceborne phased array radar is described herein, which incorporates power amplification of the transmitted signal, low noise amplification of the received signal, provision for transmission of a communication signal without amplification, 3-bit phase shifting of all three signals for collimation and beam steering, logic and diode switches for TR and polarization switching, and a threshold detector circuit to generate the logic input from received RF pulses. The performance characteristics provided are detailed in the Preliminary Specification of Attachment B.

In order to provide these complex functions at minimum weight and cost, the transceiver will be constructed by using lumped element circuits for substantially all frequency selective and impedance transforming (matching) networks, using 75 ohm microstrip circuits for all interconnections (and RF terminals), and using unpackaged chip components for all active devices and large discrete passive elements. The entire assembly will consist of the chips mounted upon a 0.010-inch thick ceramic substrate (e.g. Al_2O_3). RF connections will be made by bonding from the system cabling (e.g., 3-wire or strip transmission line) to the 75 ohm microstrip at the edge of the substrate. Installation in the system will be by means of bonding the ground plane of the substrate (underside) to metallized graphite-epoxy composite supporting webbing. The DC power will be supplied to the module through these bonds, using multiple connections to both the ground plane and the bonding pads for the high voltage terminal.

The transceiver will be composed of functional circuits (viz. low noise amplifier, CMOS logic, power amplifier, phase shifter, etc.) which will be designed as replaceable parts at the final module assembly level, and will accordingly be individually amenable to multiple source procurement. The assembly will thus be exactly akin to low frequency hybrid circuit fabrication. Thin film metallization will be employed, using a thin layer of sputtered molybdenum to form a strong bond to the ceramic, and a layer of sputtered gold with an additional electroplated layer of gold to a total thickness of 0.0005-inch to provide low RF loss. All fabrication, assembly and processing will be performed in "white rooms" providing environmental control consistent with space hardware requirements.

Appendix B

Attachment B

Preliminary Specification for a Spaceborne Radar Transceiver

Operating Frequency	408-450 MHz
Power Output (Antenna Ports)	11.0 W (min)
Transmitter Gain (Port-Port)	20.5 dB (min) ± 0.5 dB
Pulsewidth	100-200 microseconds
Repetition Rate	562 (max)
Duty Factor	0.11 (max. for 0.1 second interval) .05 (max. for 1 second and longer intervals)
Noise Figure (Antenna Ports)	3.0 dB (max.)
Receive Gain (Port-Port)	20.5 dB (min) ± 0.5 dB
Dynamic Range	45 dB (min)
Phase Shift Capability	0°-360° in 45° increments, with RMS errors less than 10°.
TR Switching	High-Isolation to Low-Loss Rise Time 2 microseconds (max) Bias current only during "on"-period (low loss)
Receiver Gating	High-loss to High-gain Rise Time 2 microseconds (max) Bias current only during "on" period (high gain)
Polarization Switching	Antenna Port 1 to Port 2 Rise Time 2 microseconds (max) Bias current only during "on"-period (low loss for Port 1 or Port 2)
Envelope Detector	Biased Diode Detector and Directional Coupler at Pick-up Port with Threshold Circuit to convert received RF pulses to video logic level waveform compatible with Internal Logic.

Attachment B
Page 2

Internal Logic	Custom CMOS to receive output pulse train from Envelope Detector, decode, supply bias to Phase Shifter, TR Switches, Polarization Switches, and Receiver Amplifier as required.
Bypass	A signal path with Port-Port gain of $-35 \text{ dB} \pm 1.5 \text{ dB}$, when both Transmit and Receive amplifiers are deactivated by means of TR Switch and Receiver Gating, shall be provided.
Size	5 x 2 x 0.05 inches (max)
Weight	0.06 pounds (max); 0.03 pounds (design goal)
Connectors	75 ohm Z_0 microstrip for Pick-up, Antenna Port 1, and Antenna Port 2; Bonding Pads for DC.
Operating Temperature	0°C to +50°C (Absorptivity, Emissivity, Heat Sink Temperature and Structural Shadowing to be jointly determined by RCA and GAC).

Appendix C
Hughes Response to Customer CMOS Logic Inquiry



MICROELECTRONIC PRODUCTS DIVISION

500 SUPERIOR AVENUE • NEWPORT BEACH, CALIFORNIA 92663 • 714-548-0671 • TWX: 910-596-1374

December 21, 1973

Grumman Aerospace Corporation
Bethpage, New York 11714

Attention: Mr. J. Greene

Dear Mr. Greene:

We have evaluated your logic diagram and have determined that we cannot design a single custom chip to encompass the entire circuit. A first estimate indicates that the circuit will require two chips each approximately 140 X 140 mils in size. For your proposal effort we would suggest you use an approximate chip (unpackaged) cost of \$20 to \$25 each and a non-recurring engineering cost of \$35,000 each.

Since your program is quite distant we are officially submitting a No-Bid but the approximations given above are accurate as to the information we have at this time. When your program is firm we shall be pleased to consider the development of these chips. Thank you for your interest in Hughes.

Sincerely,

HUGHES AIRCRAFT COMPANY

A handwritten signature in dark ink, appearing to read "H.S. Evander", written over the typed name.

H.S. Evander
MOS Marketing Manager

HSE:sc

Section 5

CONFIGURATION

The configuration (Fig. 5-1) has a 300-m diameter flat-faced phased-array antenna located near the lower end of the satellite, with a 28-m diameter satellite-to-ground link antenna at its center. A 152-m mast locates and supports the antenna via two sets of stays (Fig. 5-2). The main solar arrays are boom-mounted from the upper end of the lower systems package (LSP). The lower end of the antenna mast structure mounts the lower set of attitude control thrusters. The upper end mounts the feed support mast, a free-standing (unguyed) mast that extends upward to locate and support the upper systems package (USP) 750 m from the main antenna. The USP contains the antenna feed array, upper set of attitude control thrusters, and solar paddles.

The phased-array antenna is supported by a compression rim assembly which, in turn, is supported by the spring-tension-loaded fore and back stays. These stays are 2 mils by 5/8-in. graphite/epoxy strips arrayed in back-to-back cones between the rim and stay reels on the mast. The phased-array antenna is made of gore panel assemblies that lie in the plane of the rim and are spring-tensioned between the rim and LSP.

The compression rim assembly is a ploygon 300 m in diameter, composed of 80 thin-wall tubes 11.5 m long and 4.25 in. in diameter.

The deployed rim assembly must hold radial (in-plane) tolerances of less than 0.45 m, and axial (out-of-plane) tolerances of less than 1.12 m. These tolerances are easily met by using low-temperature-coefficient graphite/epoxy material for the rim and stays.

The 80 triangular antenna array gore panel assemblies (Fig. 5-1) are made in sections and spliced together by circumferential mini-hinged beams that provide the required inter-layer spacing. The triple-layer panels consist of the following:

- A circularly polarized target-side dipole plane located 18 cm ($\lambda/4$) from the ground plane
- The ground plane, with phased-array modules and electrical conductors
- A linearly polarized feed-side dipole plane 18 cm from the ground plane.

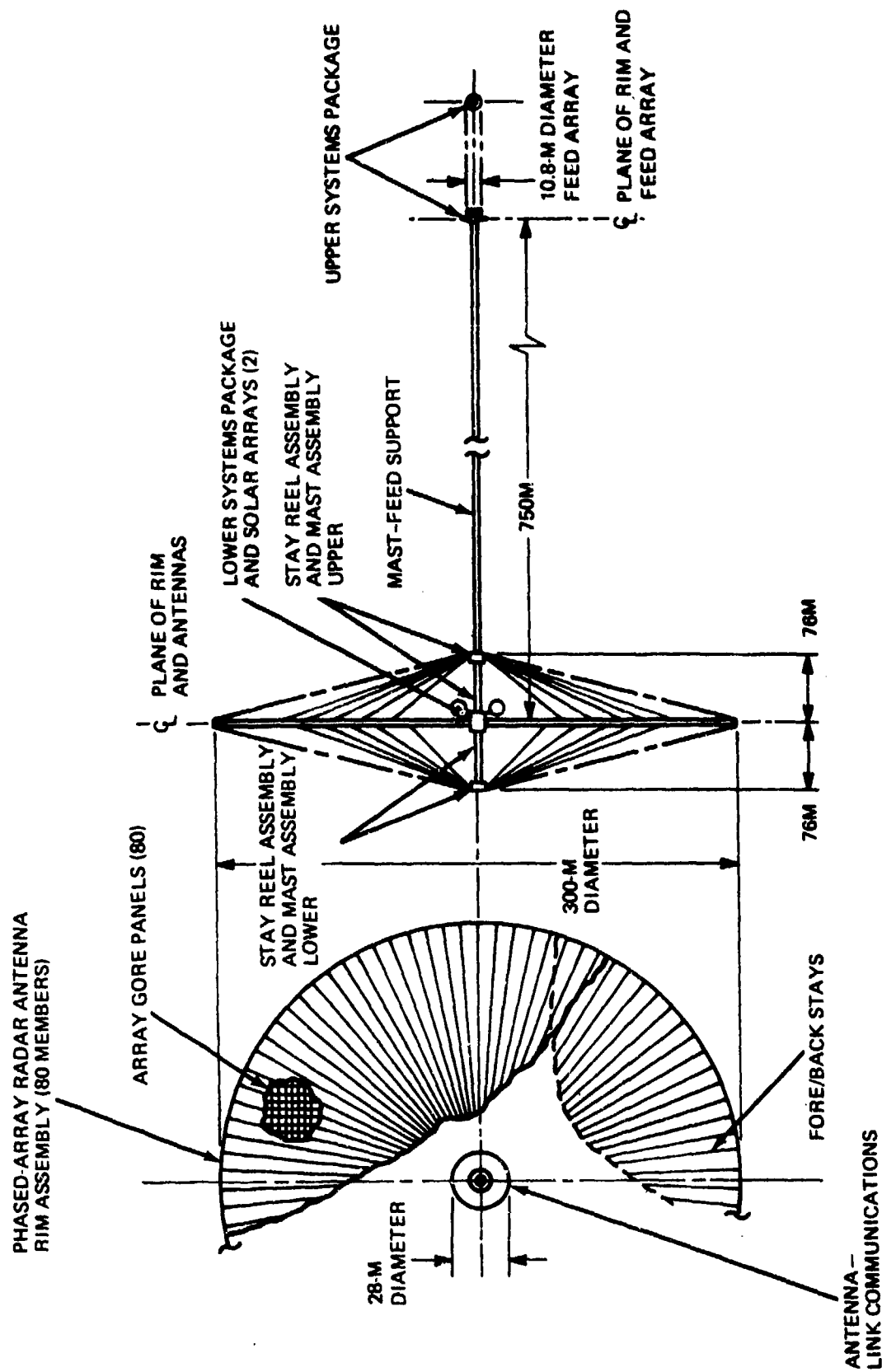


Fig. 5-1 Deployed Configuration, 300 Meter Diameter Phased-Array Radar Satellite

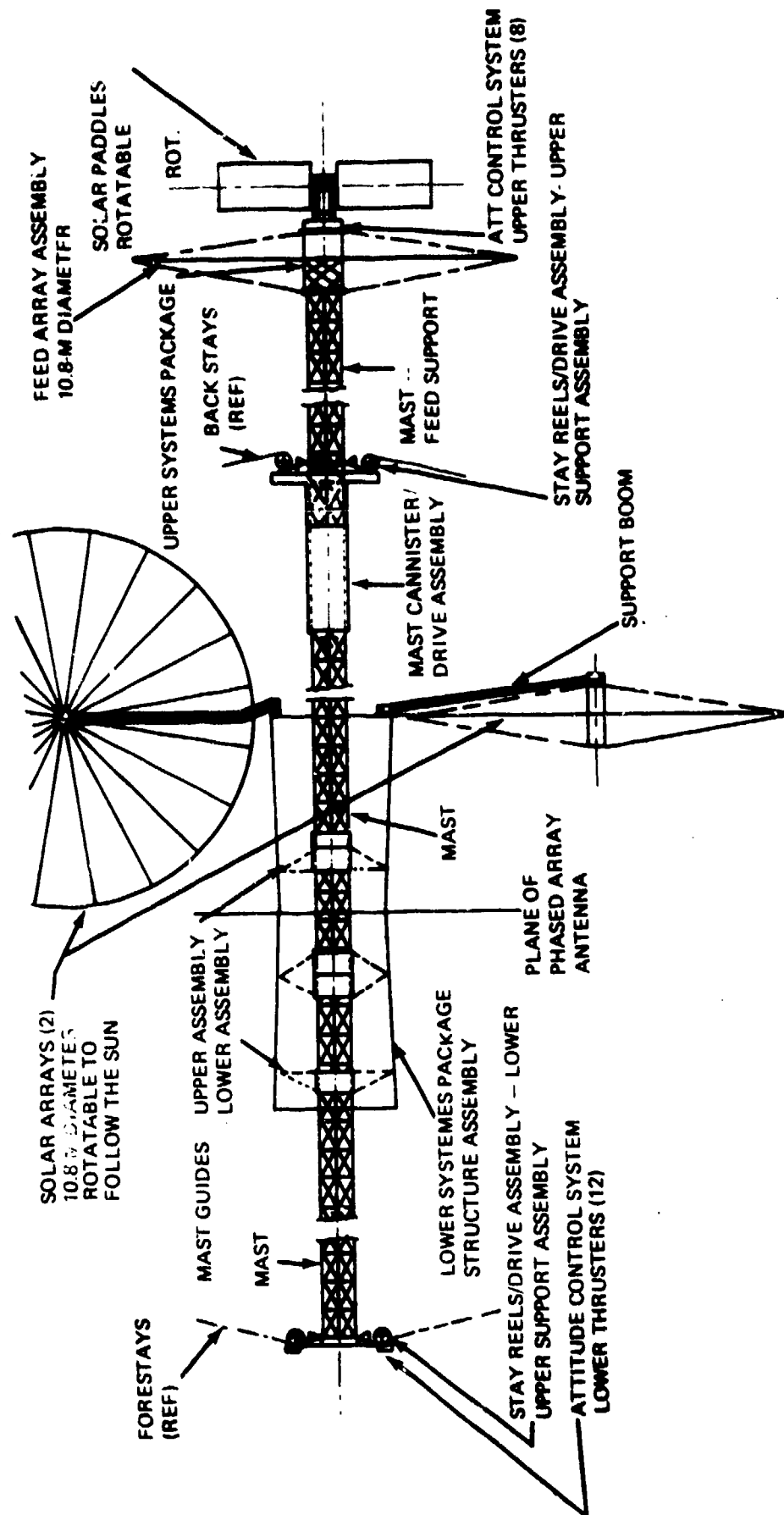


Fig. 5-2 Axially Arrayed Components Deployed

THIS PAGE HAS INTENTIONALLY

BEEN LEFT BLANK

The target-side plane consists of frame-mounted crossed-dipole subarrays. The frames, shown are assembled edge-to-edge into an axisymmetric array of rows and columns within the bounds of the gore section. Each frame is a 2.16 m square structure made of 2-mil by 0.25-in. graphite/epoxy strips. The subarrays of 16 crossed dipoles and feed lines are made of 1/2-mil aluminum mounted on a 1/2-mil TFE substrate mesh.

The ground plane consists of a square mesh of 2-mil by 20-mil tapes spaced 4.5 cm apart. The tapes are aluminum-coated, teflon-insulated graphite-epoxy mini-tapes spaced 4.5 cm apart. The mesh sections are reinforced with transverse graphite/epoxy battens spaced 2.16 m apart and bounded by radial edge tapes and transverse mini-hinges. The ground plane mesh, together with the aluminum-coated battens and aluminum conductor strips paralleling the edge tapes, provides a multiply redundant power distribution network to the T/R modules mounted on the ground plane.

The feed-side plane is the same size and arrangement as the target-side plane except as follows. The 2.16-m square frames enclose a 2.16-m diameter ring as shown in Fig. 5-4. This assembly is made of 2-mil by 0.2-in. graphite/epoxy strips. The linearly polarized 12 dipole/feed subarrays are made 1/2-mil aluminum on 1/2-mil TFE substrate mesh. Regardless of frame structural orientation, the required linear polarization is obtained by suitable subarray rotation within the circular portion of the frame.

The inboard ends of the 80 phased-array gore panels are preserved to form a 28-m diameter radar-to-ground link antenna. This antenna incorporates crossed dipoles in the target-side plane, a ground plane, and a corporate feed network plane.

The LSP, Fig. 5-2, is 11.5-m long and 3.4 m in diameter, and is fabricated principally of aluminum alloy in a stringer-and-frame reinforced, thin skin cylindrical configuration. Two external antenna rim support rings and a multiplicity of antenna gore edge/batten support studs in spiral patterns transfer antenna launch loads to the primary structure. Major components contained within are the dual-opposed 1-m diameter mast canisters and the associated mast guides. The dual main solar arrays are boom-mounted at the upper end of the LSP.

The USP, Fig. 5-2, is 2.1-m long and 1.0 m in diameter, and is fabricated in two parts. The lower section consists of quartz/epoxy rods in a cylindrical geodesic arrangement. The upper half is a cylindrical canister fabricated of aluminum. The solar array paddles are mounted on a support truss structure attached to the upper face of the canister. Stays at each end of the canister locate and stabilize the feed array.

The upper and lower stay reel and drive assemblies shown in Fig. 5-2 are basically identical except that the upper assembly includes the feed support mast canister and drive assembly while the lower assembly mounts the lower attitude control thrusters. The stay reels are mounted in a motor-driven, rotatable, jointed tubular ring. This ring, in turn, is mounted on an axially rotatable ring which is roller-supported and motor-and-pinion-gear-driven around a fixed ring. The support assembly includes a 1.0-m diameter, 0.25-m long central hub to which the mast is attached.

Each of the three masts shown in Fig. 5-2 is a wire-and-lattice-braced triangular cross-section "Astromast" with three cap members, each approximately 0.01 cm^2 in area. The mast fits within a 1.0-m diameter circle. The cap member material is uni-directional filament graphite/epoxy that minimizes thermal deflection. The antenna support masts are each 75-m long. The feed support mast is 375-m long.

The 10.8-m diameter feed array assembly, shown in Fig. 5-2, has 20 rim members and gore panels, and is mounted on the USP. The feed array structural arrangement is similar to that shown for the main radar antenna. The gore panel assemblies include only a linearly polarized dipole plane and a ground plane. The latter is used for electrical power distribution, and incorporates the RF feed network and T/R modules.

The main solar arrays, shown in Fig. 5-2 are each 10.8-m in diameter and are similar in structural arrangement to the feed array. The gore panels consist of solar cells mounted on a thin, flexible substrate. The arrays are boom-mounted from the LSP and are motor-driven to follow the sun. The arrays provide a 16 Kw to the LSP.

The 0.65 Kw upper solar paddles, shown in Fig. 5-2, are a pair of identical, rigid, flat panels with solar cells on one side. The paddles are electrically motor-driven. The paddles provide a total solar cell area of 7 m^2 .

Twenty attitude control thrusters of the pulsed-plasma, solid-propellant type are used. Required thrust levels are on the order of 50-100 μ lb per thruster. Twelve thrusters mounted on the LSP provide stationkeeping, roll control, and part of the pitch and yaw control. The remaining eight thrusters are mounted on the USP to complete the pitch and yaw control.

The preliminary weight estimate follows:

		<u>LB</u>	<u>Kg</u>
● Phased-array Main Antenna	—————→	4160	1890
- Rim assembly	600		
- Dipole plane frames - target side	440		
- Dipole plane frames - feed side	440		
- Ground plane mesh	680		
- Dipole subarrays - target side	390		
- Dipole subarrays - feed side	265		
- Edge tapes	140		
- Conductor tapes	385		
- Stays	70		
- Mini-hinges	250		
- T/R modules	500		
● Lower Systems Package (LSP)	—————→	2580	1170
- Primary cylinder structure	1070		
- Dual-opposed mast canisters/drives/masts	180		
- Feed support mast cannister/drive/mast	470		
- Stay reel assemblies - upper/lower	150		
- Main solar arrays	460		
- Other systems installations	250		
● Upper Systems Package (USP)	—————→	410	186
- Primary cylinder structure	90		
- Feed array assembly	80		
- Solar Paddles	75		
- Other systems installations	165		

	<u>LB</u>	<u>Kg</u>
● Contingency Allowance _____ (Payload Adapter, Shroud Penalty, & Misc. Hardware)	750	340
● Radar Satellite Launch Weight _____	7900	3586

Section 6

LIFE-CYCLE COST ESTIMATE

Ten-year life-cycle cost estimates were made of the geostationary radar satellite system, using a parametric cost model that relates cost to weight, size, or power. The model results account for various levels of technology and degrees of complexity. A summary of the program level cost elements and a breakdown of costs, on a per space-craft basis, are presented in Tables 6-1 and 6-2.

Although the satellites have a 5-year life, three satellites were assumed to be required for each station for a 10-year life. The ground station network is described and costed in the separate report by the Sperry Gyroscope Division.

TABLE 6-1. LIFE CYCLE COST SUMMARY

	10-Year Life Cycle Cost, M \$1974	
	3 Satellite Stations Perimeter Coverage	7 Satellite Stations Worldwide Coverage
DDT & E	241	241
Investment for S/C ⁽¹⁾	240	503
Investment for 4V ⁽¹⁾	265	619
Operations	(2)	(2)
TOTAL (Less Ops)	746 ⁽³⁾	1383 ⁽³⁾
<p>Notes:</p> <p>(1) Each S/C has a 5 yr design life, but 3 S/C per station were assumed for a 10-yr period.</p> <p>(2) Ground Station and 10-yr operations costs to be supplied by Sperry under separate cover.</p> <p>(3) Assumes 90% learning curve.</p>		

TABLE 6-2. SPACECRAFT AND LAUNCH VEHICLE COSTS

	M \$1974	
	Non Recurring RDT & E	Recurring Unit Cost
Spacecraft		
• Phased-Array Antenna	41	3 ⁽¹⁾
• Lower Systems Package	78.5	17.5
• Upper Systems Package	27	3.0
• Miscellaneous	7.5	1.5
TOTAL SPACECRAFT	154	25
System Integration & Test, Prog Mgmt 10% spares, Qual Test, etc.	54	8
AGE, Special Test Equip, Test Facilities	19.5	-
TOTAL SPACECRAFT RELATED	227.5	33
Launch Vehicle Related	14	29.5
<p>Notes:</p> <p>(1) Modules assumed @ \$100 each</p>		

Section 7

STRUCTURAL MECHANICS AND RIGID BODY DYNAMICS

The satellite configuration described in Section 5 is the final design; this Section reports on an earlier, slightly different, design. The structural analysis results indicate that the tolerances held are orders-of-magnitude smaller than the allowable tolerances. Thus, the differences between the two configurations are insignificant.

7.1 STATIC STRUCTURAL ANALYSIS

The geostationary satellite structural analysis was performed utilizing the finite-element method and the NASTRAN finite element program developed by NASA. Capable of handling very large problems, NASTRAN can perform a variety of analyses, including static and thermal stress, vibration mode, and buckling.

In the finite-element method, the structure is first "idealized" as an assemblage of individual structural components or elements. The results of the structural model computer analysis are used to predict the actual structure's behavior.

NASTRAN uses the stiffness method of structural analysis. The input data consists of node geometry, member connection data and properties, boundary conditions, and external loads. The program generates the stiffness matrix and member stress matrices used to solve the problem. Output for a statics problem consists of displacements, element stresses, and reaction. The structure can also be plotted in the deformed or undeformed state.

During the present investigation, the following analyses were performed:

- Static analysis under pretension load (reported below)
- Static analysis under pretension load with a broken stay (reported below)
- Buckling analysis ● Vibration analysis
- Thermal stress analysis

7.1.1 Structural Model

Figures 7-1 through 7-5 shows the finite element model of the geostationary satellite. It consists of a ring composed of 32 straight-beam elements stabilized by a set of 64 stays - 32 front stays and 32 back stays. Each stay bifurcates and supports two points on the rim. The gore structure supporting the phased-array antenna lies in the ring plane and is modeled with membrane triangles bounded on two sides by bar elements. The antenna feed is located at the mast end which is idealized with beam elements.

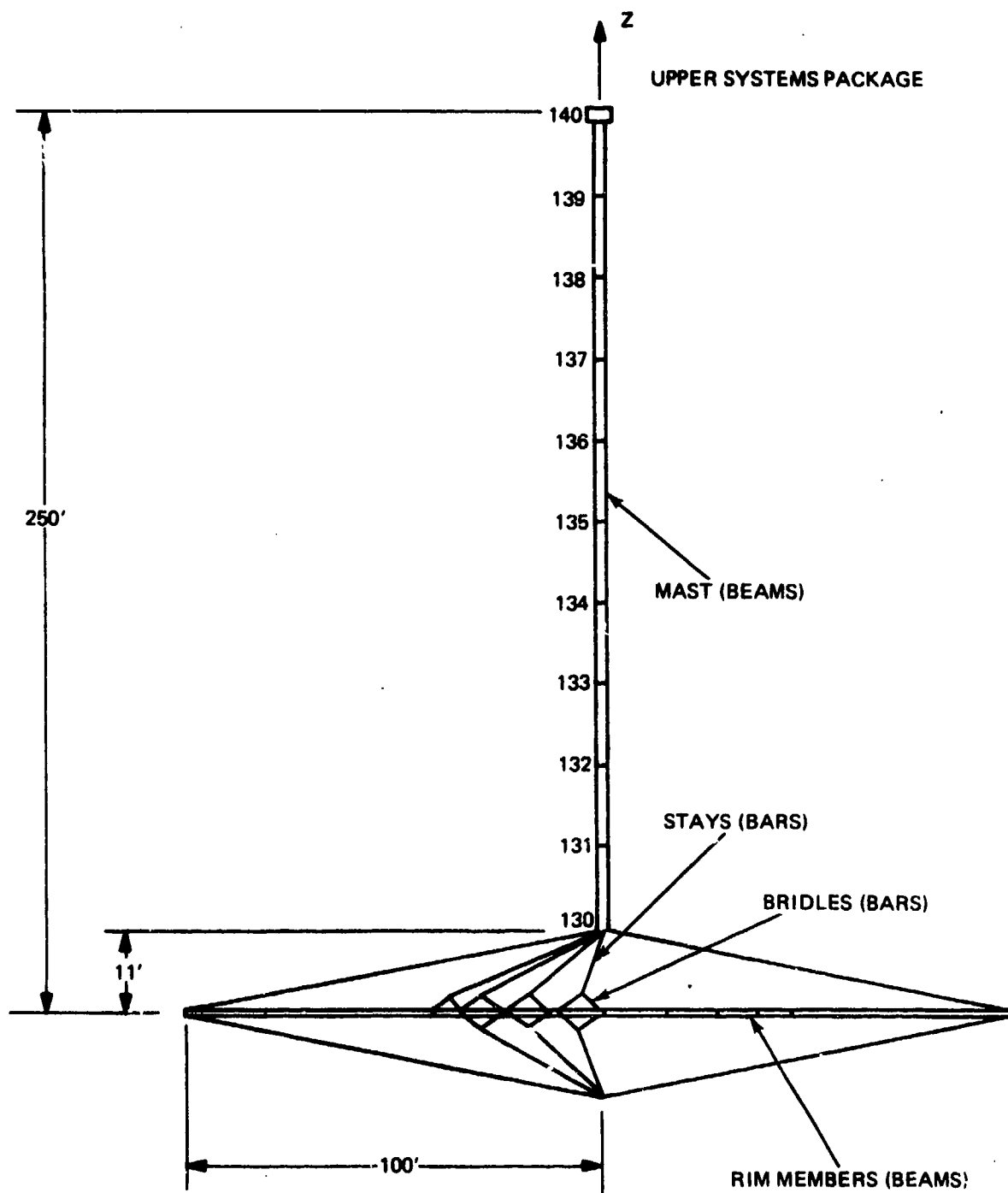


Fig. 7-1 Structural Idealization

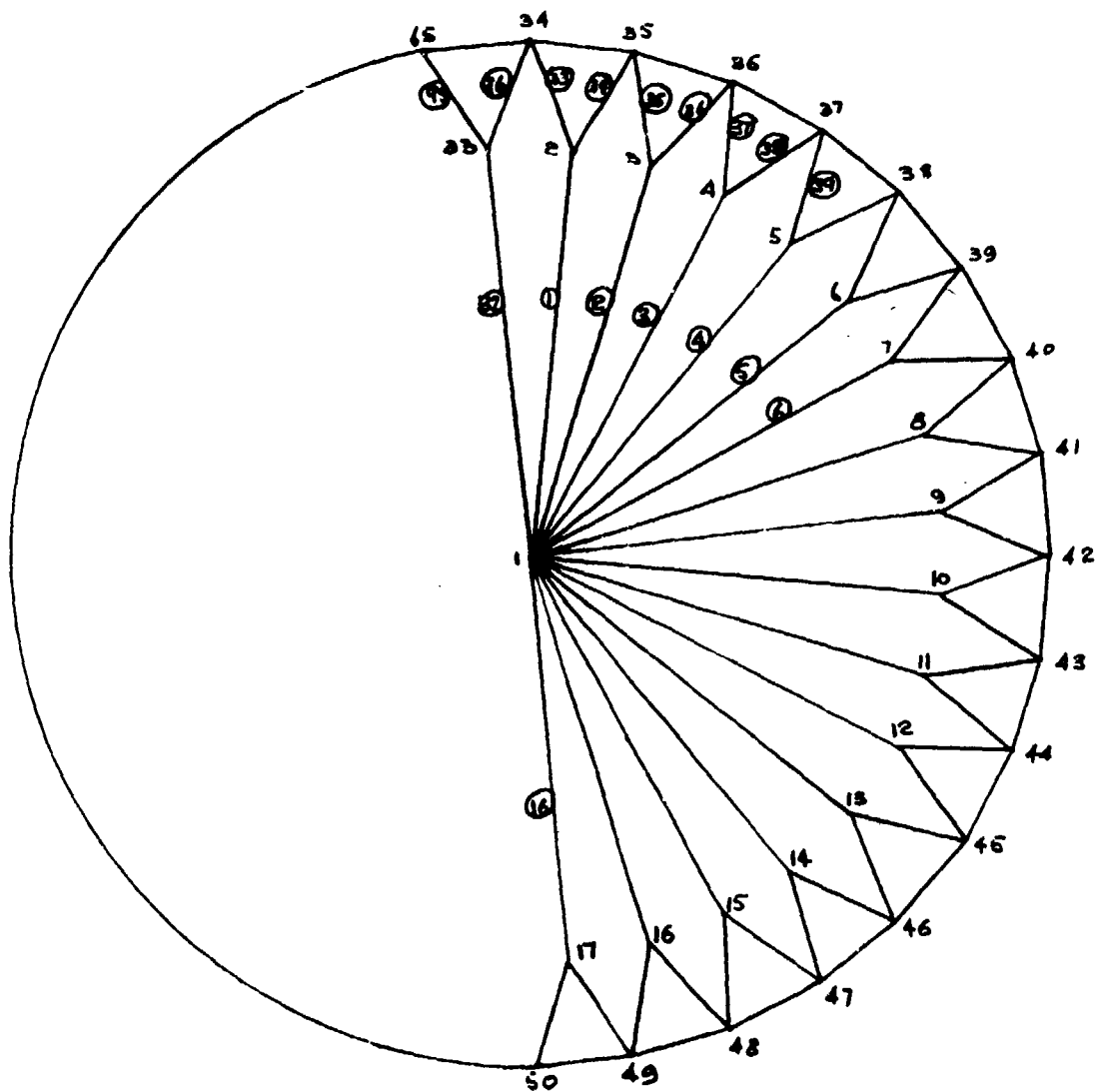


Fig. 7-2 Back Stays and Bridles

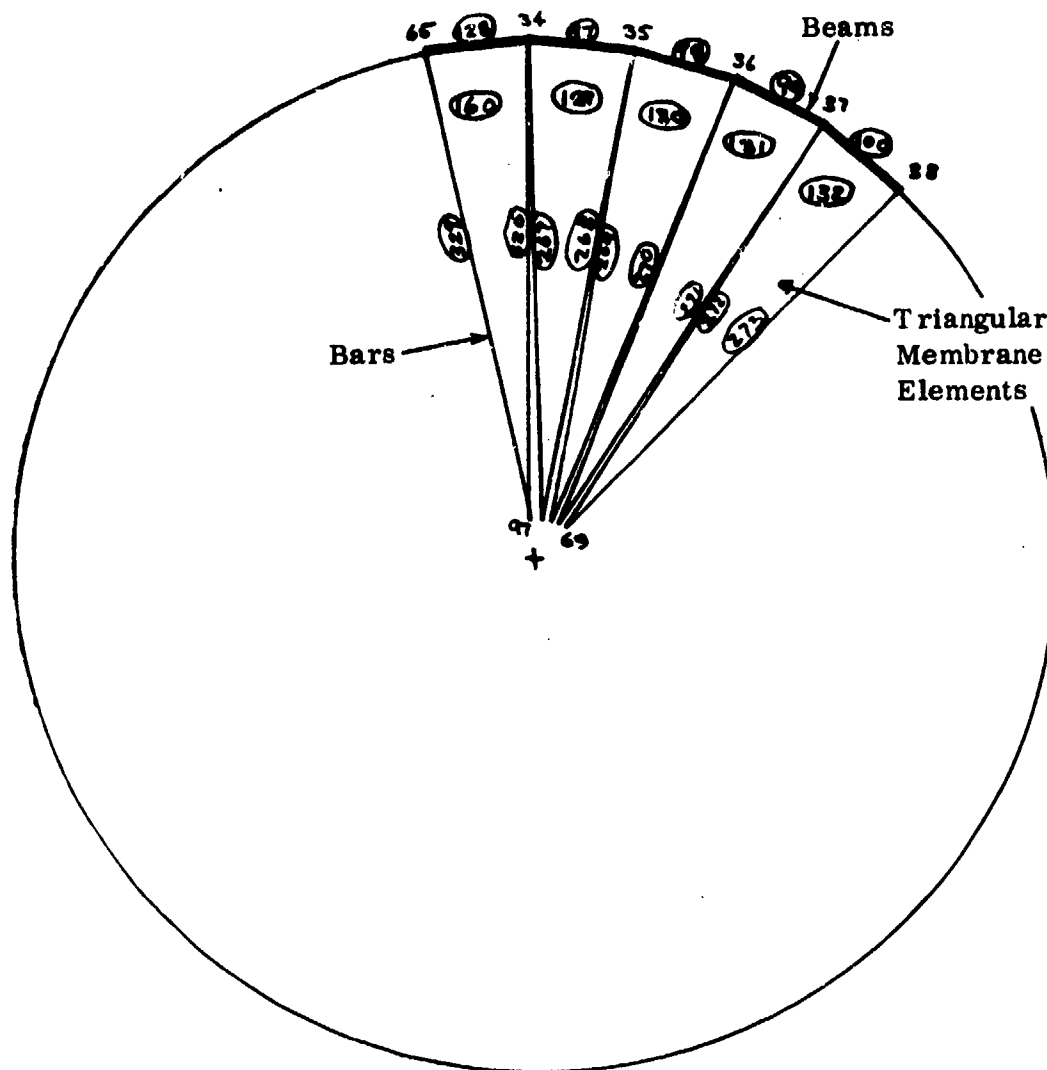


Fig. 7-3 Gore Structure and Rim

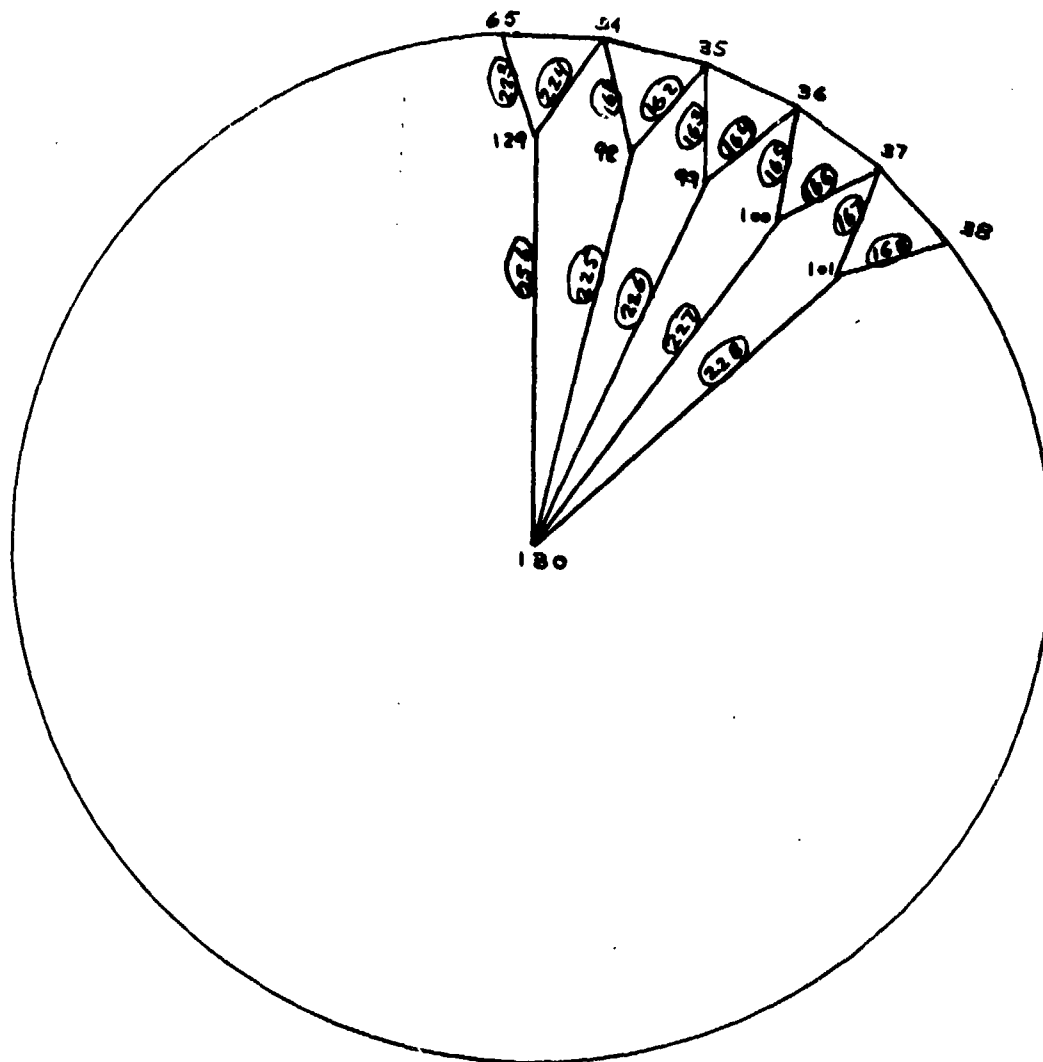


Fig. 7-4 Front Stays and Bridles

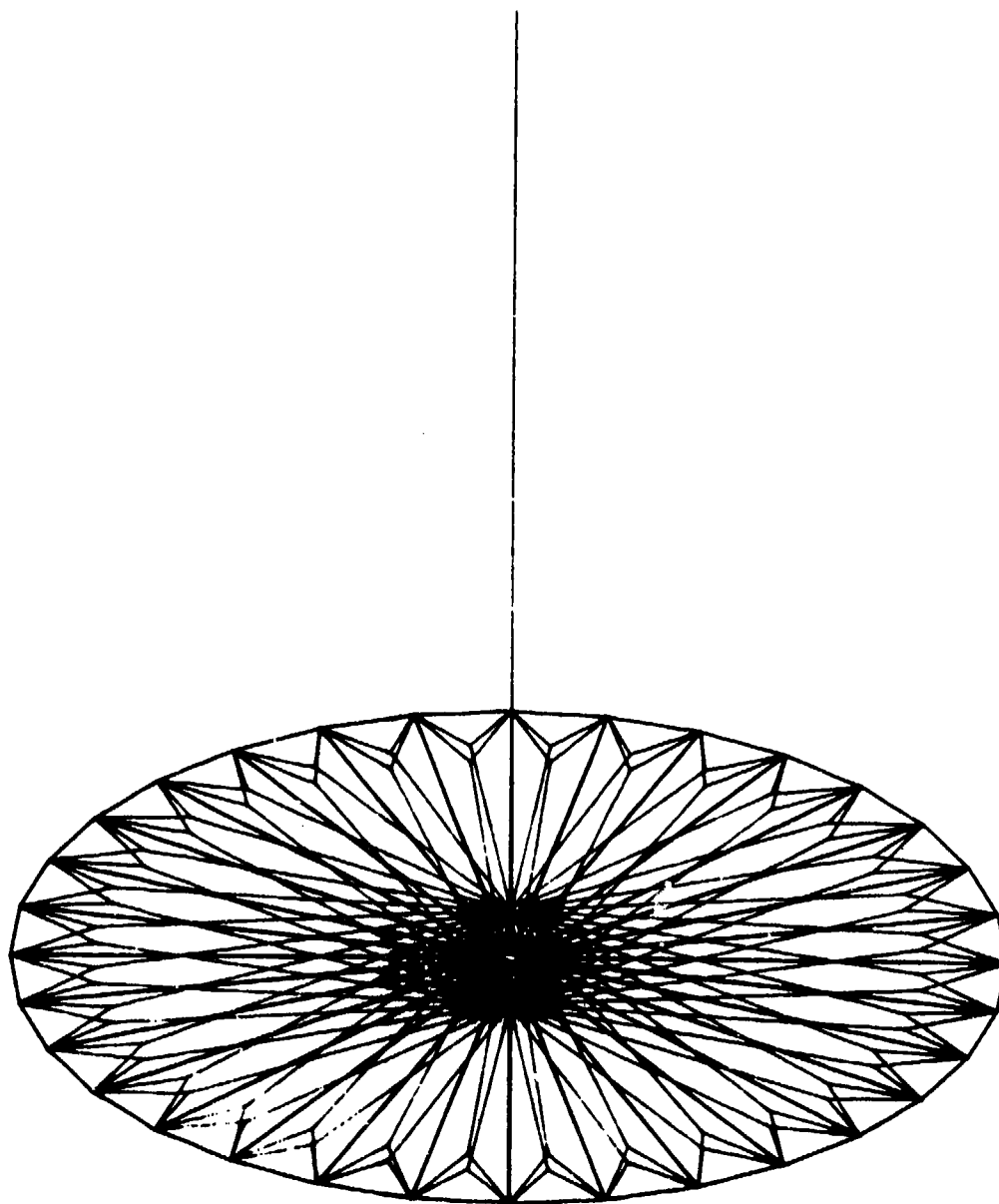


Fig. 7-5 Computer-Generated Structural Idealization

The member properties of the model are:

- Stays and Bridles

- Material: Graphite Epoxy
- Area = 0.0015 in.^2
- $E = 25 \times 10^6 \text{ psi}$

- Rim

- Material: Graphite Epoxy
- Area = 0.2128 in.^2
- $I = 0.4769 \text{ in.}^4$
- $J = 0.9538 \text{ in.}^4$
- $E = 25 \times 10^6 \text{ psi}$

- Gore

- Triangular membrane elements:
 - o Material: Quartz
 - o Effective thickness = $2.77 \times 10^{-6} \text{ in.}$
 - o $E = 7 \times 10^6$
 - o $E_r = 61.46 \times 10^6$
 - o $r = 0.0$
- Edge bars:
 - o Material: Quartz
 - o $A = 0.76 \times 10^{-3} \text{ in.}$
 - o $E = 7 \times 10^6$

- Mast

- Material: Graphite Epoxy
- $A = 0.09 \text{ in.}^2$
- $I = 14.58 \text{ in.}^4$
- $J = 4.0 \text{ in.}^4$
- $E = 25 \times 10^6$

7.1.2 Static Analysis

The structure was supported in a statically determinate fashion and two different cases were considered. In the first, the structure was subjected to a pre-tension load; and the second, a stay was broken (by removing it) in the pre-tensioned structure.

- Pre-tension Load. The stays and bridles were pre-tensioned by applying a 0.87472 load in the z direction at node 130 while holding node 1 fixed. The gore material was pre-tensioned by applying radial loads of 0.47 lb at the apex of each triangular membrane element, i. e., nodes 66 to 97 in Fig. 7-3. This loading resulted in the following member loads:
 - Stays: axial tension = 0.249 lb
 - Bridles: axial tension = 0.145 lb
 - Rim: axial compression = 5.04 lb
 - Gore-edge tapes: axial tension = 0.081 lb
 - Triangular membrane elements: $\sigma_{\theta\theta} = -6.634$ psi
 $\sigma_{rr} = 945$ psi
- Pre-tension Load with Cable Broken. The rim deflections resulting from the removal of stay number 225 and bridles 161 and 162 (see Fig. 7-4) are shown in Fig. 7-6 and 7-7. Figure 7-6 shows the rim's axial deflection in the vicinity of the broken stay while Figure 7-7 shows the radial deflection. The resulting maximum loads in the members were:
 - Stays: axial tension = 0.37 lb
 - Bridles: axial tension = 0.215 lb
 - Rim: axial compression = 5.07 lb
bending moment = 3.07 in. -lb
torque = .425 in. -lb
 - Gore: edge tapes axial tension = 0.081 lb
triangular membrane elements $\sigma_{\theta\theta} = -6.67$ psi
 $\sigma_{rr} = 945$ psi

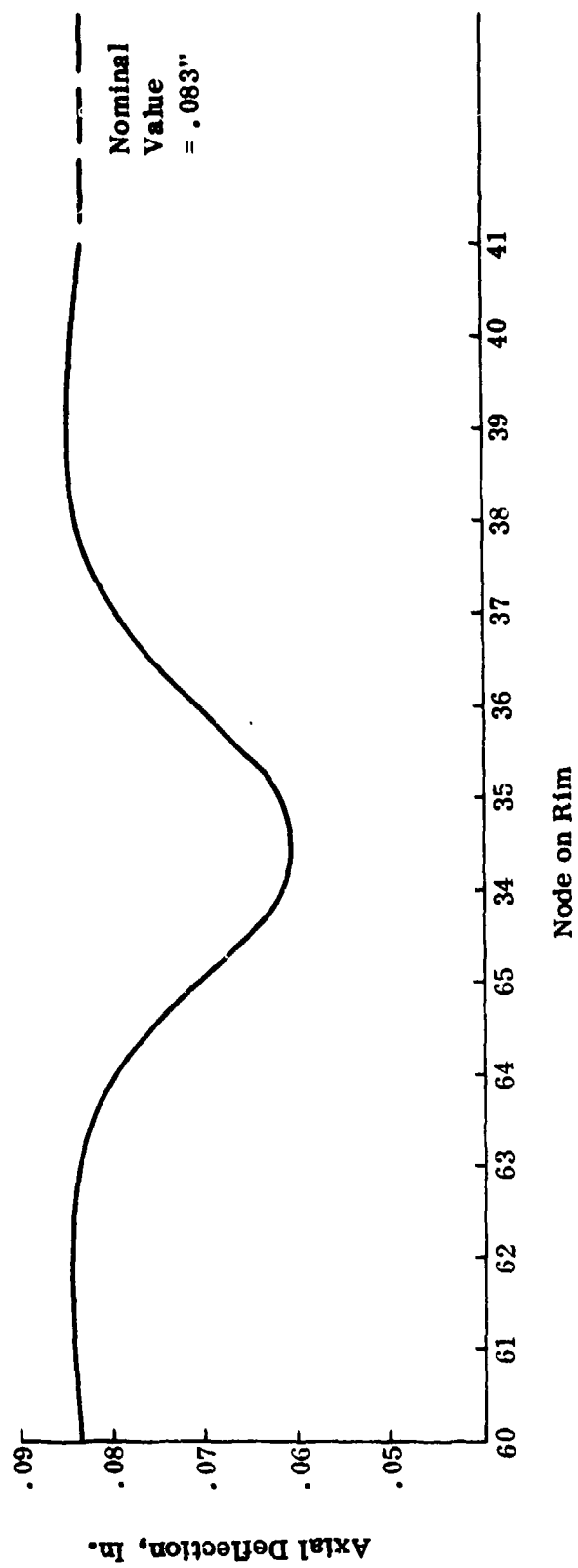


Fig. 7-6 Axial Deflection of Rim Due to Broken Cable

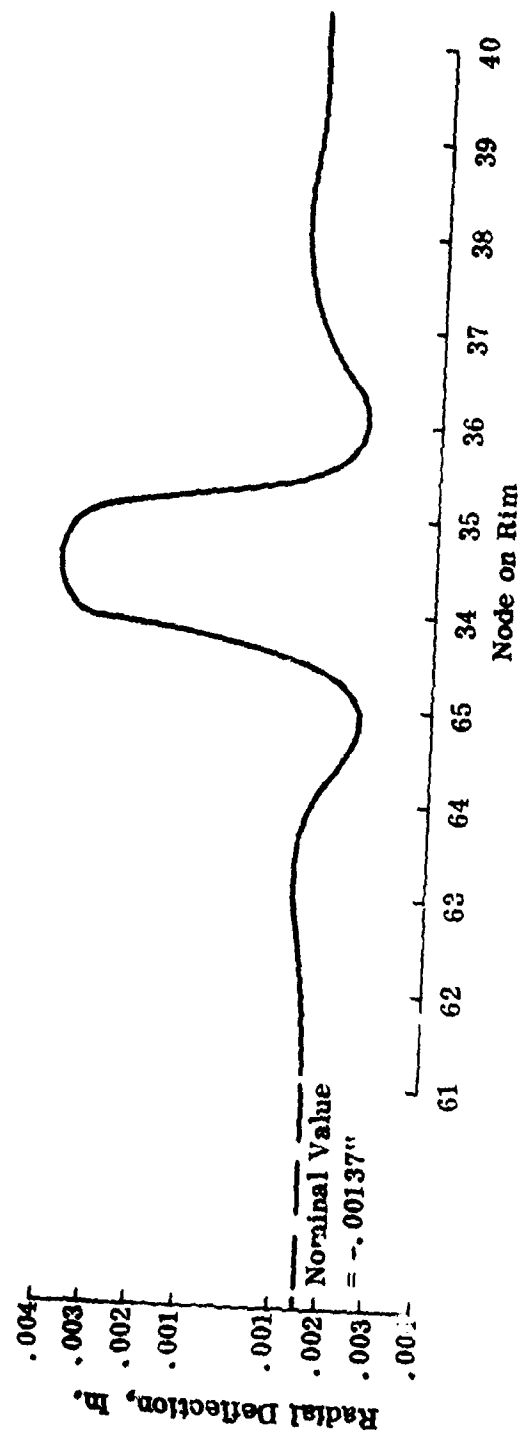


Fig. 7-7 Radial Deflection of Rim Due to Broken Cable

7.2 BUCKLING ANALYSIS

Buckling analysis of the geostationary satellite employed both manual computations and the NASTRAN finite-element program.

The structure was considered to be a circular ring under a compressive load on continuous elastic supports. The compressive load in the ring arises from pre-tensioning the structure. Table 7-1 lists the results of manual computations⁽¹⁾ and the finite-element computer program for the lowest buckling load. Figure 7-8 shows a NASTRAN-generated plot of the buckling mode shape. Note that the lowest buckling load corresponds to an out-of-plane mode shape and that the results of the manual computations are in close agreement with those of the finite-element solution. The compressive load in the ring due to pre-tensioning the structure was 5 lb.

TABLE 7-1 RESULTS OF BUCKLING ANALYSIS

	Manual Computations	Finite-Element Solution
Critical Load in ring, lb	360.7	353.7
No. of waves around circumference	5	5

7.3 VIBRATION ANALYSIS

A free-vibration analysis of the satellite structure was made using the finite-element program, and manual computations were used for checking some of the frequencies.

The mass of the structure was lumped at the model's nodes, as shown in Table 7-2. The mass of the gore material was distributed by lumping 50% of its weight on the nodes of the rim and the remaining 50% on the mast node at the rim's center. The mass of the LSP was distributed as follows: 1/6 on each of the top and bottom LSP nodes (nodes on mast where top and bottom stays are attached), and 2/3 on the center node. Table 7-3 shows the analysis results for the first 14 modes. Note that, except for the first and tenth, the modes occur in pairs. Those involving rim bending only (4 and 5, 6 and 7, 8 and 9, etc.)

¹ Chenney, J. A., "Bending and Buckling of Thin Walled Open Section Rings", ASCE, Journal Eng. Mech. Div., October, 1963.

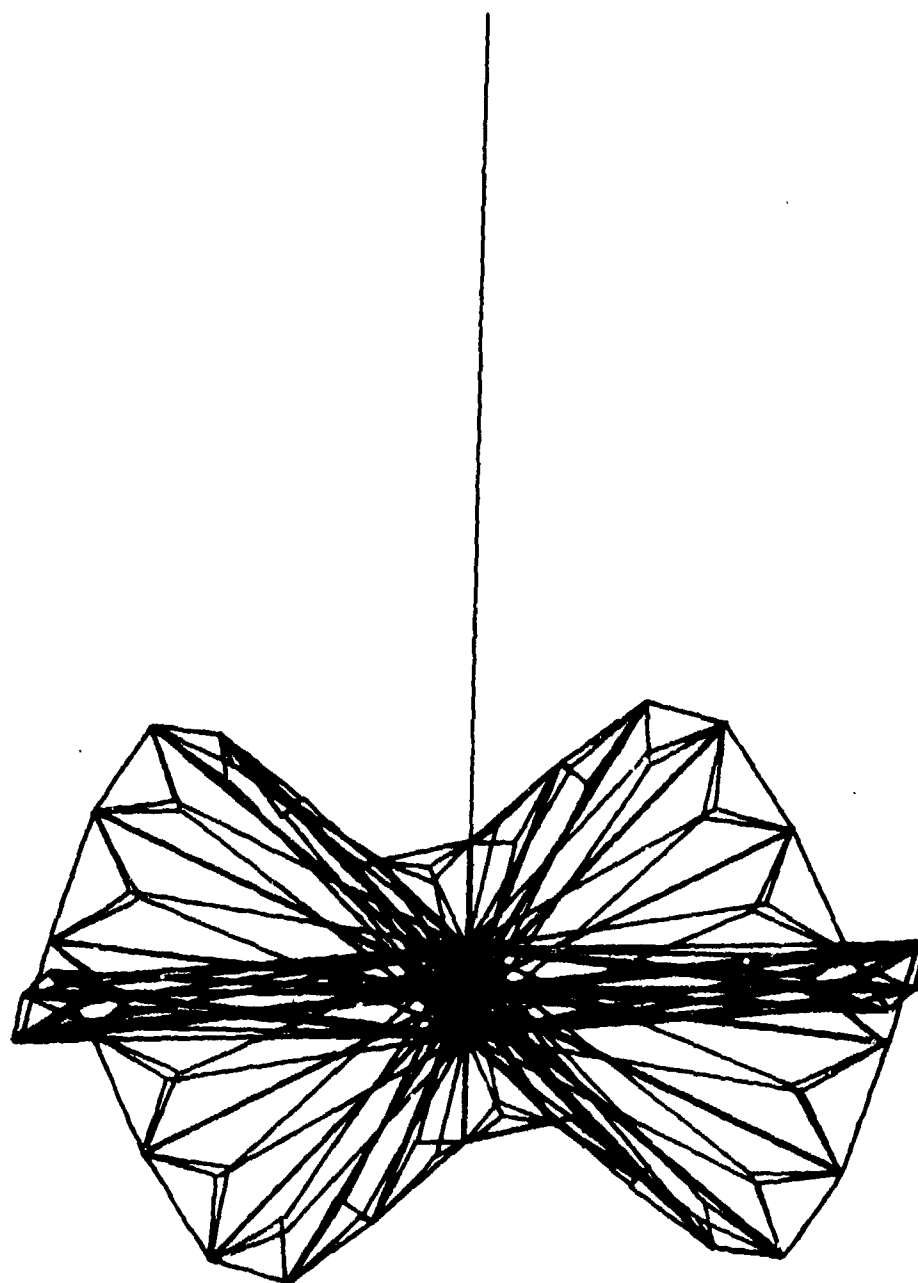


Fig. 7-8 Mode Shape for Lowest Buckling Load

TABLE 7-2 DISTRIBUTION OF LUMPED MASSES ON FINITE ELEMENT VIBRATION MODEL

Nodes		Weight, lb	Mass	I_{xx}	I_{yy}	I_{zz}
1.	Attachment Point of Back Stays	118.3	.30625	0	0	0
130.	Attachment Point of Front Stays	120.7	.31245	0	0	0
34-65.	On Rim	19.52	.0505	0	0	0
131-139.	On Mast	4.8	.01242	0	0	0
140.	At Top of Mast (Upper Systems Package)	262.4	.6799	0	4930	4930
200.	On Midplane of Ring on Mast	965	2.497	0	0	0

TABLE 7-3 NATURAL FREQUENCIES OF SATELLITE STRUCTURE

Mode Number	Frequency, cps		Type of Motion
	Finite Element Program	Hand Computations	
1	.0668	.0693	Torsional—rim rotates in one direction and mast in the other.
2	.10256	.117	Mast bending — about y axis about x axis
3	.10270		
4	.61747	.6212	$m = 2$ } $m = 3$ } Rim bending—out of plane $m = 4$ } $m = \text{No. of waves around circumference}$
5	.61747		
6	.6295		
7	.6295		
8	.6887		
9	.6887		
10	.7436		Mast moves back and forth through rim
11	.7993		Mast bending about y axis
12	.82025		$m = 5$ Rim bending out of plane
13	.82025		
14	.8680		Mast bending about x axis
23	2.09962		Mast bending about y axis
26	2.73765		Mast bending about x axis

have identical frequencies since the rim is axisymmetric. The pairs involving mast bending differ slightly in frequency because I_{xx} differs from I_{yy} for the USP. Figure 7-9 shows the second vibration mode.

7.4 THERMAL STRESS ANALYSIS

Figure 7-10 shows the temperature distribution used in the geostationary satellite stress analysis. Note that temperatures are given for the stays only, the rim, gore, and mast are assumed to remain at the structure's mean temperature (165°K). In addition to the temperature condition, pre-tensioning loads were applied to the structure. Figures 7-11, 7-12, and 7-13 show the resulting structure deformations. Figure 7-11, a computer-generated plot, shows that axial deformation of the rim is predominant. The axial and radial rim deflections are plotted in Fig. 7-12 and 7-13, respectively. The stresses in the structural members due to the temperature distribution are negligible.

7.5 BUCKLING ANALYSIS

7.5.1 Buckling of Lower Systems Package Cylinder

In the launch configuration, the gores are wound under tension on the LSP cylinder. This produces an inward radial pressure on the cylinder that can cause buckling. The 32 gore segments are wrapped so that the edge tapes do not overlap. If it is assumed that the wrapping tension loads only the edge tapes then, since there are two tapes per inch, the radial pressure on the cylinder is uniform and is

$$P = \frac{T}{R} = \frac{5}{24} = 0.208 \text{ psi}$$

If it is assumed that the wrapping tension is carried uniformly across the full gore section, then the pressure on the cylinder will vary since the gore segments are triangular sectors and the cross-sectional area increases along the length of the sector. The highest pressure that the cylinder experiences, which is at the central section, is $P = 1.36 \text{ psi}$.

The LSP cylinder is made up of two shallow conical frustrums. For this analysis the cylinder is assumed to be circular and is reinforced with rings and stringers with the following dimensions:

Cylindrical Shell	Rings	Stringers
$D = 48 \text{ in.}$	$A = 0.120 \text{ in.}^2$	$A = 0.950 \text{ in.}^2$
$t = .025 \text{ in.}$	$I = 0.104 \text{ in.}^4$	$I = 0.0205 \text{ in.}^4$
$L = 282 \text{ in.}$	$J = 0.409 \times 10^{-4}$	$J = 0.07 \times 10^{-4}$

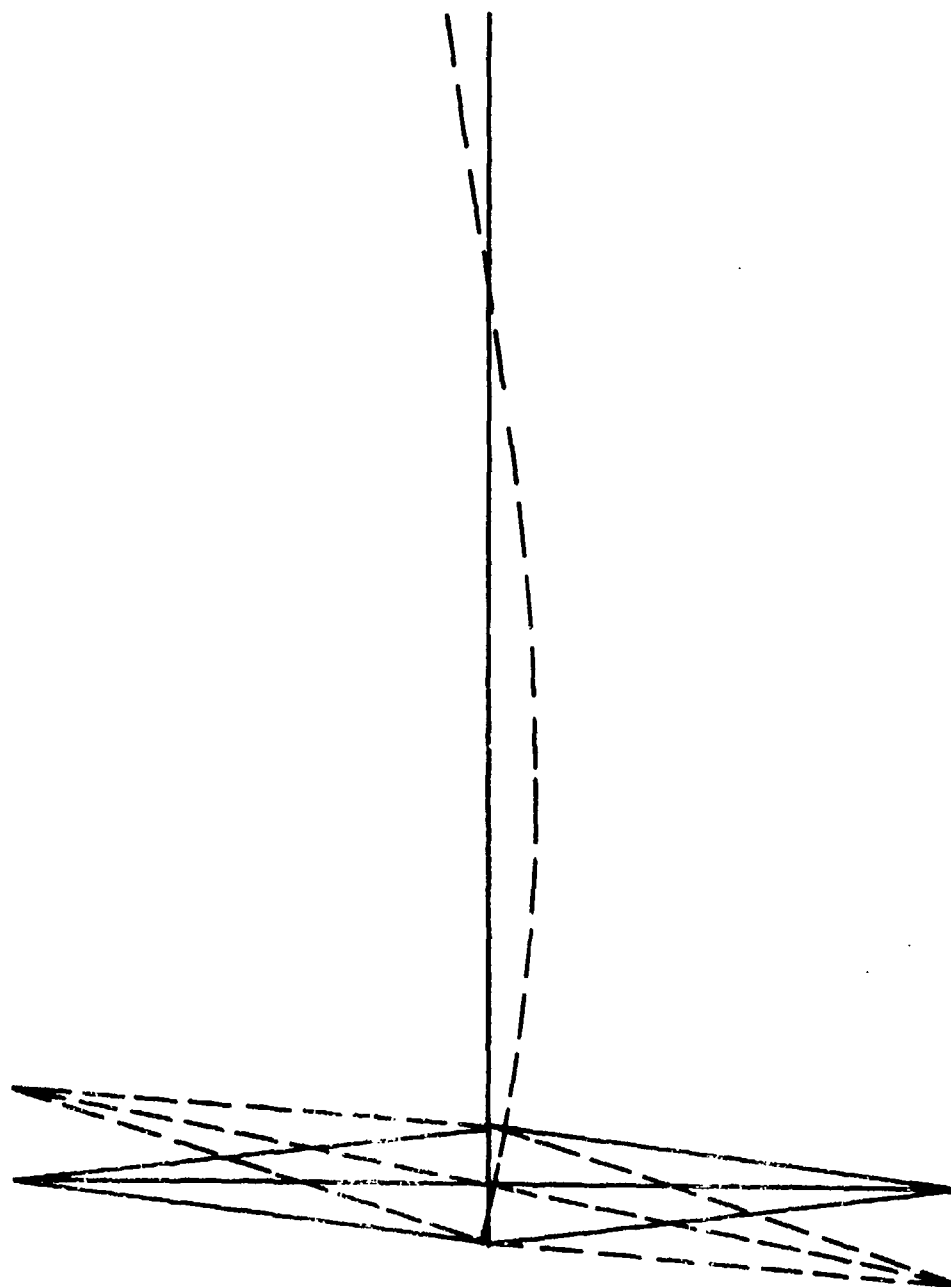


Fig. 7-9 Second Vibration Mode, $f = .10256$ cps

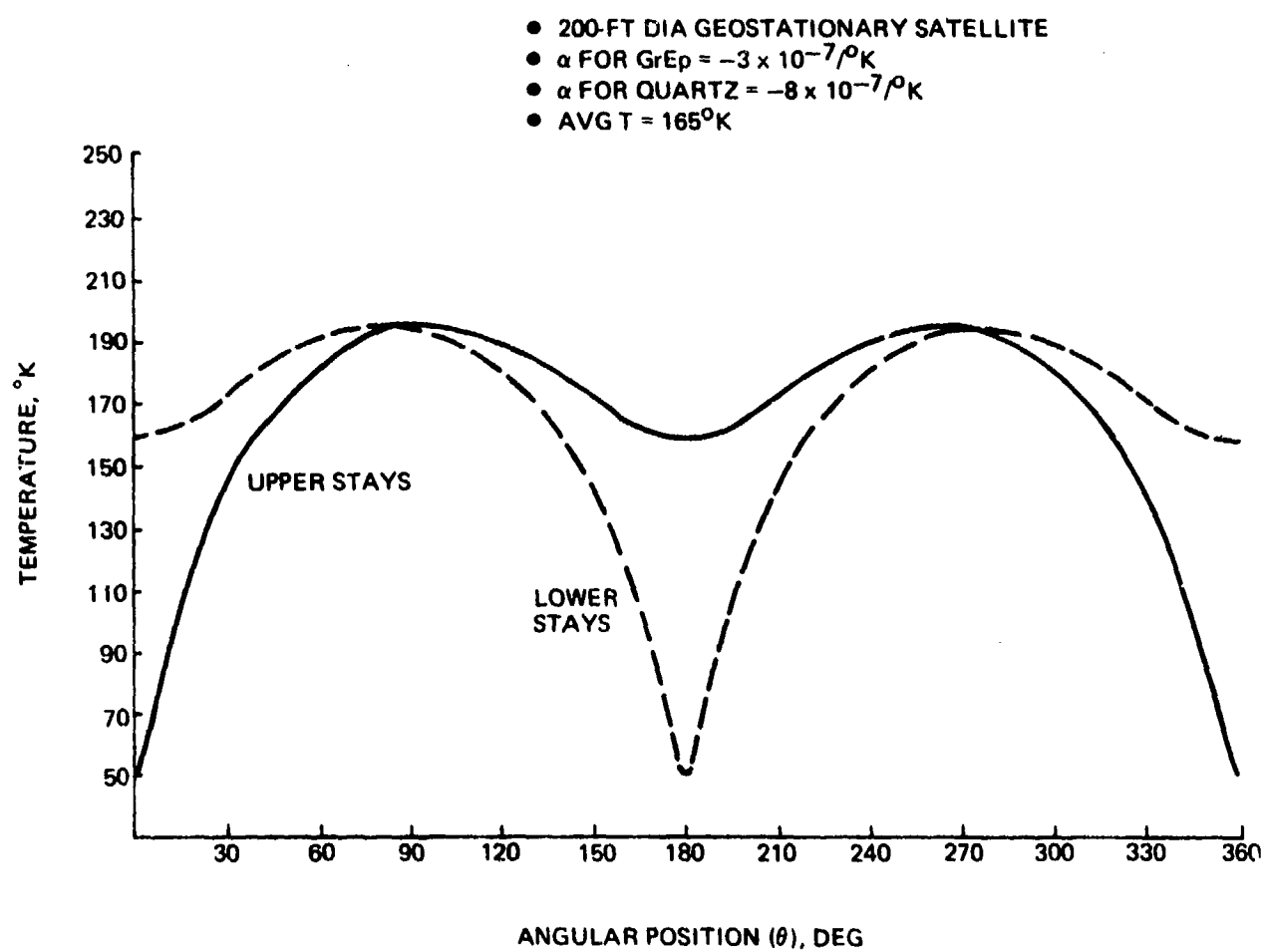


Fig. 7-10 Temperature Variation of Stays

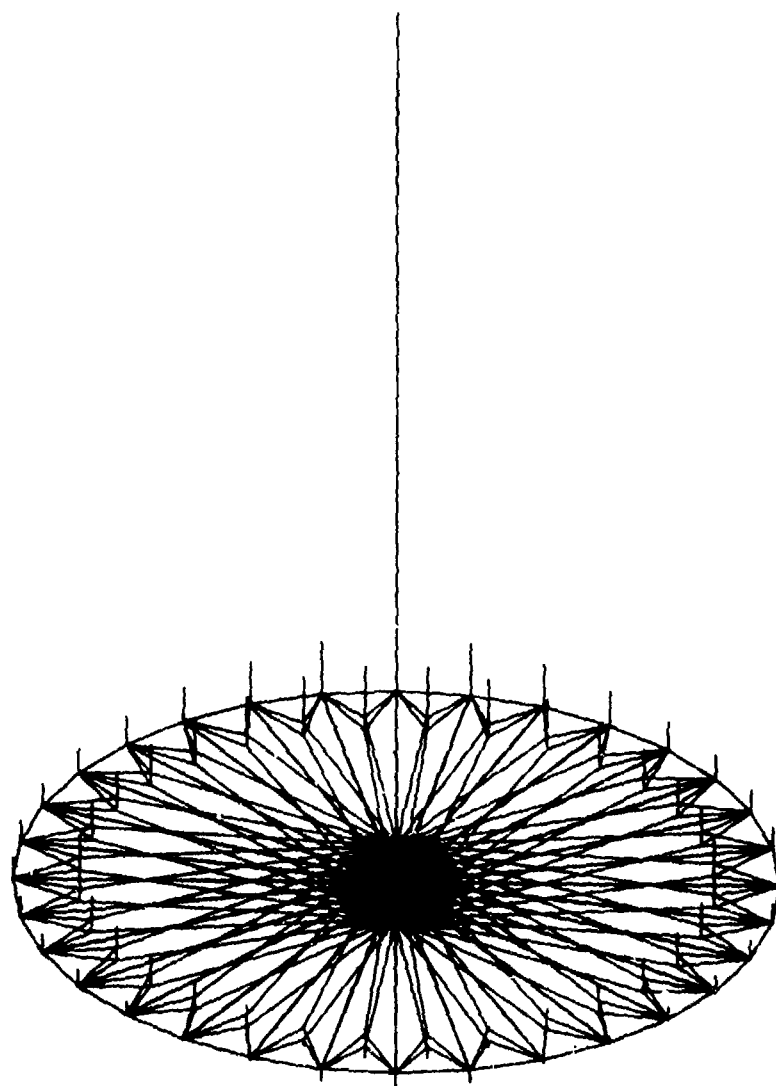


Fig. 7-11 Structural Deformations from Thermal Stress Analysis

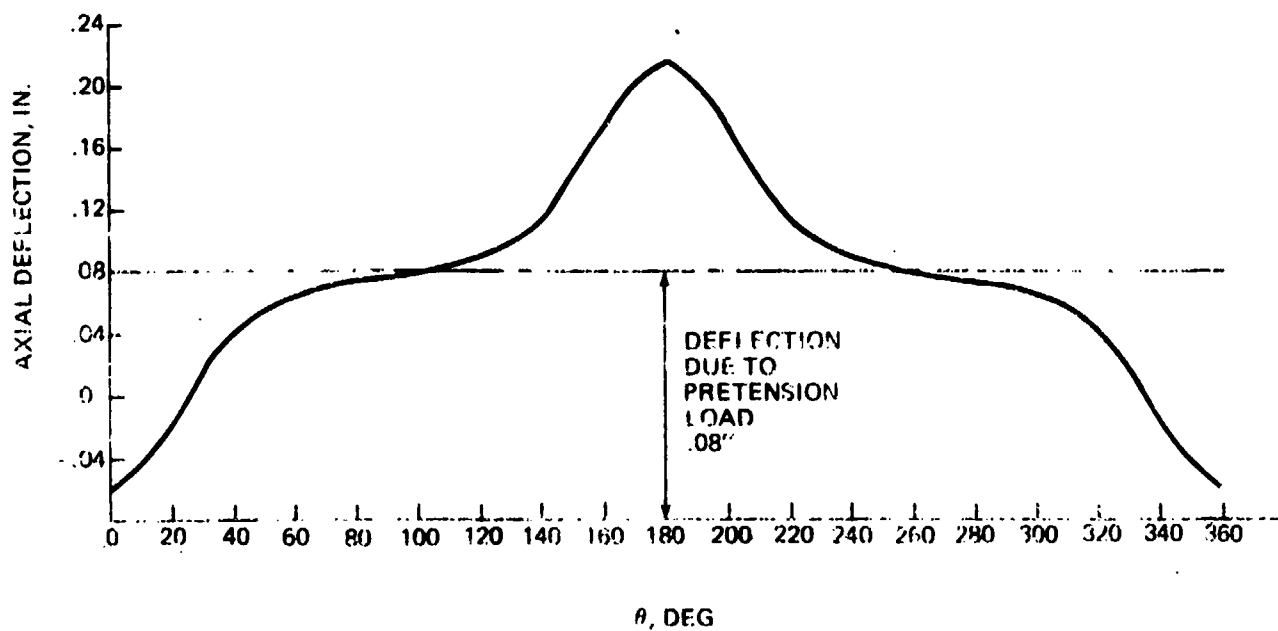


Fig. 7-12 Axial Deflection of Rim Due to Temperature Distribution

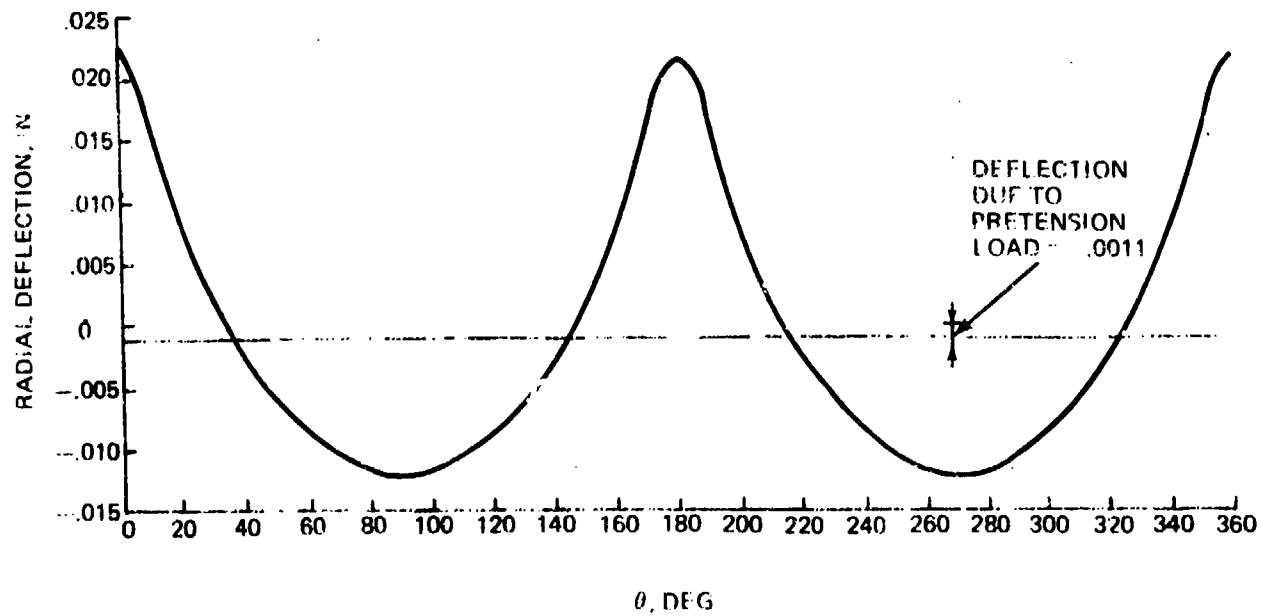


Fig. 7-13 Radial Deflection of Rim Due to Temperature Distribution

The buckling analysis used a computer program based on the formulation given in NASA TND-2960. The results are given below:

Case	Buckling Pressure
Entire Cylinder with Stringers Only	Less than 1 psi
Entire Cylinder with Stringers and Rings	36 psi
Length of Cylinder Between Rings; With Stringers	
L = 30 in.	1.1 psi
L = 15 in.	4.6 psi
L = 10 in.	10.6 psi

Note that both the overall cylinder and the length of cylinder between rings must be considered, so that both overall and local buckling are checked. The results indicate that the overall cylinder will not buckle; however, the distance between rings at the center of the cylinder where the pressure is greatest must be less than 15 in.

7.5.2 Buckling of Battens

The battens are structural members in the gores that are parallel to the rim members, as shown in Fig. 7-14. In the deployed configuration, the tension load applied to the gores puts a compressive load in the battens, while in the launch configuration with the gores wound around the LSP oscillations cause substantial compressive loads in the battens (see Subsection 7.7). The battens' stability must be considered in both configurations. In the launch configuration, however, only the outermost battens need be considered since all others are supported by the overlying gores.

We can consider the battens to behave as beams subjected to compressive loads on an elastic foundation. The quasiradials and the netting in the gore provide elastic support. Thus, the formulas in "Theory of Elastic Stability" by S. Timoshenko giving the critical load for a beam on an elastic foundation are used:

$$P_{\text{critical}} = \frac{\pi^2 EI}{L^2} \left\{ m^2 + \frac{\beta L^4}{m^2 \pi^4 EI} \right\}$$

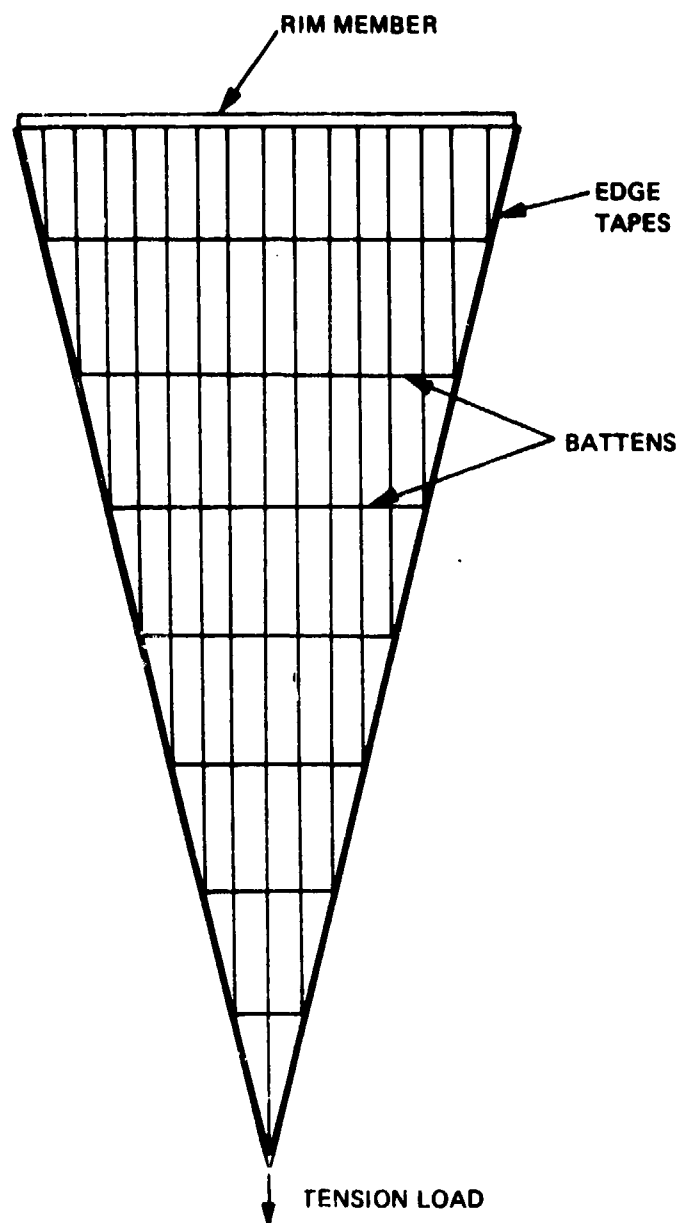


Fig. 7-14 Arrangement of Battens in Deployed Configuration

where the critical value of m (number of waves in buckling shape) is obtained from

$$\frac{\beta L^4}{\pi^4 EI} = m^2 (m+1)^2$$

and

β = stiffness constant of foundation per unit length


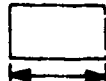
E = modulus of elasticity of beam

I = moment of inertia

L = length

The foundation stiffness is due to the tension in the quasiradials and netting in both the deployed and launch configurations. Additional stiffness is provided by nonlinear deflection effects.

For the deployed configuration, two sizes of battens were considered. The results are shown in the chart below. The longest battens were considered with $L = 235$ in.

CROSS-SECTIONS OF BATTENS				
	 2×10^{-3} in.		 10×10^{-3} in.	
	20×10^{-3} in.		30×10^{-3} in.	
	P_{crit}	m	P_{crit}	m
Linear	$.86 \times 10^{-3}$ lb	40	2.90×10^{-3} lb	21
Nonlinear	15.9×10^{-3} lb	175	17.4×10^{-3} lb	52

The compressive load in the battens in the deployed configuration is $.315 \times 10^{-3}$ lb, which is less than the critical values shown in the table. Hence, the battens will not buckle.

Results from the launch configuration are given below; nonlinear effects have been included:

P_{crit} , lb	l , in. ⁴
.65	$.25 \times 10^{-8}$
6.5	$.25 \times 10^{-6}$
20.3	$.25 \times 10^{-5}$
64	$.25 \times 10^{-4}$

Since the compressive load in the launch configuration is 13 lb as given in Subsection 7.7, a moment of inertia of $.25 \times 10^{-5}$ in.⁴ is needed for the outermost battens.

7.6 DYNAMICS OF CONTROLLED ORBITING SATELLITE

The dynamic behavior of the deployed satellite was predicted using the SPACE12 computer program*. This program simulates the satellite dynamics of any configuration by numerically integrating the equations of motion. The program was used to obtain both the rigid-body and flexible-body results presented herein.

7.6.1 Rigid-Body Attitude Dynamics

The rigid satellite attitude dynamics were simulated over a complete orbit. The results for an updated design with a 500-ft mast are presented in this subsection. Figure 7-15 shows the model with its mass properties.

The primary disturbance is the torque due to the solar radiation pressure**. The radiation reflectivity is assumed equal to one; i.e., all surfaces are in equilibrium in the sense that all incident radiation is emitted. Also, since totally diffuse emission is assumed, a shear stress as well as a normal stress will be induced. The appearance of a shear stress can be understood by contrasting the case of diffuse emission with that of specular emission (see Fig. 7-16). The radiation may be thought of as a stream of very small particles travelling at the speed of light. As these particles impact a surface and their velocity is reduced to zero, a stress of $.672 \times 10^{-9}$ lb/in.² is induced. In the case of emission (Fig. 7-16A), the angle of emission is equal to the angle of incidence and the emitted radiation produces a thrust stress, due to the jet effect, that is equal in magnitude to the incident stress. As is evident from Fig. 7-16A, the resultant of these effects is only a normal stress, since shear components of the incident and emitted stresses cancel. On the other hand, in the case of perfectly diffuse emission (Fig. 7-16B), the emitted radiation is dispersed in a symmetrical pattern with respect to the normal to the surface. Thus, the emitted radiation does not cause a shear stress for cancelling the shear stress induced by incident radiation.

* This program was developed by Grumman under contract to the NASA Langley Research Center (Contract NAS 1-10973).

** The concepts presented and equations used for computing solar radiation loads were extracted from a paper by W. Evans ("Aerodynamic and Radiation Disturbance Torques on Satellites Having Complex Geometry", Journal of the Astronautical Sciences, Volume VIX, No. IV, Winter 1962).

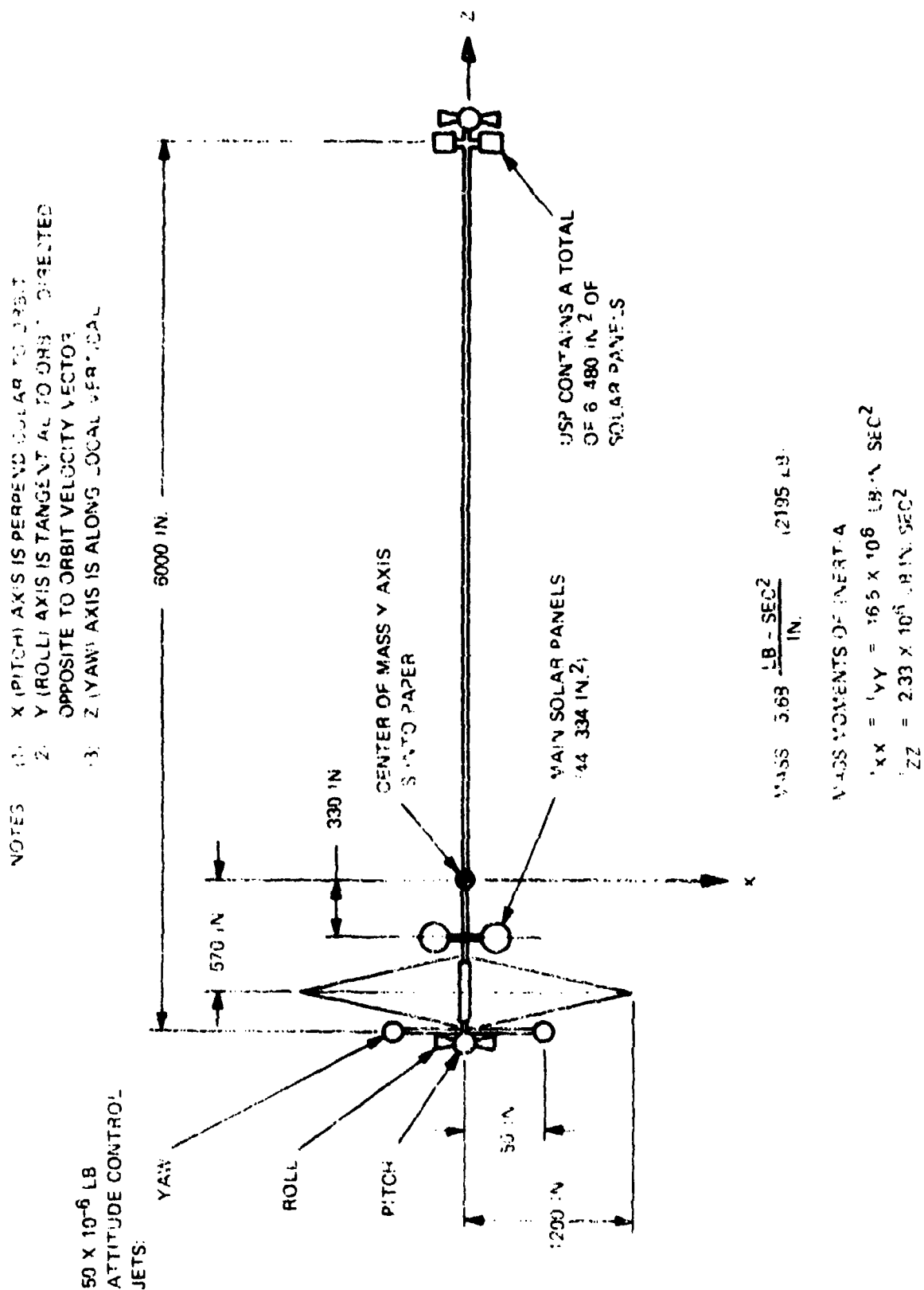


Fig. 7-15 Configuration and Mass Properties Used in Rigid Body Dynamics Studies

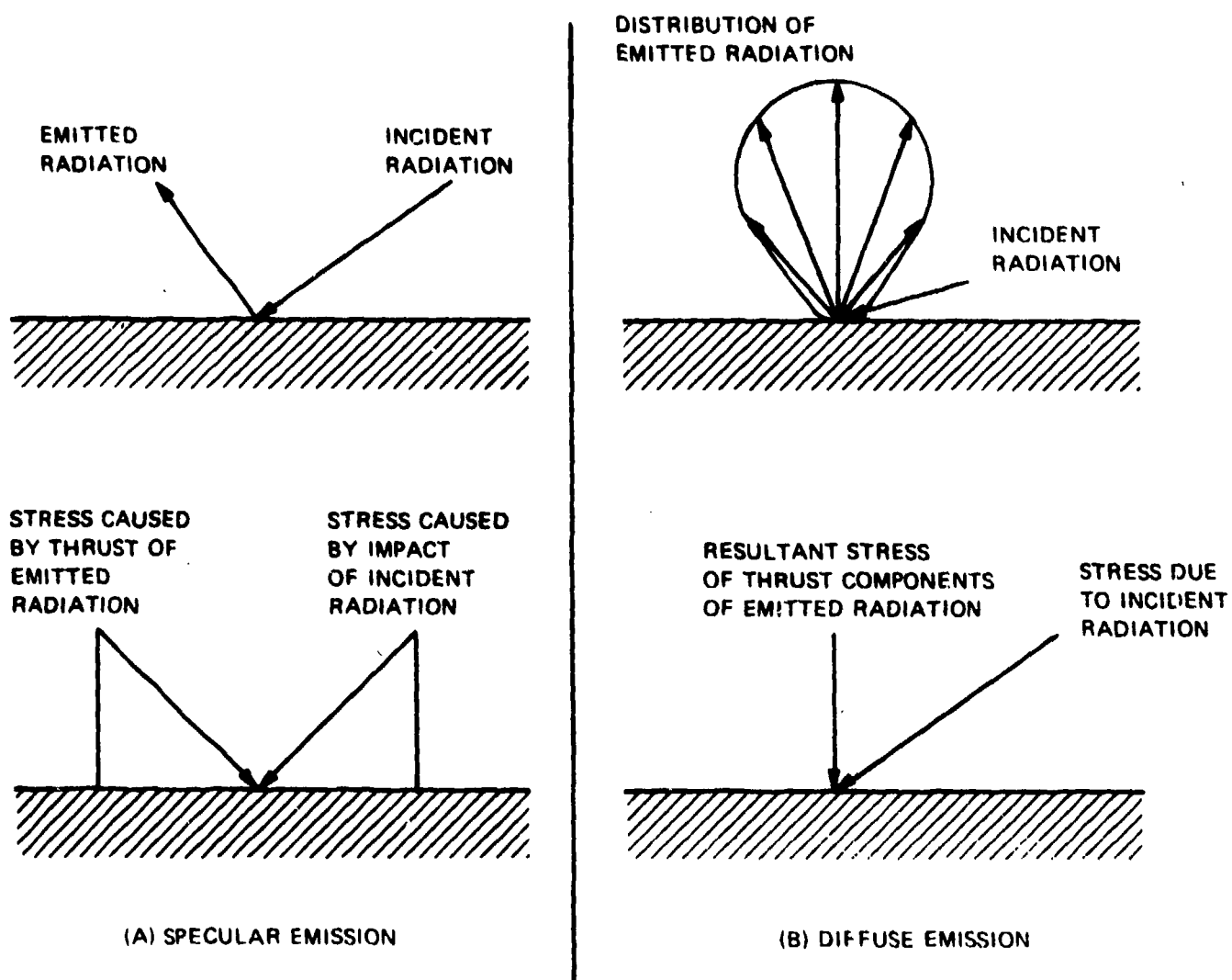


Fig. 7-16 Radiation Pressure for Specular and Diffuse Emission with Reflectivity = 1

Figure 7-17 shows the satellite's orbit. An equatorial orbit was assumed so that the angle of inclination to the plane of the earth's orbit was 23.45° . The angle locating the ascending node was assumed to be zero in the computer run to be discussed, so that the line of nodes was perpendicular to the sun's rays. Angle θ was initially zero, and the time history of the satellite's attitude motion was computed over one orbit. The lens area was assumed to be 18% dense for the purpose of computing the solar radiation load. The solar panels indicated in Fig. 7-15 are assumed to be driven about axes parallel to the x-axis at an angular velocity, relative to the satellite, equal in magnitude but opposite in direction to the orbital angular velocity. Thus the panels point approximately to the sun, although no compensation is made for the 23.45° inclination of the satellite's orbit.

Figure 7-18 shows the control law assumed about all three axes. When there is no external disturbance, the error trajectory spirals into the origin in the manner indicated; however, the control system's performance will, of course, differ in the presence of solar radiation torques. The dead band was assumed to be ± 0.00156 rad, corresponding to a ± 35 mi sweep on the earth's surface*. It was assumed that the error data was examined every 10 sec to determine whether to fire or turn off jets; consequently, the minimum jet pulse-width was 10 sec.

Figures 7-19 and 7-20 illustrate the satellite's dynamic behavior over one orbit. Figure 7-19 shows the radiation-pressure torques on the satellite about the axes of Fig. 7-15. The torque about the z (yaw) axis is zero due to the configuration's symmetry about this axis. T_y would be zero if the orbit were not inclined. This torque component is caused by the radiation shear stress. The discontinuity in the slope of both torque components at the 180° orbit angle occurs because, before reaching this angle, the radiation impinges on the back surface of the lens; after 180° , the radiation impinges on the front surface. In other words, if P is incident radiation pressure and ψ is the angle between the area (as seen in an edge view) and the sun's rays, the shear stress is $|P \sin \psi \cos \psi|$; consequently, as ψ passes through zero, the slope of the stress differs from zero, causing the discontinuity in the torque's slope. A similar discontinuity occurs at 360° . Torque calculations were coupled to the satellite's attitude; that is, the slight variations in the torque due to perturbations in the vehicle's attitude were included. The maximum torque was approximately .12 in.-lb; thus, the 50×10^{-6} lb jets (which produce .3 in.-lb torque) provide sufficient control authority.

* The roll and pitch dead band errors could combine to produce a total sweep of ± 50 miles.

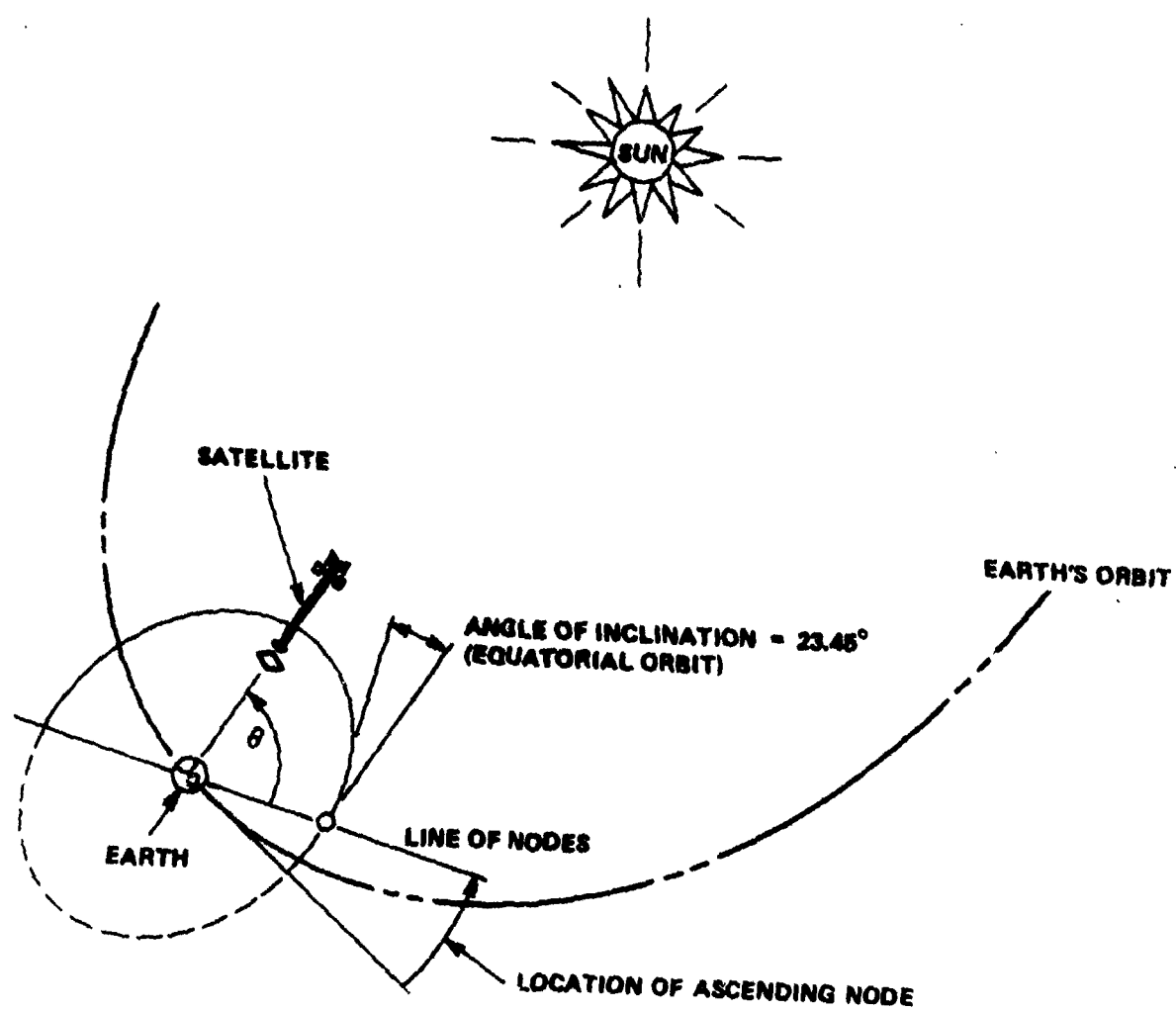


Fig. 7-17 Geometry of Orbit Assumed for Computing Solar Radiation Torques

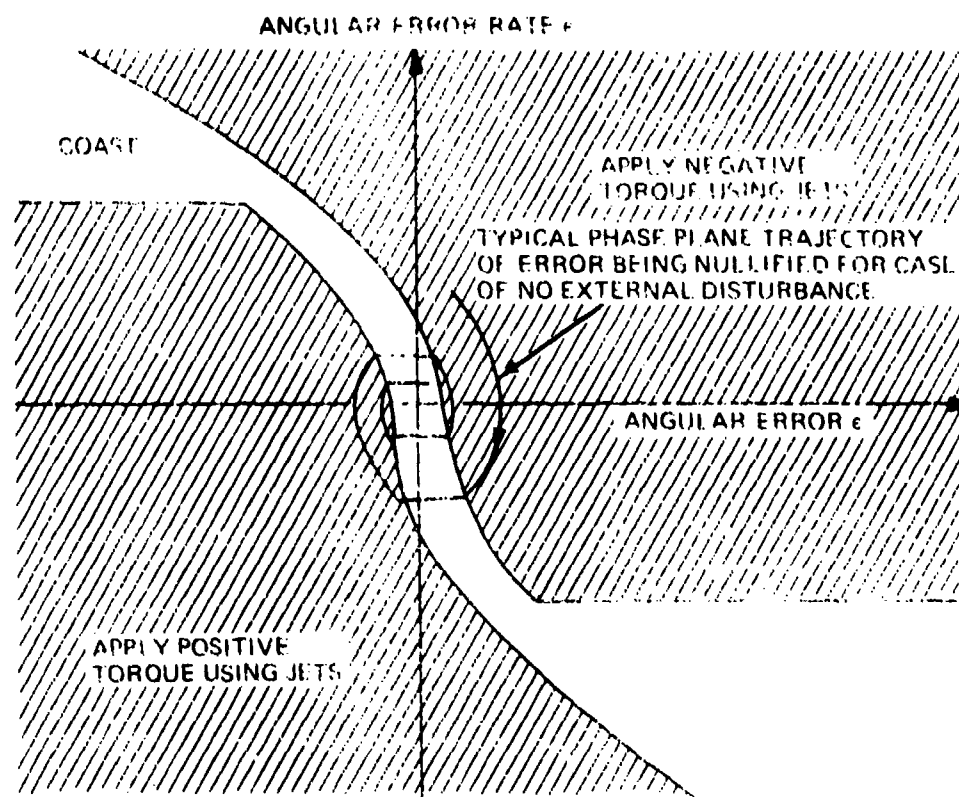
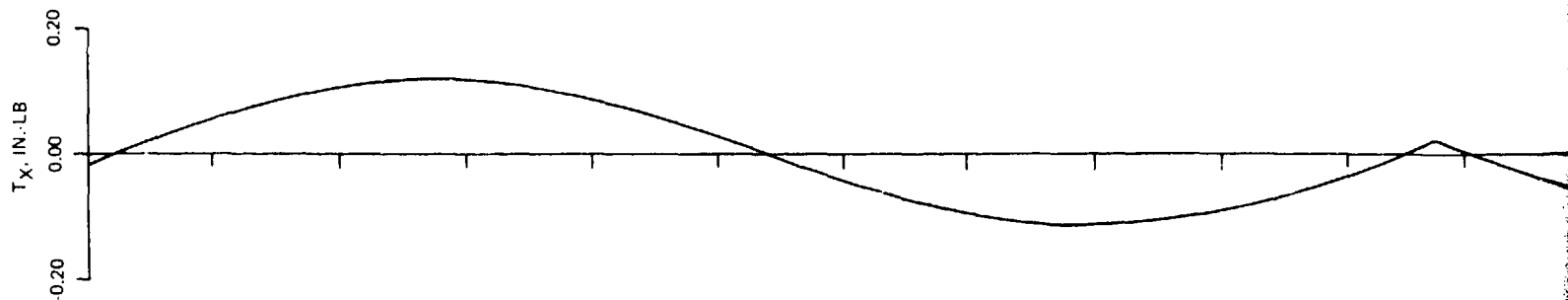
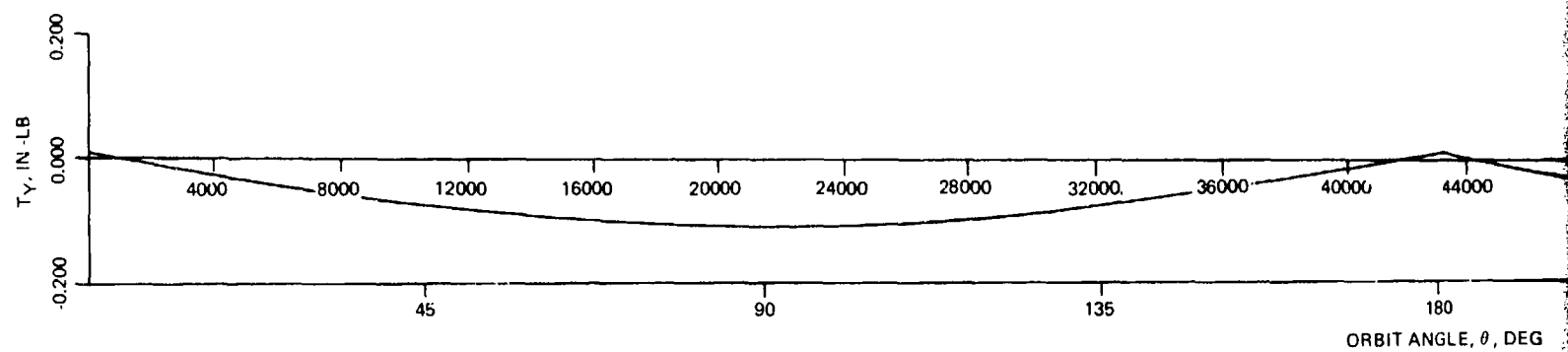


Fig. 7-13 Control Law Assumed for Attitude Position Control About Roll and Yaw Axes

THIS PAGE HAS INTENTIONALLY BEEN LEFT BLANK



(A) TORQUE ABOUT SATELLITE X (PITCH) AXIS



(B) TORQUE ABOUT SATELLITE Y (PITCH) AXIS

AXIS IS TANGENTIAL τ

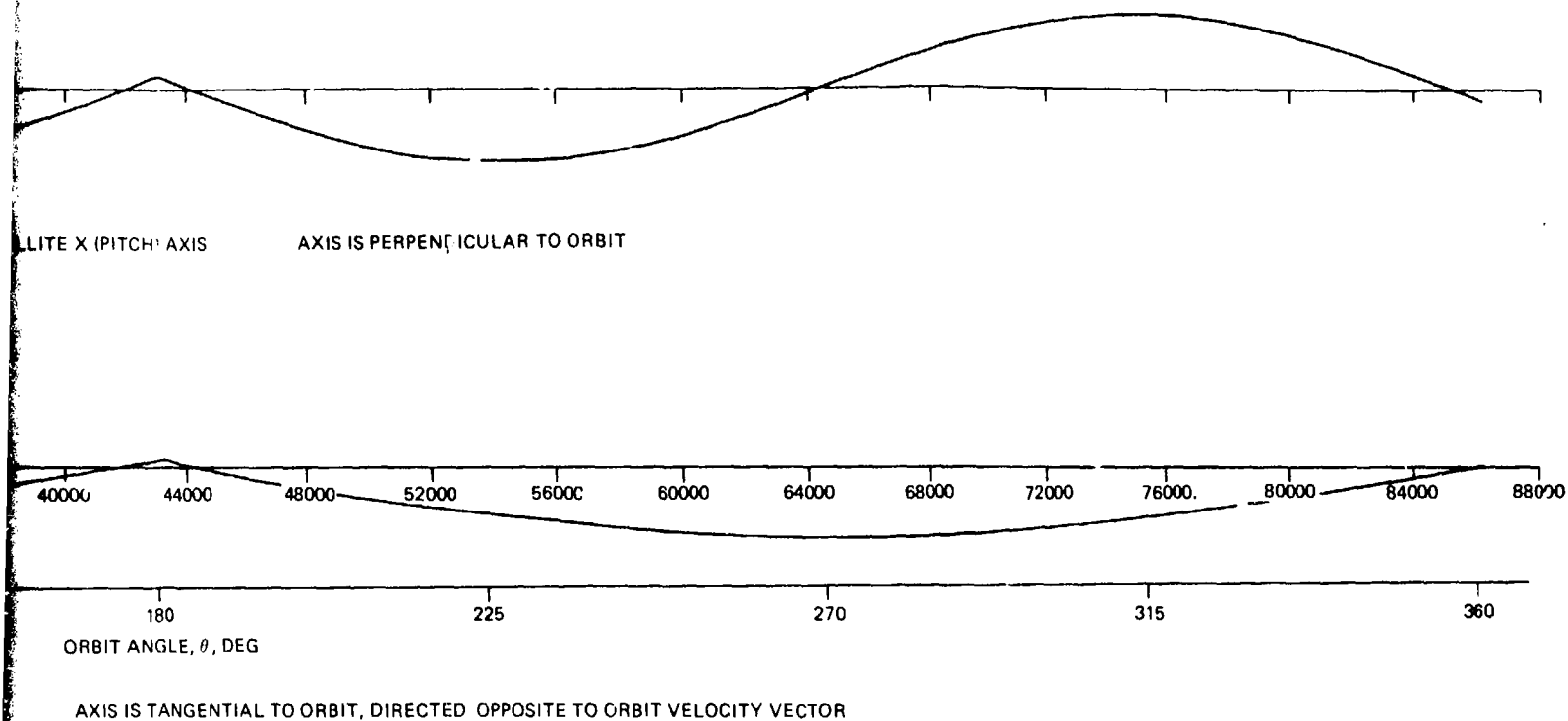
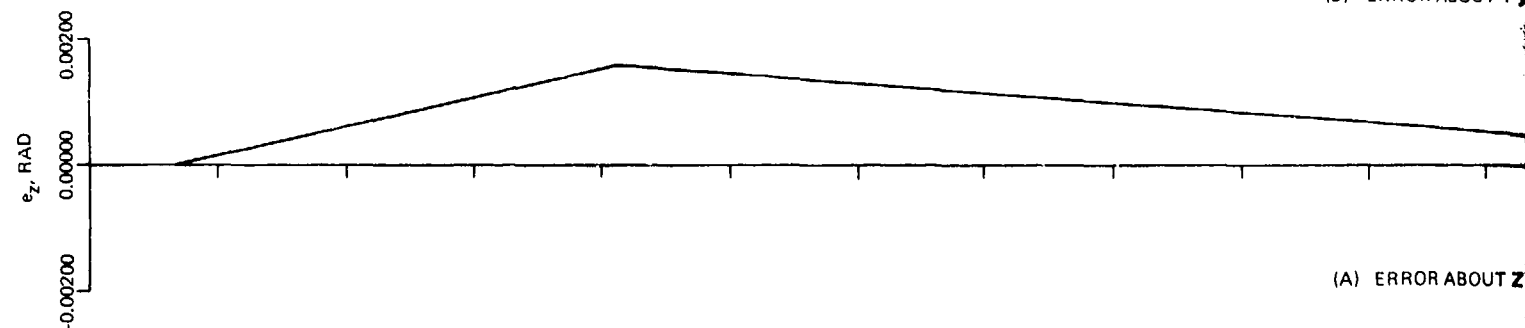
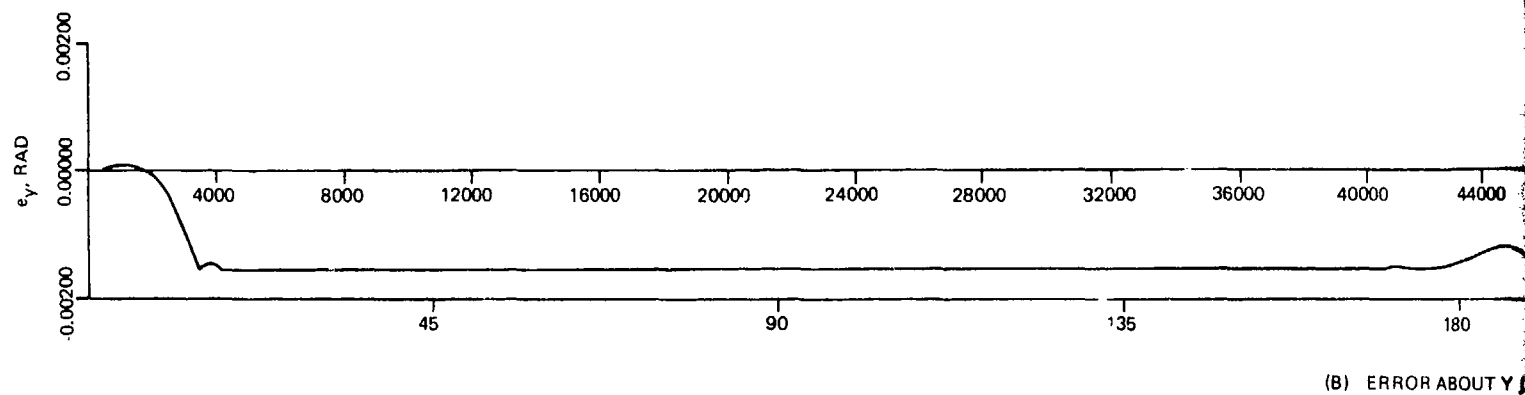
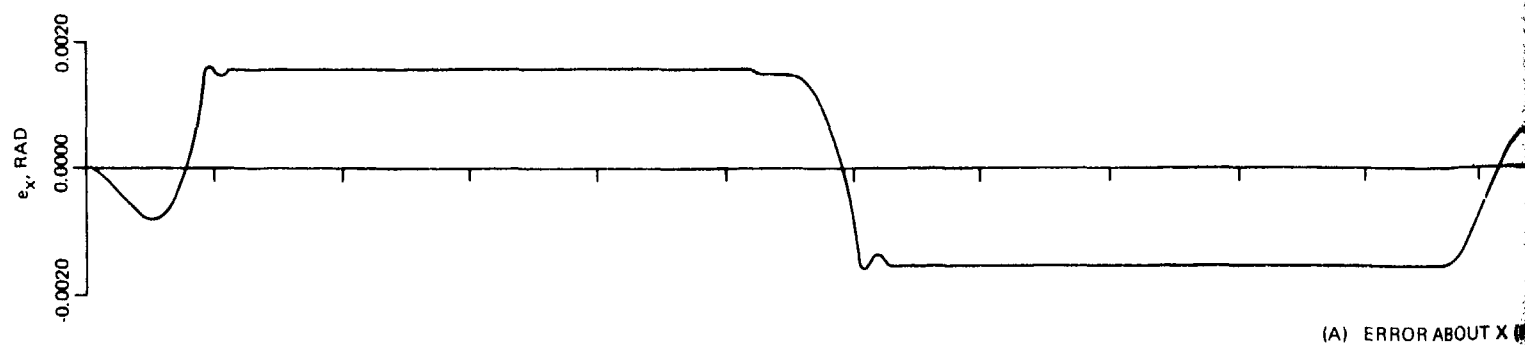


Fig.7-19 Torque Components, About Axes Fixed in Satellite, Due to Solar Radiation Pressure During One Orbit



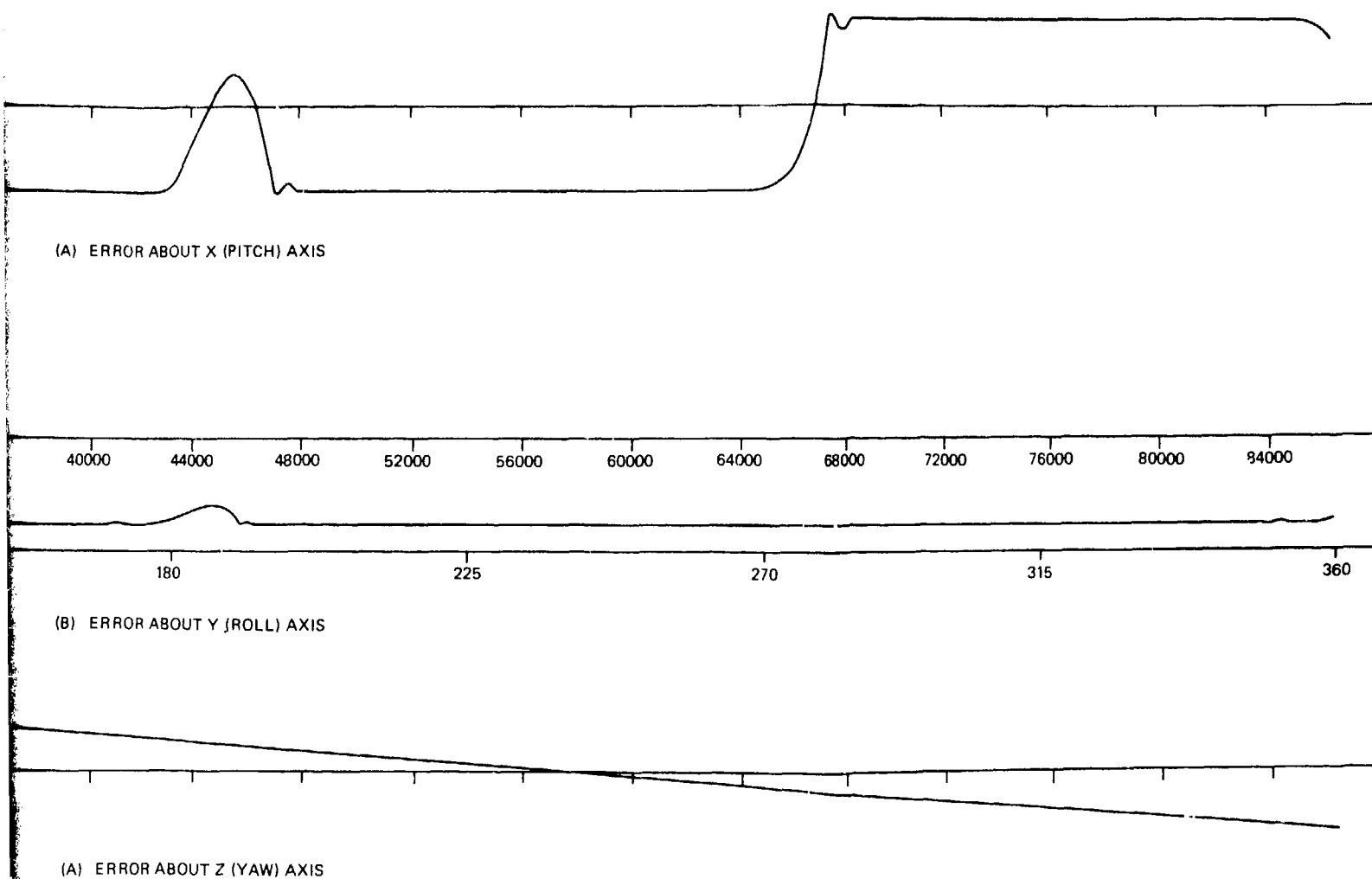


Fig.7-20 Attitude Error Components About Axes Fixed in Satellite

Figure 7-20 shows the attitude error about each axis; i.e., the actual angle minus the commanded angle. The commanded angle about the x-axis was ωt , where ω was set to the synchronous orbit rate of $.727 \times 10^{-4}$ rad/sec (1 rotation/day). Since the commanded angles about the y and z axes were zero, the corresponding error is equal to the actual angle about each of these axes. The error about the x and y axes roughly follows the direction of the applied torque. Although the errors remain approximately within the dead-band region, the torque does not reverse directions for long periods of time; thus, the satellite lingers in a rotated position, approximately at an edge of the $\pm .00156$ rad dead-band, while the jets pulse to counteract the solar torque and prevent any significant penetration beyond this dead-band region. Consequently, the lens axis is always maintained at the maximum allowable error position. However, the width of the dead-band could be significantly reduced with only a very small fuel penalty. Another possibility for performance improvement would be to introduce logic to bias the dead-band (for example to $+0$, $-.00156$ during one portion of the orbit and $+.00156$, -0 during another portion of the orbit).

While no torques were applied about the z-axis, a yaw rate appears at about 2500 sec. This rate is due to the kinematics of tilting the satellite to the dead-band angle of $.00156$ rad about the roll axis; consequently, the angular velocity has a component (equal to the orbital rate times $.00156$) in the yaw direction. The yaw jets fire at approximately 16,700 sec to correct this yawing motion.

The total jet impulse expended over the orbit was 4.01 lb-sec. This may be contrasted with the 2.46 lb-sec impulse expended during a similar computer run, where the inclination of the orbit was set to zero. During the latter run, the only disturbance was the solar radiation torque about the x-axis.

7.6.2 Flexible Response to Control Jet Excitation

The deployed satellite's dynamic behavior during attitude-control maneuvers was simulated to determine the loads induced in the structure and the influence of flexibility on control-system performance. The analysis was performed on an earlier configuration than that used for the rigid body study presented in the previous subsection. The configuration for the flexibility body study is shown in Fig. 7-1 through 7-5 and described in Subsection 7.1.1. It was found that the internal loads and deflections induced are very small; thus, only very mild stresses occur in the structure. In this study only the flexibility of the structural members (rim, mast, and stays) was considered; thus, the deformations of the gore material were not computed although its mass was included in the analysis. Since the solar panels were located only on the USP and were larger than the panels considered in the updated configuration, larger control jets were used (200×10^{-6} lb compared to 50×10^{-6} lb

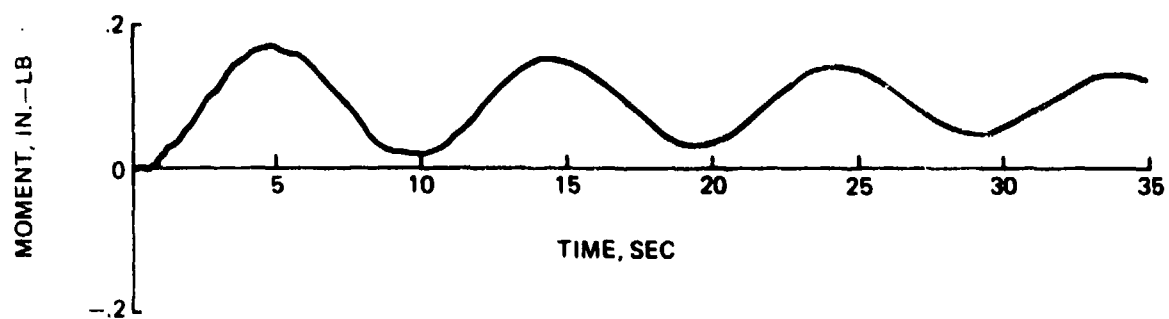
in the updated configuration). Also, it appears the the control system frequencies can be easily separated from the flexible body frequencies by adjusting the sample time increment between decisions to change the conditions of the jets (e.g., from on to off). For these reasons, the system flexibility probably will not result in any difficulty in controlling the deployed vehicle. On the other hand, the mast has nearly doubled in size, is consequently more flexible, and provides a larger jet moment arm. Thus, additional study of the final design is recommended. The control law described in the previous subsection was used with a control system dead-band of $\pm .001191$ rad. In each run the initial attitude error was assumed equal to the negative dead-band value with an initial angular velocity of $-.116 \times 10^{-4}$ rad/sec. The modes described in Subsection 7.3 were used, and structural damping was assumed to be 4% of critical in each mode.

Because of the symmetry of the configuration, the results for pitch and roll are identical except, of course, that the loads and deformations occur in perpendicular directions. Four modes of vibration (2nd, 3rd, 14th, and 26th) were used to compute the transient response of the deployed satellite due to firing the pitch attitude control jets. These were all mast-bending modes (the only modes which can be excited by the jets); only the 2nd mode contributed significantly to the response. Figure 7-21 presents some of the results obtained, including the force and moment time histories of node 130 (the point on the mast where the front stays are attached) and the displacement time history of node 140 (the USP). The jets remained on for the entire run. It can be seen that the responses induced are small.

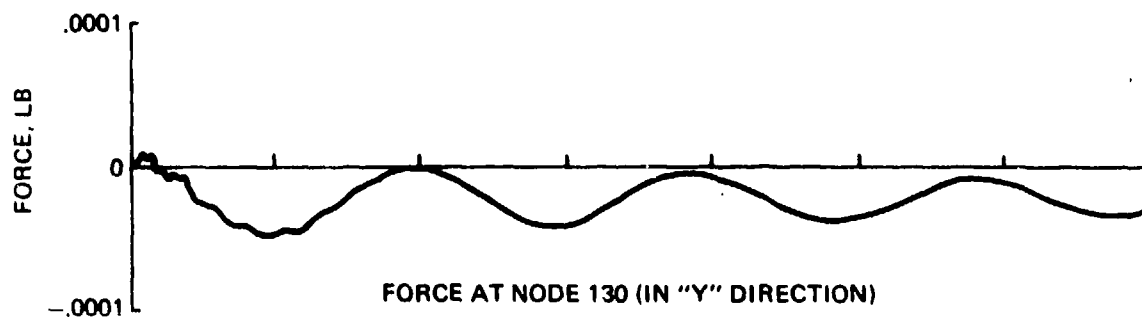
As indicated in Table 7-3, the frequency in torsion is rather low due to the high torsional flexibility between the rim and the mast. This frequency is excited during the yaw control maneuver (see Fig. 7-22). The yaw control jet moment arm was 60 in. After 2 sec, the jets shut down for approximately 2 sec because the mast, with its low torsional mass moment of inertia, was rotated to a reduced error-rate and the sensor located on the LSP signalled the jets to turn off. The rim, with its higher inertia, did not initially follow the mast. After 4 sec the rim followed the sensor and the jets remained on for the balance of the run. The time increment between jet firing decisions was 1 sec in this run. The induced torque in the mast was less than .02 in.-lb, and the maximum angular deformation between the mast and rim was $.26 \times 10^{-4}$ rad.

7.7 DYNAMIC ANALYSIS OF GORE MATERIAL DURING LAUNCH

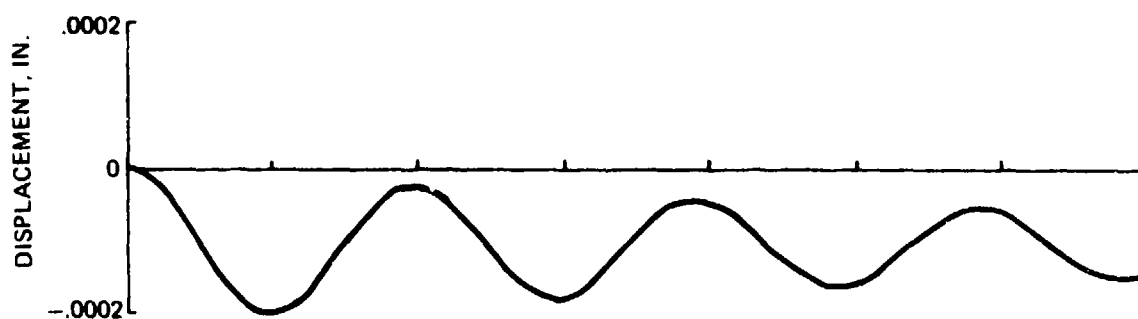
In the launch configuration, the gore material is wrapped on the drum as indicated in Fig. 7-23. A dynamic analysis of this subsystem was conducted to ensure that excessive loads do not occur in the gore and to establish the tiedown loads required to hold the gore material on the drum.



MOMENT AT NODE 130 (ABOUT "X" AXIS)

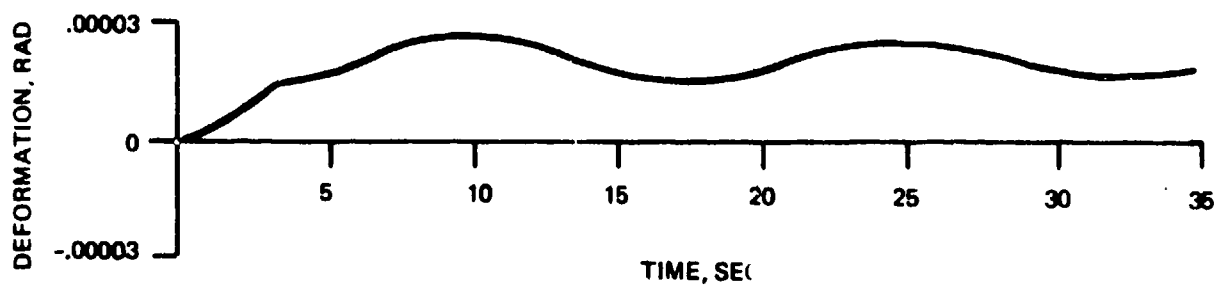


FORCE AT NODE 130 (IN "Y" DIRECTION)

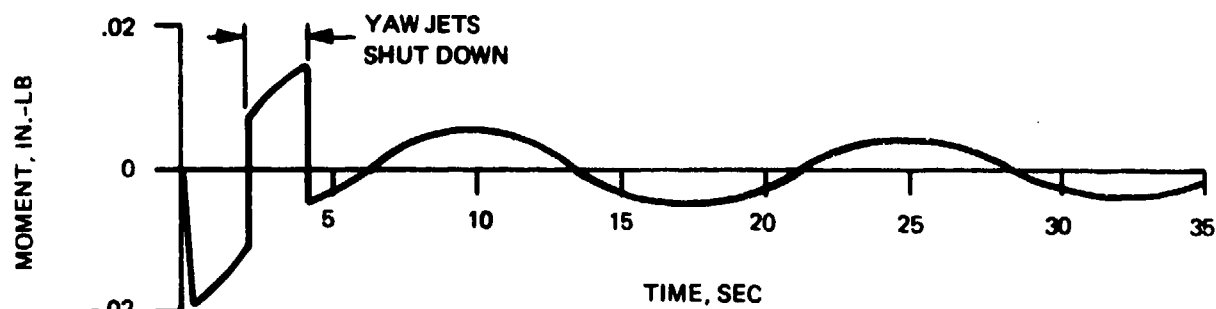


DISPLACEMENT AT NODE 140 (IN "Y" DIRECTION)

Fig. 7-21 Transient Response of Deployed Satellite Due to Firing Pitch Control Jets



(A) DEFORMATION OF MAST RELATIVE TO RIM



(B) MOMENT ABOUT "Z" AXIS AT NODE 130

Fig. 7-22 Transient Response of Deployed Satellite Due To Firing Yaw Attitude Control Jets

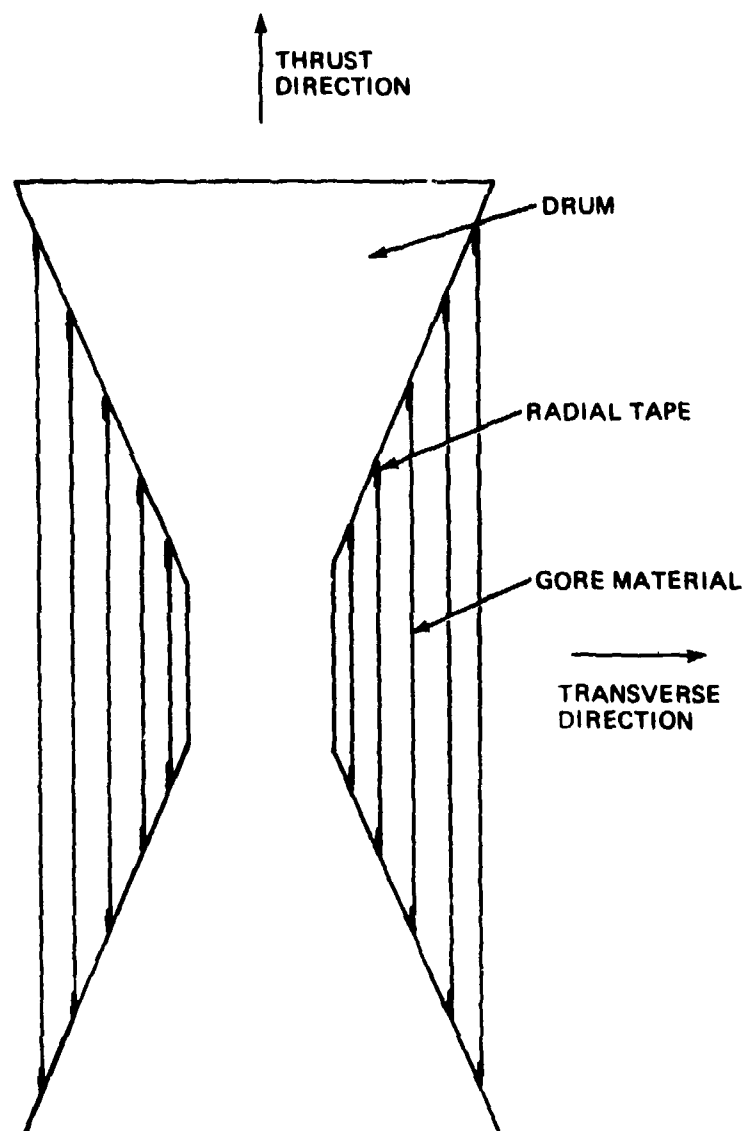


Fig. 7-23 Gore Material Packed for Launch

The idealization employed in this analysis accounted for vibration in the thrust direction only, since transverse vibration will be small due to layer overlapping, which restrains transverse motion. The principal load-carrying members in the thrust direction are the quartz battens spaced every 16 in., as shown in Fig. 7-24. These battens were idealized as uniform bars, fixed to a rigid drum at both ends. All of the stiffness of a bar was contributed by the batten which it represented, while the bar's mass included the total mass of the gore material 8 in. on either side of the batten. The batten cross-section was .010 by .030 in. Damping was taken to be 4% of critical damping for sinusoidal response calculations, and zero for the transient analysis.

Sinusoidal acceleration levels 50% higher than those shown in the Titan/Centaur D-1T frequency spectrum were applied to the drum, and the battens' steady state responses computed. Only the lowest resonant frequency of each batten was considered, since it was shown that this resulted in the maximum response. Figure 7-25 shows the force at the ends of each batten as a function of its location (R) defined in Fig. 7-24. The discontinuities in the frequency spectrum appear in the curve since the resonant frequencies are a function of batten length which is, in turn, a function of location. Figure 7-26 shows the distribution of force and stress in the outermost batten, which is the one that is most heavily loaded. The tiedown loads at the drum are equal to the forces at the ends of the battens. The loads presented here exclude gravity.

This analysis established the dynamic loads for the sinusoidal vibration environment during launch. A similar analysis was performed for the transient launch excitation using the same idealization. Since the rise times for the Centaur burns and the first two Titan stages (Stage 0 and Stage 1) are long compared to the period of the lowest mode of the system, these excitations induce only static loads. The maximum transient response is produced by the instantaneous cutoff of the Titan Stage 1, followed by the instantaneous buildup of Titan Stage 2 thrust. Due to the nature of the transient loading responses could be hand-calculated, making the use of a computer program unnecessary. Transient acceleration levels 50% higher than those specified for the Titan/Centaur D-1T were applied to the drum, and the batten responses computed. Figure 7-25 shows the maximum force at the ends of each batten as a function of its location. It should be noted that the transient response is significantly lower than the sinusoidal response.

These linear analyses assumed no free play in the attachment between the gore material and the drum. The existence of significant free-play could necessitate a nonlinear analysis.

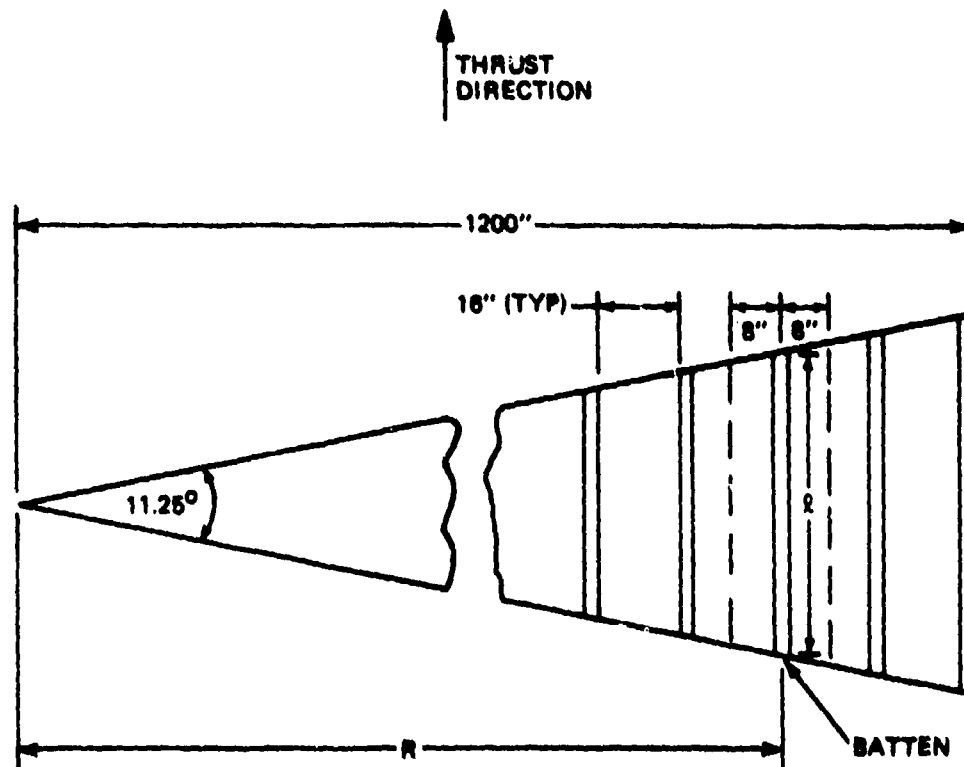


Fig. 7-24 Unwrapped Gore Material

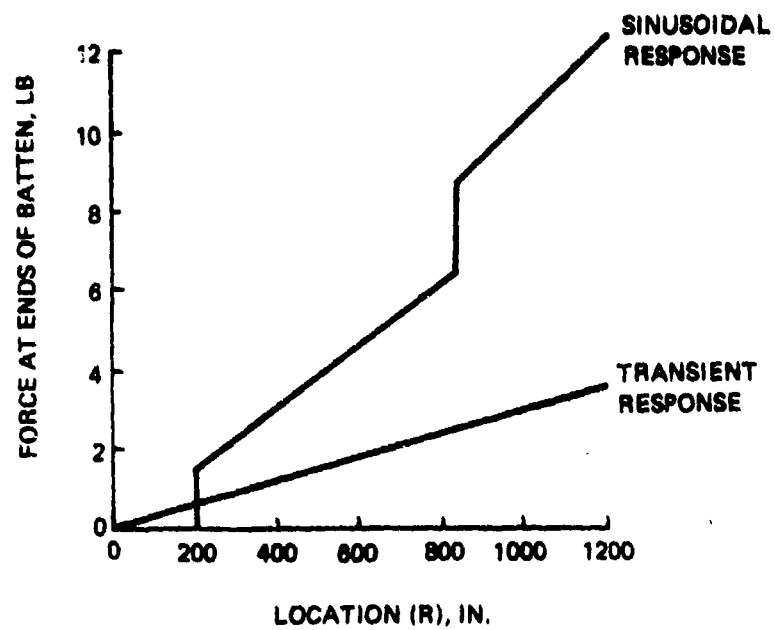


Fig. 7-25 Force at Ends of Batten

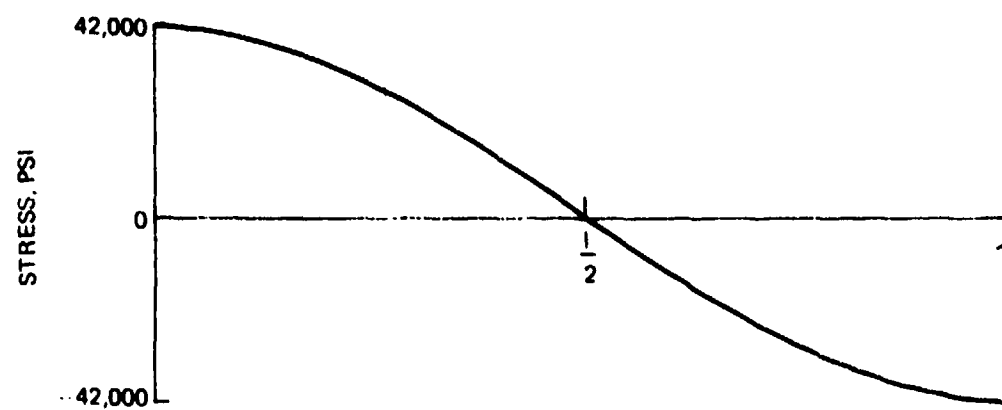
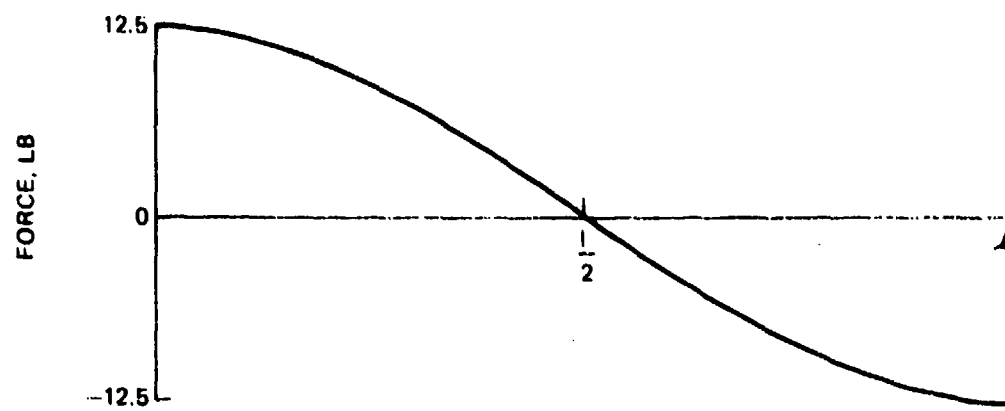


Fig. 7-26 Force and Stress Distribution Along the Length of the Outermost Batten Due to Sinusoidal Excitation

SPACEBORNE RADAR STUDY

REPORT SUPPLEMENT

TABLE OF CONTENTS

<u>SECTION</u>	<u>TITLE</u>	<u>PAGE</u>
0	Introduction	145
1.0	Aircraft Track Initiation	145
2.0	Aircraft Traffic	145
2.1	Aircraft Fence Crossings	145
2.2	Traffic Density	149
3.0	Radar Average Power Calculation	151
3.1	Radar Range Equation Parameters	152
3.2	Fence Generation	152
3.3	Target Tracking	157
3.4	Power Summary	160
4.0	Integration Loss	161
5.0	Use of Shuttle	169

THIS PAGE HAS INTENTIONALLY BEEN LEFT BLANK

SECTION 0 INTRODUCTION

This is a supplement to the Spaceborne Radar Study report, Grumman number 74-21AF-1, submitted earlier on Air Force Contract F19628-74-R-0140. Reference will be made to that report in the presentation of the material covered by this supplement.

The items covered herein are:

1. Aircraft track initiation
2. Aircraft traffic
3. Radar average power calculations
4. Integration loss in pulse burst Doppler filters
5. Use of the Shuttle

SECTION 1 TRACK INITIATION

Track initiation is done in addition to the fence generation, without interrupting the fence. A track initiate routine is started whenever a target is detected. The routine consists of several looks at the target at a sufficient rate so that target speed and heading can be established within a few minutes. Thereafter, the track is maintained by pointing the beam periodically at the aircraft at a rate determined by its speed, maneuvers, and traffic density.

SECTION 2 AIRCRAFT TRAFFIC

2.1 Aircraft fence crossings

Figure 2-1 is a plot of the average hourly traffic crossing longitude 10°W in August of 1972 (data provided to us by the IAS study group). The average number of aircraft crossing the line per day is 217 eastbound and 203 westbound. The number of crossings in both directions is 2,975 per week. A major portion of this traffic goes to Canada, South America, Mexico and Islands. We estimated the amount of oceanic traffic crossing our radar fence using per week Flight Information Regions (FIR) data given in table 2-1, and part of the 10°W traffic.

In 1985 we expect 900 aircraft per week to be crossing the portion of the fence located off the U.S. Atlantic coast. This number was obtained by taking the projected oceanic traffic, 451 flight per week, listed in table 2-1 and doubling it to account for VFR traffic and for flights not handled by the FIR centers.

The total number of flights in each direction is then 65 per day or 2.7 per hour. The peak number of aircraft crossing the line is about 3 times the average as indicated by the data for the 10° longitude line. Using this ratio gives a peak rate of crossings of 8 aircraft per hour in the incoming direction.

Using analysis similar to that done for the Atlantic coast above, the expected fence crossings were determined for the other portions of the fence. Table 2-1 shows the results.

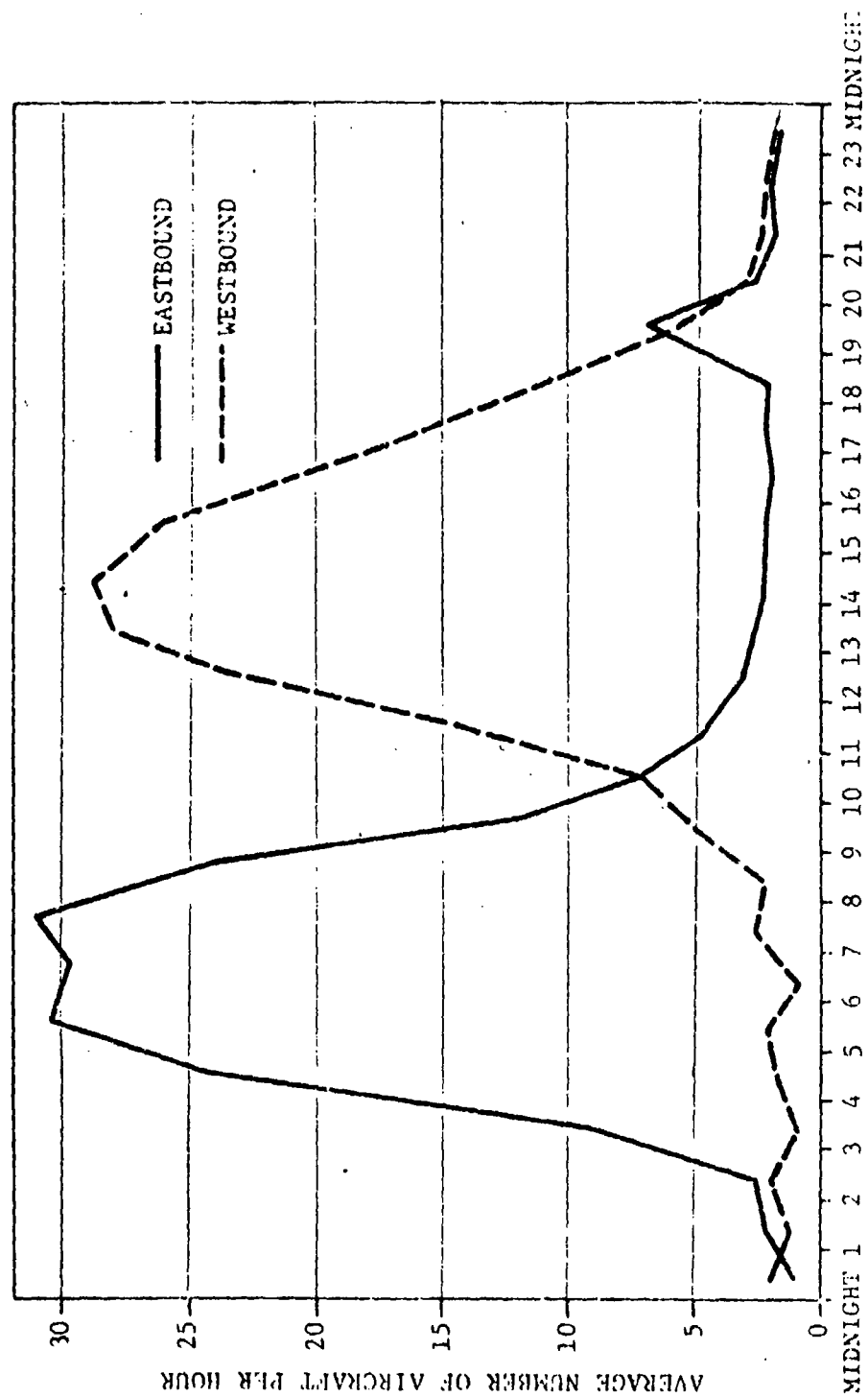


FIGURE 2-1
AVERAGE HOURLY TRAFFIC CROSSING LONGITUDE 10°W IN AUGUST 1972

TABLE 2-1 Oceanic Over Traffic by Flight Information Regions (FIR) (Weekly)

REGION		FY 1972	PROJECTED FY 1985	INCREASE NO.	%
A.	<u>Atlantic</u>	<u>234</u>	<u>451</u>	<u>217</u>	<u>93</u>
	New York FIR	99	142	43	43
	Miami FIR	135	309	174	129
B.	<u>Gulf of Mexico</u>	<u>156</u>	<u>350</u>	<u>194</u>	<u>124</u>
	Miami FIR	135	309	194	129
	Houston FIR	21	41	20	95
C.	<u>Pacific</u>	<u>292</u>	<u>294</u>	<u>31</u>	<u>12</u>
	Oakland FIR	87	110	23	26
	Anchorage FIR	39	40	1	3
	Honolulu FIR	100	122	22	22
	Guam FIR	37	22	(15)	(41)
D.	<u>San Juan FIR</u>	98	174	76	78
E.	<u>Balboa FIR</u>	26	34	8	31

TABLE 2-2

Expected Aircraft Fence Crossings for FY-1985

<u>Fence Portion</u>	<u>Peak number of crossings per hour in one direction</u>	
U. S. Atlantic Coast	8	
Gulf of Mexico and the Caribbean	8	
Mexico and Central America Coasts	3	
Pacific Coast	5	
Canadian Coast	8	
Alaskan Coast	<u>0.5</u>	
	Total	32.5 use 33

The length of time an aircraft detected crossing the fence may have to be tracked, assuming the worst case that all aircraft must be tracked 1200 miles until they reach the U.S. borders, and that the average aircraft speed is 450 knots, is 2.67 hours per aircraft. Therefore the peak number of aircraft that have to be tracked at any one time is 33×2.67 or 87, of which 21 of these are off the Atlantic coast. Dividing this number among the five ARTCCs covering the Atlantic coast makes it 4 aircraft per center.

2.2 Traffic Density

The worst case traffic density is the portion of the fence on the approaches to the Boston, New York, and Washington areas. Table 2-3 gives a listing of the projected number of domestic IFR aircraft that will be handled by the ARTCCs in FY-1985 (provided to us by the LAS study group). The New York area is taken as an example for the traffic density calculations. The number of 2,354 flights per week is doubled to 4,708 to account for VFR and any non-controlled traffic. This is equal to an average of 670 aircraft per day or 28 per hour.

The area covered by the New York ARTCC is approximately 50,000 square miles. The region is roughly a square of 220 nautical miles on a side. The average time an aircraft spends in this area is assumed to be on the order of one hour, to include low speed general aviation aircraft, scheduled commercial aircraft, holding times, and take-offs and landings.

Therefore, the average number of aircraft in the air at any one time in the New York ARTCC region will be 28, which is an average traffic density of one aircraft every 180 square miles. The peak density may be one aircraft per 60 square miles.

Another source of data for the traffic density in the New York region is the flights made by aircraft equipped with search radars.

The Grumman/Navy E-2C flying in the vicinity of New York is another source of air traffic data. At an altitude of 30,000 ft. with a radar/IFF range of 250 miles the E-2C sees about 200 IFF replies from aircraft during busy periods. Adding an estimated 100 non-IFF aircraft brings the total traffic to 300. The area covered by the radar is 188,000 square miles. Nearly all of the aircraft are seen over land and near the coast, in only about one half of the total area radar coverage, 94,000 square miles. If the aircraft were evenly distributed, the density would be one aircraft per 313 square miles. Using a peak density factor of 3 results in a peak density of one aircraft per 104 square miles, and increasing the amount of traffic by 68% as predicted for 1985 brings the traffic density to one aircraft per 62 square miles. This result agrees very closely with the peak traffic of one aircraft per 60 square miles obtained from the ARTCC data.

This high density traffic will exist over land and near the shore. The density progressively decreases with the distance from the coast and is considerably less at the radar fence.

TABLE 2-3

Domestic IFR Aircraft Handled by ARTCCs (Weekly)		FY 1972	Projected FY 1985	Increase # %	
A.	<u>Atlantic Coast</u>	<u>5,927</u>	<u>9,928</u>	<u>4,001</u>	<u>68</u>
	Boston ARTCC	933	1,491		
	New York ARTCC	1,526	2,354		
	Washington ARTCC	1,342	2,406		
	Jacksonville ARTCC	1,105	1,840		
	Miami ARTCC	1,021	1,837		
B.	<u>Guam Mexico</u>	<u>3,307</u>	<u>5,521</u>	<u>2,214</u>	<u>67</u>
	Miami ARTCC	1,021	1,837		
	Jacksonville ARTCC	1,105	1,840		
	Houston ARTCC	1,181	1,844		
C.	<u>Mexican Border</u>	<u>2,904</u>	<u>4,775</u>	<u>1,871</u>	<u>64</u>
	Houston ARTCC	1,181	1,844		
	Albuquerque ARTCC	699	1,298		
	Los Angeles ARTCC	1,024	1,633		
D.	<u>Pacific Coast</u>	<u>2,524</u>	<u>4,092</u>	<u>1,568</u>	<u>62</u>
	Los Angeles ARTCC	1,024	1,633		
	Oakland ARTCC	941	1,442		
	Seattle ARTCC	559	1,017		
E.	<u>Canadian Border</u>	<u>4,373</u>	<u>7,485</u>	<u>3,112</u>	<u>71</u>
	Seattle ARTCC	559	1,017		
	Great Falls ARTCC	202	-		
	Salt Lake City ARTCC	393	1,012		
	Minneapolis ARTCC	736	1,362		
	Cleveland ARTCC	1,550	2,603		
	Boston ARTCC	933	1,491		
F.	<u>Off-shore ARTCCs/CERAPs*</u>				
	Anchorage ARTCC	257	400	143	56
	Balboa*	44	55	11	25
	Guam*	79	74	(5)	(6)
	Honolulu ARTCC	398	564	166	42
	San Juan ARTCC	304	648	344	113

* Combined Center and Terminal facilities, i.e., Center RAPcon.

Section 2.2.2 of the main report shows how the look rate for tracking the aircraft is determined. Section 3.7 discusses the capability of the satellite radar in resolving one aircraft from all others. The high resolution is a major factor in minimizing the number of track mix-ups. The area covered by one range bin of the radar is 3 square miles (300 feet x 60 miles). The probability that another aircraft will be in the same range bin as the one being tracked for the density of one aircraft per 60 square miles is .05. The probability that both aircraft will have the same radial speed component so that they appear in the same doppler filter is about .015. The combined probability of interference during any one look is then 7.5×10^{-4} . Since two radars look at the aircraft from different angles, the probability of not resolving one aircraft from the other drops to $(7.5 \times 10^{-4})^2$ or 56×10^{-6} .

The other factor that minimizes the chance of track mix-up is the advance knowledge obtained on other aircraft in the path of the one being tracked. All aircraft in the vicinity of the target aircraft are detected simultaneously with the target aircraft with the same look of the radar beam because of the large footprint. Aircraft on possible mixup courses are tracked along with the target aircraft at an increased look rate until the danger is past. This increases the number of tracks that must be processed over the 87 crossing the fence, however, the processing is done at the ground station and it does not increase the burden on the satellite.

SECTION 3 RADAR AVERAGE POWER CALCULATIONS

3.1 Radar Range Equation Parameters

The radar signal energy required to detect a target in a single look is given by the following standard radar equation:

$$E = \frac{4\pi R^4 \lambda^2 K T S/N L}{A^2 \sigma} \text{ in watt-sec. (Joules)}$$

For the proposed radar satellite the parameters are as follows:

R = Range in meters (variable with segment location, see sec. 3.2).

λ = Wavelength, 0.72 meters.

K = Boltzman constant, 1.38×10^{-23} joules per degree, Kelvin.

T = Effective system temperature, 470° Kelvin.

S/N = Signal to noise ratio, 28.8 (14.6db).

L = System loss (variable with segment location, see sec. 3.2).

A = Area of antenna, 70,500 square meters (300 meters dia.).

σ = Target R.C.S., 1 square meter.

The average power in watts required to generate the fence and track the aircraft is a product of the energy per look in watt-sec. times the number of looks per second.

The effective system temperature of the satellite repeater radar receiving system is 470° Kelvin referred to the antenna input. Part a Figure 3-1 is a block diagram of the R. F. portion of the radar showing the loss budget for each portion. Part b is the equivalent loss diagram with the equation used to calculate the effective temperature.

The signal-to-noise ratio, S/N , is optimized for the least average R.F. power required to generate the fence. For the specified probability of detection, P_D of .999, and with a probability of false alarm, P_{FA} of 10^{-6} , the S/N would have to be 15.5db. The number of opportunities for a false alarm for one fence cycle is equal to the number of footprints, 330, times the number of looks per footprint, 6, times the average number of range bins per footprint, 1800, or 1.24×10^6 . The number of false alarms per fence cycle would be 1.24 for the P_{FA} of 10^{-6} . If the S/N were reduced, there would be more false alarms, and more repeat radar looks would be necessary to check out the false alarms which would increase the average power. It turns out that up to a point a reduction in S/N ratio results in less average power because the drop in power due to lowering the S/N ratio is more than the increase in power required to check out the false alarms. The optimum S/N ratio is 14.6db. This increases the number of looks by 7.3 percent and reduces the power by 0.5db. Figure 3-2 is a plot of the power curves used for the optimization.

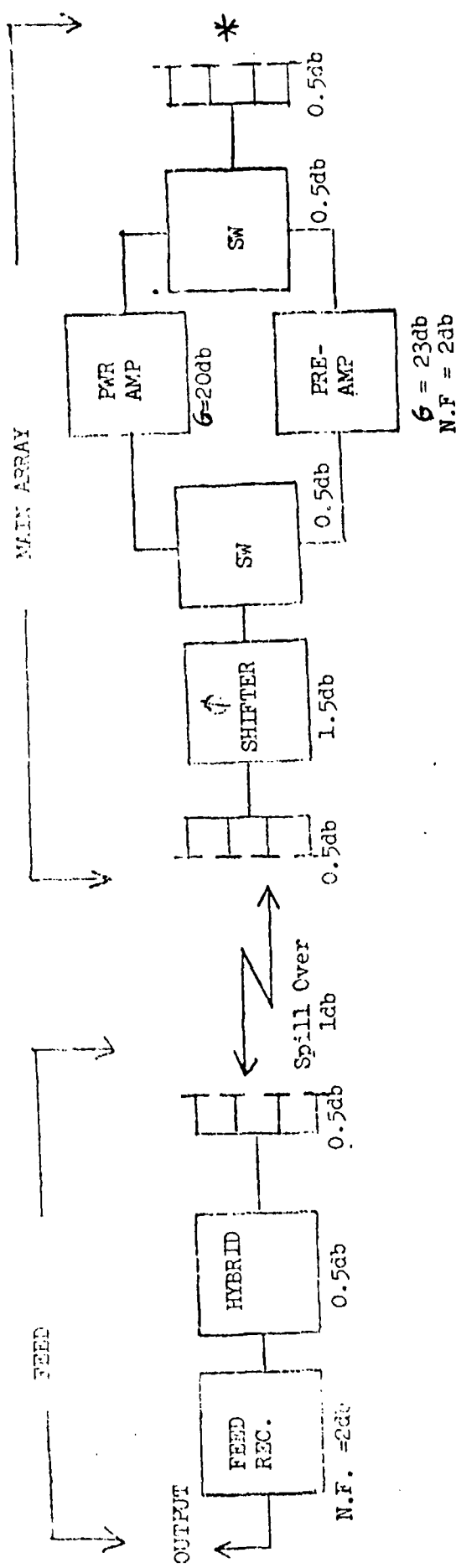
The system loss, L , consists of two parts: a fixed part, and a variable part that is a function of the scan angle. The fixed part consists of 1db for the resistive loss between the transmitter modules and the dipoles, up to 1db for polarization loss and up to 0.3db for integration loss, making a total of 2.3db. The polarization loss results when the polarization of the radar echo deviates from the transmitted circular polarization, which is caused mainly by the ionosphere. Integration loss occurs because the detection filters are not entirely power matched when optimized for maximum clutter rejection. Section 4 covers the integration losses in more detail.

The variable losses consist of the antenna subarray pattern loss and the bandwidth loss. To minimize the effect of these losses, the satellite antenna boresight is directed at Mexico City, which puts the lowest scan angle losses where the number of looks per segment is the highest. The scan losses vary from 0.36db to 3.76db over the length of the fence.

3.2 Fence generation

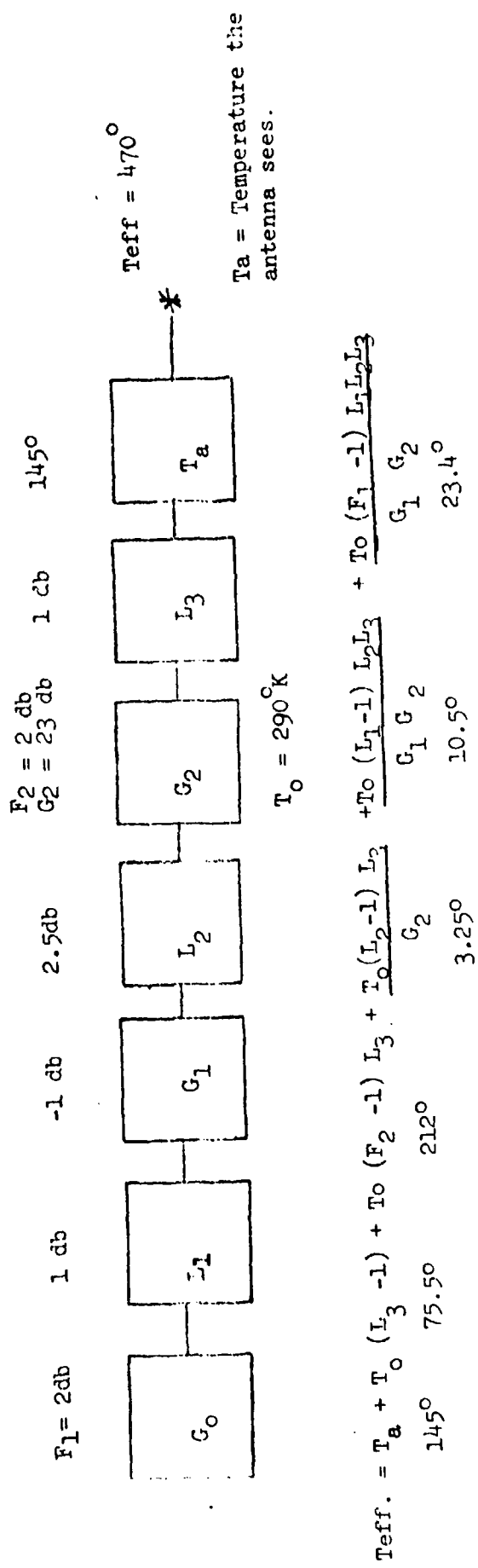
Section 2.2.1 of the main report describes the technique of generating the fence. To simplify the power calculations the fence is divided into 13, 1000 mile segments as shown in figure 3.2-1.

The number of footprints required to generate a segment of the fence varies with its location in the fence. The location determines its range from the satellite, the grazing angle of the beam, and the aspect angle. Table 3.2-1 gives the geometry parameters for each one of the 13 segments.



* Effective Temp. Point

Part a Loss budget for Radar System



Part b Equivalent Loss Diagram and Equation for Effective Temp. Calc.

FIG. 3-1 Effective System Temperature

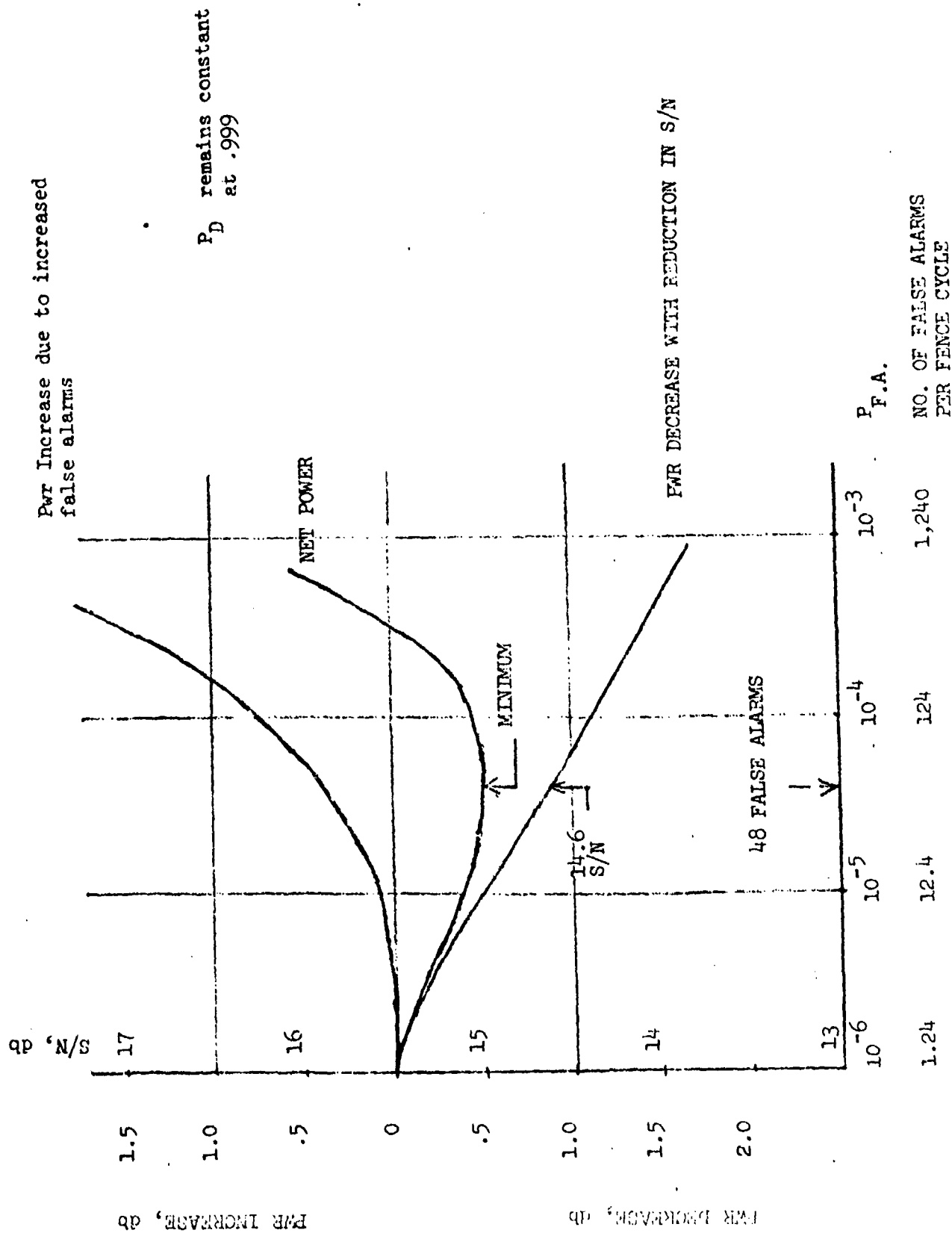
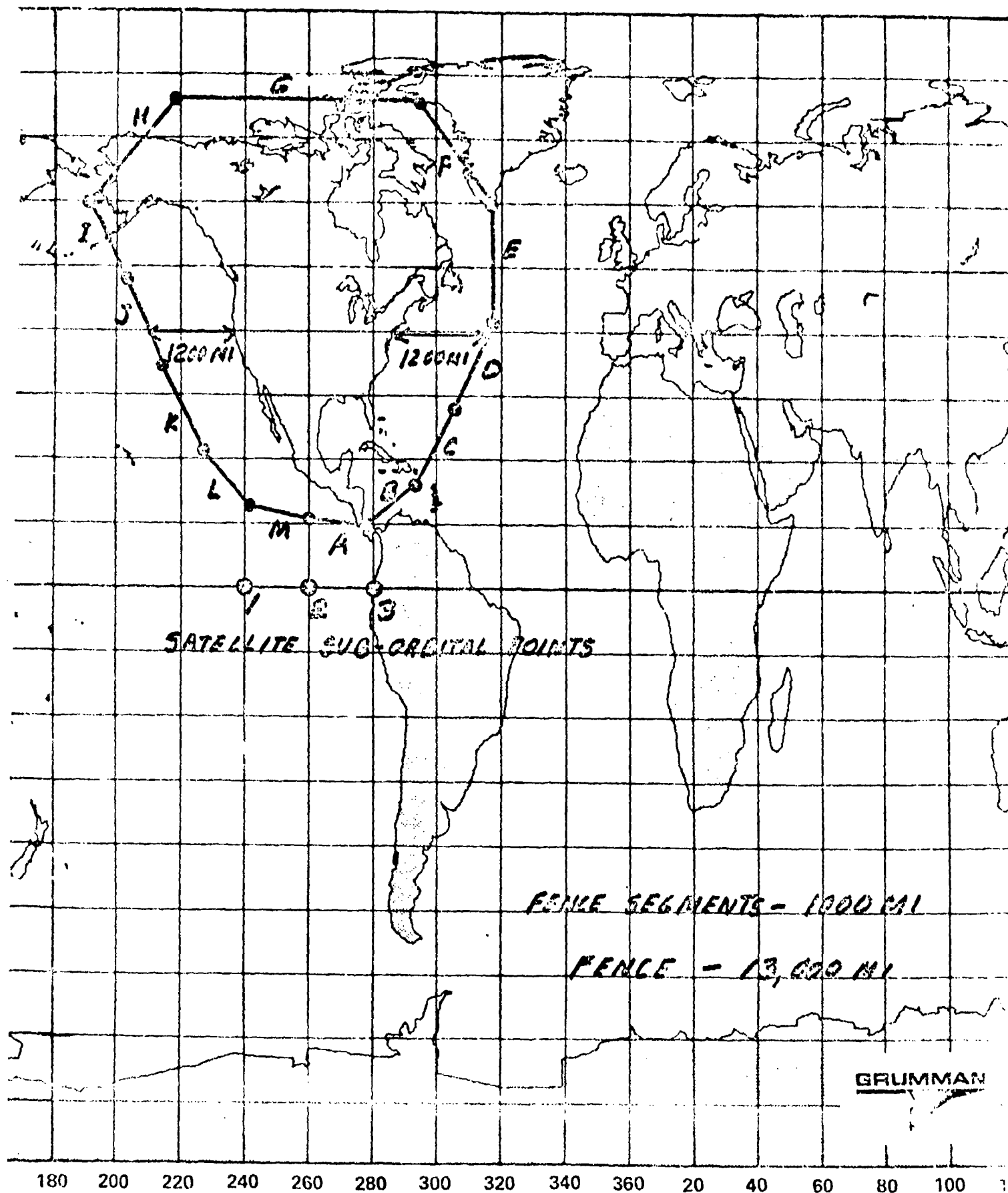


FIG. 3-2 OPTIMIZATION OF S/N VS POWER

Figure 3.2-1. FENCE LOCATION



SEGMENT	RANGE	GRAZING ANGLE	ASPECT ANGLE	ELLIPSE SIZE MINOR	MAJOR	NO. OF BEAM FOOTPRINTS	SHORTEST DISTANCE ACROSS FENCE
A	19,414 Mi.	74.4°	45°	56mi.	58.5mi.	34.2	48.8 Mi.
B	19,760	97.2	1.12	57	67.8	29.4	50
C	20,382	40	24.01	58.7	91.3	24.4	60.5
D	21,129	24	18.22	60.9	148	16.5	66
E	21,851	10.8	30.80	62.9	335.7	16.7	164
F	22, 216	4.5	50.5	64	815.7	24.1	556
G	22,321	2.7	90	64.3	905.1	31.1	800
H	22,364	2	60.46	64.4	1003.4	27.1	780
I	21,938	9.2	11.70	63.2	395.3	7.8	88
J	21,076	25	9.98	60.7	143.6	14.9	61
K	20,299	42	4.75	58.5	87.4	38.2	86.5
L	19,669	61.3	1.23	56.6	64.5	31.0	50.5
M	19,400	75	47.99	56	58.5	34.25	50
Total						329.7	use 330

Table 3.2-1 FENCE GEOMETRY PARAMETERS

The number of beam footprints varies from 7.8 to 34.25 per segment for a total of 330 for the fence. The shortest distance across the fence, its width, varies from 48.8 mi. at the high grazing angle to 800 mi. at the low grazing angle. The width is especially important since it determines how often a segment of the fence must be cycled to prevent an aircraft from passing through between the looks. A look consists of pointing the beam at a spot in the fence, transmitting a pulse burst, and receiving the echo.

Two looks are made during the time it takes an aircraft to cross the fence. The two looks and the overlapped footprints result in a cumulative probability of detection exceeding .999. Table 3.2-2 gives the time for crossing the fence and the look rate required for each one of the segments. The look rate varies from 125 per hour where the fence is the widest to 2520 per hour where the fence is the narrowest. The look rate for the total fence is 15,258 looks per hour. Look repeats because of false alarms increase this by 7.3 percent to 16,400 looks per hour. Since there are 330 beam footprints in the fence, and two looks are made per footprint, the average time required to generate one fence cycle is 2.92 minutes.

Table 3.2-3 gives the system losses and the calculated transmitter power for each segment of the fence. The highest system loss used in the calculation of the power is 6.06db. This is equivalent to 8.64db if the radar equation were used differently where the temperature is kept at ambient 290° and the receiver noise figure and circuit resistance are treated as losses. Except for false alarms, average power required to generate the fence is 4833.7 watts. Increasing this by 7.3% to cover the repeat looks for the false alarms brings it to 5200 watts. Dividing this equally among the three satellites makes it 1,734 watts per satellite.

3.3 Target Tracking

The number of aircraft crossing the fence per hour during the peak period as shown in table 2-2 is 33. It is estimated that on the average about 6 looks per aircraft are required to initiate the tracks. This results in a peak load of 33×6 or 198 looks per hour for track initiation.

87 tracks are being maintained by the satellite system during the peak period. For most of the time after penetrating the fence the aircraft are tracked in a low density traffic area. Assuming an average speed of mach 1, the look rate required to track an aircraft is once every three minutes. As the aircraft approaches the coast or busy land areas, the traffic density increases and the look rate may have to be increased. The amount of increase depends on the geometry of any cross tracks and on the speed of the other aircraft. The average speed of the penetrating aircraft may also be considerably less than mach 1 at this point. It is estimated that the average look rate will be increased to once per minute for the close-in traffic.

SEGMENT	TIME TO CROSS FENCE (1500 KT)	TIME BETWEEN LOOKS (2 per crossing)	NO. OF BEAMS	LOOKS PER HOUR
A	.0270HR.	.0135HR.	34.2	2533
B	.0277	.0139	29.4	2115
C	.0336	.0168	24.4	1452
D	.0366	.0183	16.5	901.6
E	.0909	.0455	16.7	367.4
F	.3086	.1543	24.1	156.2
G	.4444	.2222	31.1	140.0
H	.4329	.2165	27.1	125.2
I	.0488	.0244	7.8	319.8
J	.0339	.0169	14.9	879.1
K	.0481	.0240	38.2	1589
L	.0280	.0140	31.0	2214
M	.0278	.0139	34.25	2466
		Total	330	15,258

Table 3.2-2 FENCE LOOK RATE

SEGMENT	SCAN ANGLE (Degrees)	STARRAY PATTERN LOSS (db)	BAUMWITZ LOSS (db)	FIXED LOSS (db)	TOTAL LOSS (db)	EMPTY FOOK (Watt-sec.)	RAJAR LOSS (170 MC)	AVERAGE PWR (Watts)
A	2.3	.4	.07		2.77	734	.705	515
B	4.2	1.55	.14		3.99	1030	.558	605
C	5.1	2.3	.18		4.78	1380.	.403	556
D	6.1	3.3	.28		5.88	2060	.249	514
E	5.5	2.7	.23		5.23	2030	.102	207
F	5.6	2.85	.24	2.3 dB	5.39	2250	.0434	97.6
G	5.3	2.5	.21	I ² R	5.01	2110	.0389	82.1
H	5.4	2.6	.22	POLARIZATION	5.12	2160	.0348	75.0
I	5.0	2.2	.18	INTEGRATION	4.68	1820	.0888	161
J	5.9	3.2	.56		6.06	2130	.244	520
K	4.0	1.4	.14		3.84	1100	.442	486
L	3.4	.9	.12		3.32	870	.615	535
M	2.0	.3	.06		2.66	700	.686	480
Total Average Pwr.								4833.7

Table 3.2-3 SYSTEM LOSSES AND TRANSMITTER POWER

Assuming that the high density traffic begins at 250 miles out, this puts $\frac{250}{1200}$ x 87 or 18 aircraft in this area. Therefore, 69 of the aircraft are tracked at an average look rate of once every three minutes per aircraft or 1380 looks per hour, and 18 are tracked with an average look rate of once per minute per aircraft or 1080 looks per hour. The average rate for tracking all 87 aircraft is then 1380 + 1080 or 2460 looks per hour.

The radar signal energy required in each look for tracking is the same as that required in each look for detecting aircraft crossing the fence. The same radar equation is used, but instead of dividing the area where aircraft may have to be tracked into sections and treating each separately, like the fence, the whole area is treated as one with an average range and system loss.

The average range of 21,080 is obtained by taking the 4th root of the average of the sum of the 4th power of the maximum and minimum ranges. An average loss of 5db is used which is biased towards the high side. The energy required in each look to track an aircraft with these parameters is 1700 watt-seconds. The average power required for track initiation and tracking of the 87 aircraft is then $1700 \times \frac{2,658}{3,600}$ (looks per sec.) or 1260 watts.

3.4 Power Summary

The average R.F. transmitter power that must be produced by all three satellites to generate the 13,000 mile of fence for aircraft with speeds up to mach 3, and including the repeat looks for false alarms, is 5,200 watts.

The average power required for track initiation and for tracking the peak number of 87 aircraft that are expected to be in the system at any one time is 1260 watts.

The total system power required is then 5,200 + 1,260 or 6,460 watts. Dividing the load equally among the three satellites requires $\frac{2,154}{3}$ watts per satellite. This power is the combined R.F. average power output from the 12,000 modules in the phased array.

The energy per look varies from 734 watt-sec. to 2,350 watt-sec. If this were transmitted in one 0.6 μ sec pulse (300 feet range resolution), the peak power would have to vary from 1.22×10^9 watts to 3.75×10^9 watts. In the satellite radar transmitter the energy is distributed over the 64 pulses and a varying pulse width. The peak power is kept constant at 12 watts per module or 144,000 watts for the array. The energy per look is varied by changing the pulse compression ratio over the range from 133 to 406.

SECTION 4 INTEGRATION LOSS

Integration loss occurs because the Doppler filters are not completely power matched when they are optimized for clutter rejection. The amount of clutter rejection and associated loss are a function of the weighting given to the amplitude and phase of each one of the 64 pulses in the transmitter pulse burst. The weighting is done on receive during the processing of the radar echoes at the ground stations.

A computer program has been written and executed that determines the weighting of the coefficients for an optimum filter characteristics with respect to clutter attenuation and integration loss. An important point to recognize is that in the radar signal processor at the ground station, the filters are generated with a computer program using functions such as the Fourier transform, and consequently, they can be made as complex as necessary without the penalty of any hardware losses. Each of the 64 filters has its own coefficient weighting for optimum clutter rejection and integration loss.

The pertinent parameters of the radar system and of the clutter are as follows:

Signal-to-noise ratio, S/N	—	+14.3 dB after integration -3.46 dB before integration
No. of Doppler filters	—	64
Doppler filter bandwidth	—	10 Hz (.707 kt)
First blind speed	—	640 Hz (450 kt)
Clutter area	—	10 ⁷ square meters
Clutter σ_0	—	-13 dB
Clutter σ	—	2.5 Hz (frequency distribution)

The σ_0 of -13 dB is chosen to be on the conservative side for these calculations. In actual operation, the σ_0 is expected to be considerably less in most cases.

The clutter-to-noise ratio, C/N, for this σ_0 is 53.4 dB before integration and 71.4 dB after. The clutter reduction of 71.4 dB obtained from the filters, with coefficient weighting as determined by the computer analysis, results in a S/C ratio of 14.6 dB--the same as the S/N ratio--for all filters except the ones close in to the clutter spectrum.

The principle of the optimization consists of choosing the coefficient weighting such that the filter characteristics will have a null in the portion of the spectrum where the clutter is located and minimum attenuation at the doppler filter frequency.

The equations that were used for the optimization are shown in Figure 4-1.

$$\begin{aligned}
V(\vec{W}) &= \frac{\left| \sum_{k=1}^N W_k e^{j2\pi k f_0 T} \right|^2}{\int_{-f/2}^{f/2} S(f) \left| \sum_{k=1}^N W_k e^{j2\pi k f T} \right|^2 df} \\
&= \frac{\left| \vec{W}_T \vec{U}(f_0) \right|^2}{\sum_{k=1}^N \sum_{l=1}^N W_k W_l^* \int_{-f/2}^{f/2} S(f) e^{j2\pi(k-l)fT} df} \\
&= \frac{\left| \vec{W}_T \vec{U}(f_0) \right|^2}{\sum_{k=1}^N \sum_{l=1}^N h_{kl} W_k W_l^*} = \frac{\left| \vec{W}_T \vec{U}(f_0) \right|^2}{\vec{W}_T \tilde{H} \vec{W}^*}
\end{aligned}$$

WHERE $h_{kl} = \int_{-f/2}^{f/2} S(f) e^{j2\pi(k-l)fT} df$

$$\begin{aligned}
\left| \vec{W}_T \vec{U}(f_0) \right|^2 &= \left| \vec{W}_T \tilde{H}^{\frac{1}{2}} \tilde{H}^{-\frac{1}{2}} \vec{U}(f_0) \right|^2 \\
&\leq (\vec{W}_T \tilde{H}^{\frac{1}{2}} \tilde{H}^{\frac{1}{2}} \vec{W}^*) (\vec{U}_T^*(f_0) \tilde{H}^{-\frac{1}{2}} \tilde{H}^{-\frac{1}{2}} \vec{U}(f_0)) \\
&= (\vec{W}_T \tilde{H} \vec{W}^*) \vec{U}_T^*(f_0) \tilde{H}^{-1} \vec{U}(f_0)
\end{aligned}$$

$$\therefore V(\vec{W}) \leq \vec{U}_T^*(f_0) \tilde{H}^{-1} \vec{U}(f_0) \approx \text{MTI GAIN}$$

WITH EQUALITY iff. $\vec{W}^* = \tilde{H}^{-1} \vec{U}(f_0)$

CONTINUED

FIGURE 4-1. EQUATIONS FOR FILTER OPTIMIZATION

$$\text{LIT } S(f) = \frac{1}{\sigma\sqrt{2\pi}} e^{-\frac{1}{2\sigma^2} f^2} + \frac{1}{\rho f_r}$$

WHERE $\rho = C/N$ RATIO

$$h_{k,l} = \int_{-f_r/2}^{f_r/2} \left[\frac{1}{\sigma\sqrt{2\pi}} e^{-\frac{1}{2\sigma^2} f^2} + \frac{1}{\rho f_r} \right] e^{j2\pi(k-l)fT} df$$

$$\approx \frac{1}{\sigma\sqrt{2\pi}} \int_{-\infty}^{\infty} e^{-\frac{1}{2\sigma^2} f^2} e^{j2\pi(k-l)fT} df + \frac{1}{\rho f_r} \int_{-f_r/2}^{f_r/2} e^{j2\pi(k-l)fT} df$$

$$h_{k,l} = e^{-\frac{1}{2} [2\pi(k-l)\sigma T]^2} + \frac{1}{\rho} f_{k,l}$$

NOTATION:

W = WEIGHTING

f = DOPPLER FREQUENCY

f_0 = FILTER CENTER FREQ

$S(f)$ = SPECTRAL FUNCTION OF
CLUTTER PLUS NOISE

FIGURE 4-1. EQUATIONS FOR FILTER OPTIMIZATION
(CONTINUED)

The optimization was performed for 12 of the filters located from 5 Hz to 320 Hz. The points are 5, 10, 20, 30, 40, 80, 120, 160, 200, 240, 280, and 320 Hz. The filter responses from 320 Hz to 640 Hz are a mirror image of the first group. Figure 4-2 is a plot of the clutter reduction and integration loss for these filters, with an envelope drawn through the points to indicate the filter characteristics for the other filters in between.

Figure 4-3 is a plot of the frequency response of the filter optimized for 80 Hz. Note the nulls at the clutter frequencies. The lines of the spectrum repeat at the PRF in both directions from zero, with the amplitude falling off as the envelope of the spectrum of the transmitted pulse.

Table 4-1 is a computer run-off showing the amplitude and phase weightings for each one of the 64 pulses for the filter at 80 Hz.

The amplitude and phase figures are not normalized. The ratio of the amplitude numbers indicate the weighting. The phase weightings are given with respect to zero phase. The constant phase variation of 45° must be subtracted from each phase change increment. Except for a few points at the ends, the amplitude weighting variation is on the order of 5%, and the phase weighting on the order of one degree. These small weightings result in a filter only slightly mismatched giving an integration loss of 0.12 dB. The clutter reduction for this filter is 71.33 dB.

In the calculation of the average power for the radar in section 3, a maximum integration loss of 0.3 dB is used. This says that an aircraft with an RCS of one square meter, in heavy clutter with the σ of -13 dB and Δ of 2.5 Hz, must have a minimum radial speed of 35 kt ($50 \text{ Hz} \times .707 \text{ kt/Hz}$) to be detected. This restriction will have very little effect on the performance of the radar system since an aircraft travelling tangentially to one satellite radar beam cannot be travelling tangentially to the other satellite radar beam except at the equator.

WEIGHTING ON RECEIVE ONLY

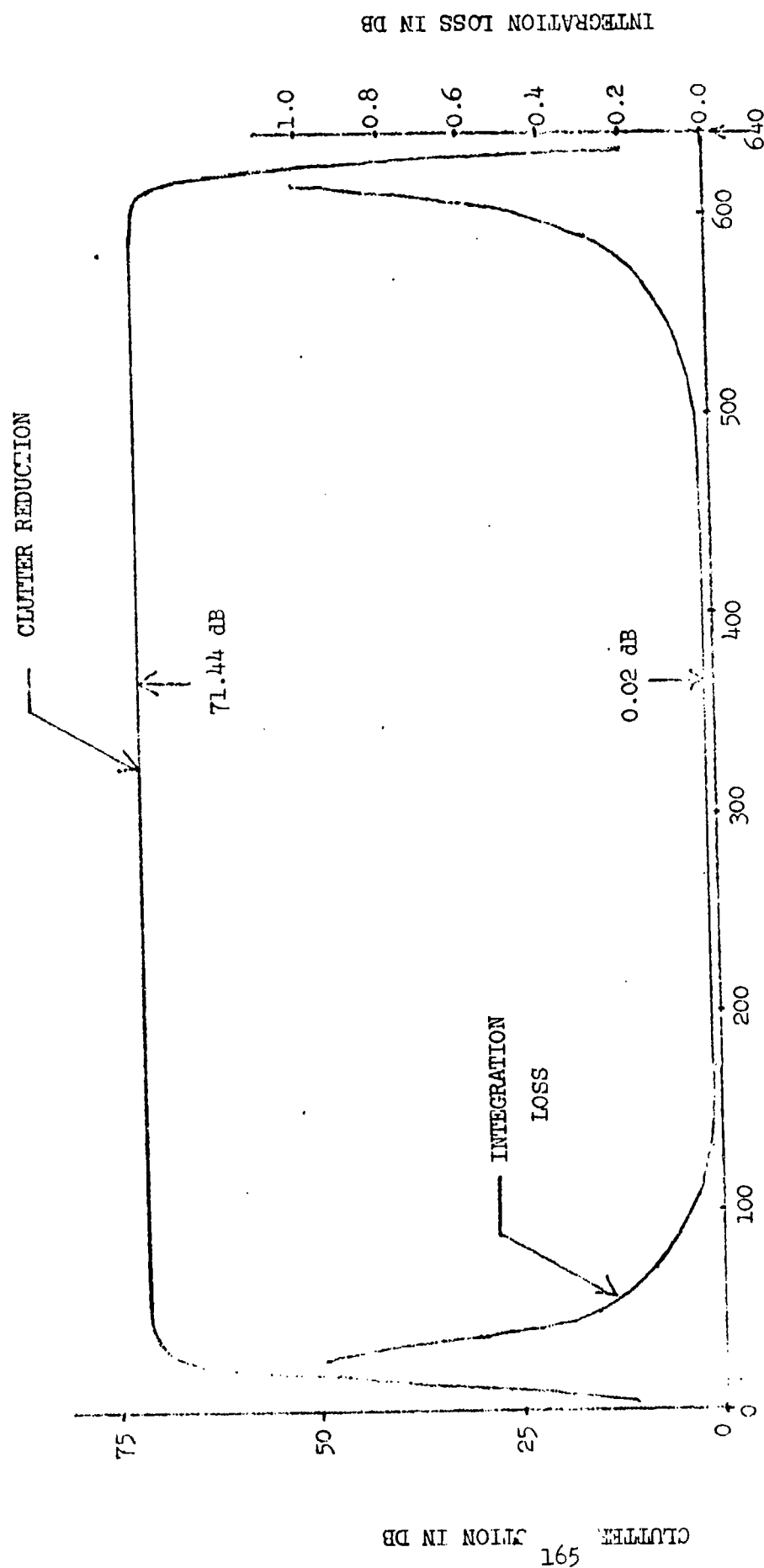


Figure 4-2 OPTIMIZED DOPPLER FILTER(S) CHARACTERISTICS
(Envelope)

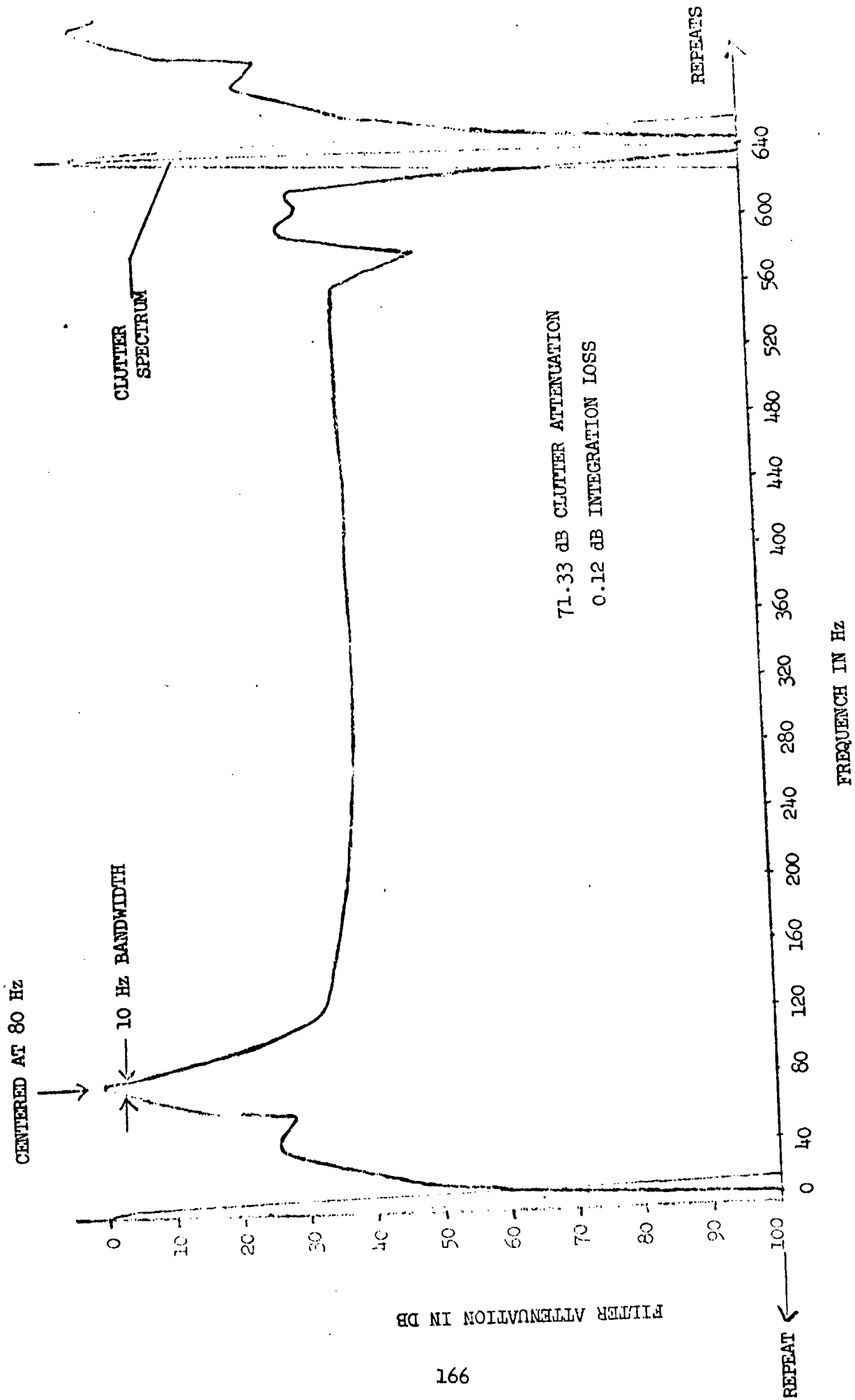


Figure 4-3 RESPONSE OF FILTER CENTERED AT 80 Hz

Table 4-1 Coefficient Weighting for 8 Hz Filter

Amplitude	Phase
WA(1) = 0.172670 00	WPH(1) = 35.26 DEG
WA(2) = 0.115030 00	WPH(2) = 171.55 DEG
WA(3) = 0.102220 00	WPH(3) = -121.53 DEG
WA(4) = 0.222940 00	WPH(4) = -78.03 DEG
WA(5) = 0.227590 00	WPH(5) = -38.20 DEG
WA(6) = 0.225490 00	WPH(6) = 2.58 DEG
WA(7) = 0.220300 00	WPH(7) = 47.50 DEG
WA(8) = 0.225050 00	WPH(8) = 93.64 DEG
WA(9) = 0.226520 00	WPH(9) = 127.61 DEG
WA(10) = 0.226180 00	WPH(10) = 179.21 DEG
WA(11) = 0.225040 00	WPH(11) = -139.52 DEG
WA(12) = 0.215800 00	WPH(12) = -96.13 DEG
WA(13) = 0.203050 00	WPH(13) = -49.10 DEG
WA(14) = 0.210350 00	WPH(14) = 0.01 DEG
WA(15) = 0.218430 00	WPH(15) = 47.85 DEG
WA(16) = 0.215870 00	WPH(16) = 92.64 DEG
WA(17) = 0.222300 00	WPH(17) = 136.22 DEG
WA(18) = 0.221490 00	WPH(18) = 179.93 DEG
WA(19) = 0.217530 00	WPH(19) = -134.52 DEG
WA(20) = 0.217730 00	WPH(20) = -88.83 DEG
WA(21) = 0.223020 00	WPH(21) = -43.40 DEG
WA(22) = 0.222430 00	WPH(22) = 0.46 DEG
WA(23) = 0.222290 00	WPH(23) = 45.37 DEG
WA(24) = 0.221440 00	WPH(24) = 86.79 DEG
WA(25) = 0.211630 00	WPH(25) = 132.16 DEG
WA(26) = 0.200210 00	WPH(26) = 179.37 DEG
WA(27) = 0.209120 00	WPH(27) = -123.10 DEG
WA(28) = 0.217450 00	WPH(28) = -57.22 DEG
WA(29) = 0.222420 00	WPH(29) = -43.23 DEG
WA(30) = 0.222560 00	WPH(30) = 0.07 DEG
WA(31) = 0.221570 00	WPH(31) = 44.07 DEG
WA(32) = 0.217230 00	WPH(32) = 89.45 DEG
WA(33) = 0.217230 00	WPH(33) = 135.55 DEG
WA(34) = 0.221570 00	WPH(34) = -179.07 DEG
WA(35) = 0.225560 00	WPH(35) = -135.07 DEG
WA(36) = 0.222420 00	WPH(36) = -91.77 DEG
WA(37) = 0.217450 00	WPH(37) = -47.78 DEG
WA(38) = 0.209120 00	WPH(38) = -1.90 DEG
WA(39) = 0.210210 00	WPH(39) = 45.63 DEG
WA(40) = 0.211630 00	WPH(40) = 92.90 DEG

Continued

Copy over to PDC does not
permit fully for the correction

Table 4-1 Continued

Amplitude	Phase
WA(41) = 0.221440 06	WPH(41) = 138.21 DEG
WA(42) = 0.228390 06	WPH(42) = -170.37 DEG
WA(43) = 0.226430 06	WPH(43) = -135.46 DEG
WA(44) = 0.223020 06	WPH(44) = -91.60 DEG
WA(45) = 0.217780 06	WPH(45) = -46.17 DEG
WA(46) = 0.217580 06	WPH(46) = -0.09 DEG
WA(47) = 0.221490 06	WPH(47) = 45.07 DEG
WA(48) = 0.223580 06	WPH(48) = 81.77 DEG
WA(49) = 0.218870 06	WPH(49) = 132.10 DEG
WA(50) = 0.208420 06	WPH(50) = 177.15 DEG
WA(51) = 0.200350 06	WPH(51) = -135.01 DEG
WA(52) = 0.203850 06	WPH(52) = -85.84 DEG
WA(53) = 0.218660 06	WPH(53) = -38.87 DEG
WA(54) = 0.235030 06	WPH(54) = 4.52 DEG
WA(55) = 0.241870 06	WPH(55) = 45.79 DEG
WA(56) = 0.236520 06	WPH(56) = 87.35 DEG
WA(57) = 0.225650 06	WPH(57) = 121.36 DEG
WA(58) = 0.220600 06	WPH(58) = 177.44 DEG
WA(59) = 0.225450 06	WPH(59) = -137.58 DEG
WA(60) = 0.227380 06	WPH(60) = -96.20 DEG
WA(61) = 0.209400 06	WPH(61) = -56.97 DEG
WA(62) = 0.163220 06	WPH(62) = -13.47 DEG
WA(63) = 0.119030 06	WPH(63) = 53.15 DEG
WA(64) = 0.173070 06	WPH(64) = 129.74 DEG

5.0 USE OF SHUTTLE

The radar satellite required to perform the IAS mission is similar to the one proposed in the Spaceborne Radar Study report. Some redesign of the packaged configuration is necessary to shorten the long dimensions for a two satellite launch by the shuttle.

The shuttle can be used to launch the radar satellite as follows:

1. Launch two satellites at one time into low orbit. Use a tug, already parked in orbit, to boost the satellites into synchronous orbit.
2. Share shuttle with a heavy high density payload and launch only one radar satellite at a time. Use tug to put satellites into synchronous orbit. A somewhat larger deployed antenna diameter is permitted when only one is launched.
3. Launch one radar satellite and Centaur booster with Shuttle. Use Centaur to boost the satellite to synchronous orbit.
4. Use any of the above three but with a heavier radar satellite.
 - a. more modules for higher frequency.
 - b. more average power for greater work load.